Eur. Phys. J. A (2017) **53**: 54
DOI 10.1140/epja/i2017-12237-2

THE EUROPEAN PHYSICAL JOURNAL A

Review

Probing exotic phenomena at the interface of nuclear and particle physics with the electric dipole moments of diamagnetic atoms: A unique window to hadronic and semi-leptonic CP violation*

N. Yamanaka[1,2], B.K. Sahoo[3], N. Yoshinaga[4], T. Sato[5], K. Asahi[5,6], and B.P. Das[6,a]

[1] iTHES Research Group, RIKEN, Wako, Saitama 351-0198, Japan
[2] Complex Simulation Group, School of Biomedicine, Far Eastern Federal University, Vladivostok 690950, Russia
[3] Atomic, Molecular and Optical Physics Division, Physical Research Laboratory, Ahmedabad-380009, India
[4] Graduate School of Science and Engineering, 255 Shimo-Okubo, Sakura-ku, Saitama City, Saitama 338-8570, Japan
[5] Nishina Center, RIKEN, 2-1 Hirosawa, Wako-shi, Saitama, 351-0198, Japan
[6] Department of Physics and International Education and Research Center of Science, Tokyo Institute of Technology, 2-12-1 Ookayama Meguro-ku, Tokyo 152-8550, Japan

Received: 16 December 2016 / Revised: 13 February 2017
Published online: 16 March 2017 –
Communicated by B. Ananthanarayan

Abstract. The current status of electric dipole moments of diamagnetic atoms which involves the synergy between atomic experiments and three different theoretical areas, *i.e.* particle, nuclear and atomic, is reviewed. Various models of particle physics that predict CP violation, which is necessary for the existence of such electric dipole moments, are presented. These include the standard model of particle physics and various extensions of it. Effective hadron level combined charge conjugation (C) and parity (P) symmetry violating interactions are derived taking into consideration different ways in which a nucleon interacts with other nucleons as well as with electrons. Nuclear structure calculations of the CP-odd nuclear Schiff moment are discussed using the shell model and other theoretical approaches. Results of the calculations of atomic electric dipole moments due to the interaction of the nuclear Schiff moment with the electrons and the P and time-reversal (T) symmetry violating tensor-pseudotensor electron-nucleus are elucidated using different relativistic many-body theories. The principles of the measurement of the electric dipole moments of diamagnetic atoms are outlined. Upper limits for the nuclear Schiff moment and tensor-pseudotensor coupling constant are obtained combining the results of atomic experiments and relativistic many-body theories. The coefficients for the different sources of CP violation have been estimated at the elementary particle level for all the diamagnetic atoms of current experimental interest and their implications for physics beyond the standard model is discussed. Possible improvements of the current results of the measurements as well as quantum chromodynamics, nuclear and atomic calculations are suggested.

1 Introduction

The important predictions of the standard model (SM) of particle physics [1–3] have been verified largely due to the remarkable advances in accelerator technology [4, 5]. A number of ingenious high-energy experiments are currently underway to search for new phenomena beyond the SM. Many of these experiments are being performed using the Large Hadron Collider (LHC) at the TeV scale. A complementary approach to search for new physics beyond the SM is characterized by non-accelerator low-energy precision tests of fundamental physics. It involves measuring observables and comparing the experimental results with the predictions of the SM. This is an indirect approach to new physics beyond the SM, but the observation of rare or forbidden phenomena is an indubitable proof of the existence of a new theory. Although conclusions reached by such an approach may in some case not be as specific in identifying the underlying fundamental theory as in the direct high-energy physics approach, its sensitivity to new physics may well exceed the energy of collider experiments.

The combined charge conjugation (C) and parity (P) symmetry (CP) violation is considered to have relevance

* Contribution to the Topical Issue "Exotic phenomena at the interface of nuclear and particle physics" edited by Balasubramanian Ananthanarayan, Bastian Kubis, Rishi Sharma.

[a] e-mail: bpdas.iia@gmail.com

to the huge discrepancy from the SM prediction which is observed in the matter-antimatter asymmetry of the Universe [6], and is currently an issue of primary importance in elementary particle physics [7–9]. CP violation has been studied in various physical systems, but has so far been observed only in the K [10] and B mesons [11–14], in which cases the experiments are in agreement with predictions of the SM. In the SM, it arises from the complex phase of the Cabibbo-Kobayashi-Maskawa (CKM) matrix [15,16]. It is well known that this phase cannot generate excess of matter over antimatter in the early Universe [17–19]. It is therefore imperative to find one or several new sources of CP violation beyond the SM. A variety of studies on CP violation including experiments to observe the electric dipole moments (EDMs) of different systems have lent themselves to searches for new physics beyond the SM [20–30].

A non-degenerate physical system can possess a permanent EDM due to violations of P and time-reversal (T) symmetries [31,32]. T violation implies the CP violation as a consequence of the CPT theorem [33]. An atom could possess an EDM due to the possible existence of i) the electron EDM (d_e) ii) P- and T-violating (P,T-odd) electron-nucleus interactions and iii) the hadronic CP violation. EDMs of open shell (paramagnetic) atoms arise primarily due to d_e and the P,T-odd electron-nucleus scalar-pseudoscalar (S-PS) interaction, but the dominant contributions to the EDMs of closed-shell (or diamagnetic) atoms come from the hadronic CP violation and the electron-nucleus tensor-pseudotensor (T-PT) interaction. Atomic EDMs are sensitive to new physics beyond the standard model (BSM) and can probe CP-violating interactions corresponding to mass scales of tens of TeV or larger [34–37]. The results of atomic EDM experiments and theory currently constrain various extensions of the SM. Experiments are underway to improve the limits of EDMs in paramagnetic (open-shell) [38–40] and diamagnetic (closed-shell) atoms [41–47]. Their results in combination with state of the art theoretical calculations can extract various CP-violating coupling constants at the elementary particle level via the hadronic, nuclear and atomic theories [7,36,48–52].

It is necessary at this stage to emphasize the importance of the study of EDMs of the diamagnetic atoms. Many low-energy observables used in the precision tests of fundamental physics, including EDMs of the paramagnetic atoms, are sensitive to limited sectors (*e.g.*, leptonic, hadronic, Higgs, etc.) of a particular particle physics model. However, the EDMs of diamagnetic atoms arise from new physics in multiple sectors of a variety of extensions of the SM, since the hadronic sector opens up many possible scenarios for CP violation at the elementary level (quark EDMs, quark chromo-EDMs, gluon chromo-EDMs, quark-quark (q-q) interactions, etc.). This means that one experimental constraint cannot in principle determine the unknown coupling constants of the models. Unraveling new physics beyond the SM in the context of EDMs of diamagnetic atoms is equivalent to finding the values for the couplings of new interactions that are solutions of a set of coupled equations obtained from experiments on atomic EDMs. The number of systems for EDM experiments must be at least equal to the number of coupling constants in order to uniquely determine those constants; assuming that uncertainties associated in all the results are of similar order. It is therefore desirable to perform EDM experiments on a number of different diamagnetic atoms.

The experimental limit on the EDM of mercury atom (^{199}Hg) has improved several times since the first measurement in 1987 [21], and it is currently the lowest limit reported for the EDM of any system ($d_{\rm Hg} < 7.4 \times 10^{-30} e\,{\rm cm}$) [29]. Improvements are expected in the EDM measurements of other diamagnetic systems such as the Xe and Ra in the near future. However, since the EDMs of the diamagnetic atoms depend on many fundamental sectors, considerable theoretical effort has to be put in relating these EDMs to new physics beyond the SM (see fig. 1). In particular, the atomic and nuclear level many-body physics as well as the non-perturbative effects of quantum chromodynamics (QCD) contribute to the theoretical uncertainties in the determination of their sensitivity to fundamental theories. Recent advances in the atomic and nuclear many-body as well as QCD calculations using numerical methods have reduced these uncertainties, but further progress is necessary in this direction.

The focus of this review article is the recent advances in the EDMs of the diamagnetic atoms which arise predominantly from the nuclear Schiff moment (NSM) [53] and CP-violating electron-nuclear interaction. The former arises from CP-violating nucleon-nucleon (N-N) interactions and EDMs of nucleons, which in turn originate from CP-violating quark level. The latter is fundamentally due to the CP-violating electron-quark (e-q) interactions. We shall summarize our current understanding of physics beyond the SM that has been obtained by combining the results of experiment as well as atomic theory, nuclear theory and QCD relevant in the evaluation of the EDMs of diamagnetic atoms. The theoretical uncertainty in the determination of these EDMs is the combined uncertainties resulting from the calculations in these three different theories. It is therefore important to identify the large sources of errors in extracting the CP-violating couplings at the particle physics level from the EDM experimental data.

The article is organized in the following manner: sect. 2 covers CP violations at the particle physics level that are suitable for the kind of atomic EDM that is considered in this review. The derivation of hadron level effective CP-odd interactions are then presented in sect. 3. Section 4 deals with the NSM and the nuclear structure issues involved in its calculation. Different features of relativistic many-body theories which are necessary to calculate the EDMs of diamagnetic atoms are presented in sect. 5.1. An introduction to the principles of the measurement of EDMs of diamagnetic atoms and the current status of the search for EDMs of these atoms are given in sect. 6. We summarize the effect of CP-odd interactions at the particle physics level on the EDMs of diamagnetic atoms in sect. 7, and analyze the candidates for BSM physics which can be constrained. Finally, our concluding remarks regarding

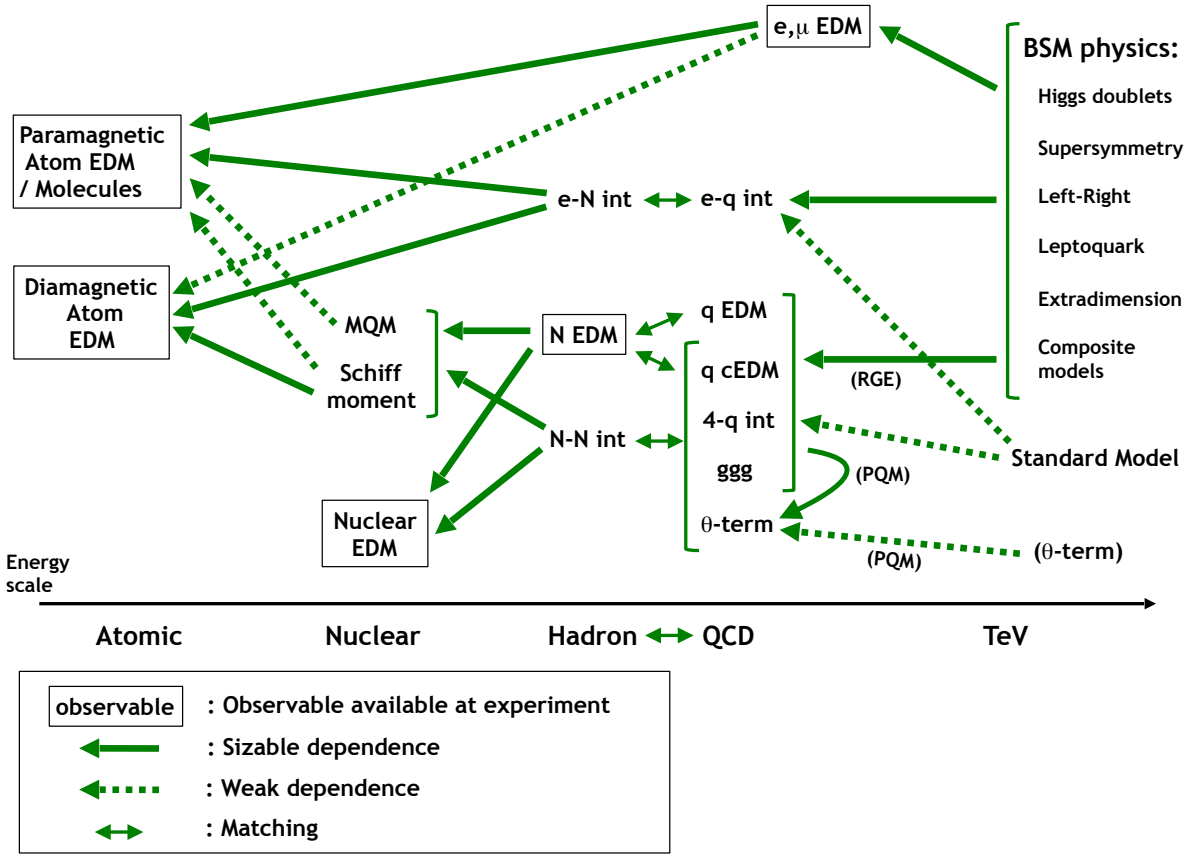

Fig. 1. Flow diagram of the dependence of the elementary level P,CP-odd processes on the EDMs of composite systems, whose EDMs can be measurable. "RGE" means renormalization group evolution and "PQM" means Peccei-Quinn mechanism.

the search for the EDMs of diamagnetic atoms are made in sect. 8.

2 Sources of P and CP violations in particle physics

In this section, we describe the physics of CP violation at the level of elementary particle physics. First, we present the relevant CP-violating operators, and then show that the SM contribution to them is small. We then briefly review several motivated candidates of new theories beyond SM. We also introduce the Peccei-Quinn mechanism which is almost mandatory to resolve the problem of too large QCD θ-term. We finally see the procedure to renormalize the CP-odd operators from the elementary physics to the hadronic scale, to pass on to the hadron level analysis.

2.1 CP-violating operators after integration of heavy degrees of freedom

After integrating out heavy new physics particles of BSM, the Higgs boson and massive electroweak gauge bosons (and eventually the top quark), we are left with an infinite number of operators which form the quark and gluon level effective interactions. As the coupling constants of those interactions are suppressed by the power of the energy scale of new physics, operators with the lowest mass dimension are important in the physics of strong interaction. Here we list the CP-violating operators generated at the elementary level up to mass dimension six, which are relevant in the physics of the EDM of atoms:

– θ-term:

$$\mathcal{L}_\theta = \frac{g_s^2}{64\pi^2}\bar{\theta}\,\epsilon^{\mu\nu\rho\sigma}G^a_{\mu\nu}G^a_{\rho\sigma}. \tag{1}$$

– Fermion EDM:

$$\mathcal{L}_{\rm EDM} = -\frac{i}{2}d_f\,\bar{\psi}\sigma_{\mu\nu}\gamma_5\psi F^{\mu\nu}, \tag{2}$$

where ψ denotes the electron or the quark and also it follows $\bar{\psi} = \gamma_0\psi^\dagger$.

– Quark chromo-EDM:

$$\mathcal{L}_{\rm cEDM} = -\frac{i}{2}d_q^c\,g_s\bar{\psi}_q\sigma_{\mu\nu}t_a\gamma_5\psi_q G_a^{\mu\nu}, \tag{3}$$

where ψ_q is the field operator of the quark q.

– Weinberg operator:

$$\mathcal{L}_w = \frac{1}{6} w f^{abc} \epsilon^{\alpha\beta\gamma\delta} G^a_{\mu\alpha} G^b_{\beta\gamma} G^{\mu,c}_{\delta}, \tag{4}$$

where f^{abc} is the $SU(3)$ structure constant of the Lie algebra.

– P, CP-odd or equivalently P,T-odd 4-quark interactions:

$$\begin{aligned}\mathcal{L}_{4q} = \sum_q & [C^q_4 \bar{q} q\, \bar{q} i\gamma_5 q + C^q_5 \bar{q} \sigma^{\mu\nu} q\, \bar{q} i\sigma_{\mu\nu}\gamma_5 q] \\ & + \frac{1}{2} \sum_{q\neq q'} \Big[2\tilde{C}^{q'q}_1 \bar{q}' q' \bar{q} i\gamma_5 q + 2\tilde{C}^{q'q}_2 \bar{q}'_\alpha q'_\beta \bar{q}_\beta i\gamma_5 q_\alpha \\ & + \tilde{C}^{q'q}_3 \bar{q}' \sigma^{\mu\nu} q' \bar{q} i\sigma_{\mu\nu}\gamma_5 q \\ & + \tilde{C}^{q'q}_4 \bar{q}'_\alpha \sigma^{\mu\nu} q'_\beta \bar{q}_\beta i\sigma_{\mu\nu}\gamma_5 q_\alpha \Big], \end{aligned} \tag{5}$$

where the color indices α and β were explicitly written when the color contraction is not taken in the same fermion bilinear.

– P, CP-odd or equivalently P,T-odd e-q interactions:

$$\begin{aligned}\mathcal{L}_{eq} = -\frac{G_F}{\sqrt{2}} \sum_q & \Big[C^{\rm SP}_{eq} \bar{q} q\, \bar{e} i\gamma_5 e + C^{\rm PS}_{eq} \bar{q} i\gamma_5 q\, \bar{e} e \\ & + \frac{1}{2} C^{\rm T}_{eq} \epsilon^{\mu\nu\rho\sigma} \bar{q} \sigma_{\mu\nu} q\, \bar{e} \sigma_{\rho\sigma} e \Big], \end{aligned} \tag{6}$$

where superscripts SP, PS, and T denote the scalar-pseudoscalar (S-PS), pseudoscalar-scalar (PS-S), and T-PT e-q interactions, respectively.

We must note that these effective interactions are defined at some energy scale. In perturbative evaluations, they are usually given at the energy scale where the new particle BSM is integrated out (typically at the TeV scale).

2.2 The SM contribution

Let us start with the SM contribution to the elementary level CP violation [1–3]. Apart from the strong θ term, CP violation comes from the Kobayashi-Maskawa phase [15] in the form of Jarlskog invariant [16]. The standard form of Cabibbo-Kobayashi-Maskawa (CKM) matrix is given by

$$V \equiv \begin{pmatrix} c_{12}c_{13} & s_{12}c_{13} & s_{13}e^{-i\delta} \\ -s_{12}c_{23} - c_{12}s_{23}s_{13}e^{i\delta} & c_{12}c_{23} - s_{12}s_{23}s_{13}e^{i\delta} & s_{23}c_{13} \\ s_{12}s_{23} - c_{12}c_{23}s_{13}e^{i\delta} & -c_{12}s_{23} - s_{12}c_{23}s_{13}e^{i\delta} & c_{23}c_{13} \end{pmatrix},$$

and the Jarlskog invariant is

$$J_{CP} \equiv \left| \Im(V_{\alpha j} V^*_{\beta j} V^*_{\alpha k} V_{\beta k}) \right| = s_{12}s_{23}s_{13}c_{12}c_{23}c^2_{13} \sin\delta. \tag{7}$$

Here $\Im$ implies an imaginary part and $s_{ij} = \sin\theta_{ij}$ and $c_{ij} = \cos\theta_{ij}$. This combination of CKM matrix elements is the minimal requirement to generate CP violation.

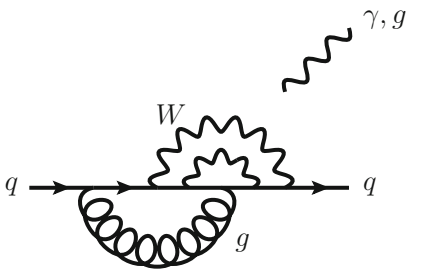

Fig. 2. Example of a diagram contributing to the EDM (chromo-EDM) of light quark at the three-loop level in the SM [58]. The external electromagnetic (or color) field, denoted by the isolated wavy line, is to be inserted in all possible propagators of electrically charged (colored) particles.

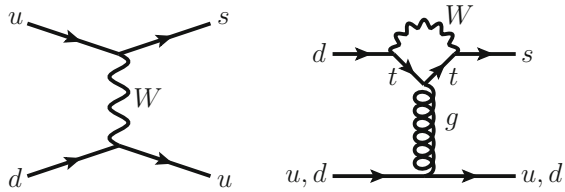

Fig. 3. Tree level $|\Delta S| = 1$ W boson exchange diagram (left) and the penguin diagram (right).

The CP violation in the SM therefore requires at least two W boson exchanges. For the quark EDM and the chromo-EDM, the two-loop level contribution is also known to vanish due to the GIM mechanism [54–57], and the leading-order one is given by at the three-loop level [58] (see fig. 2). Their effect on the nucleon EDM is around $d_N \sim 10^{-35} e\,\text{cm}$, much smaller than the present experimental limit of that of the neutron ($d_n < 10^{-26} e\,\text{cm}$) [24,30].

The EDM of the electron is also generated by the CP phase of the CKM matrix. This effect starts from the four-loop level, and its value is $d_e \sim 10^{-44} e\,\text{cm}$ [59–61]. We must note that the effect of the CP phase of the neutrino mixing matrix is negligible due to the small neutrino mass. If the neutrinos are Majorana fermions the effect of additional CP phases can generate the electron EDM from the two-loop level, and a larger value will be allowed for d_e [62–65].

Purely gluonic CP-odd processes such as the θ-term or the Weinberg operator are also known to be very small. The θ-term generated by the CKM phase is $\bar{\theta} \sim 10^{-17}$ [66, 67], which yields a nucleon EDM of $|d_N| \sim 10^{-33} e\,\text{cm}$. The Weinberg operator gives an even smaller nucleon EDM, of order $10^{-40} e\,\text{cm}$ [68].

In the strongly interacting sector, the most widely accepted leading hadronic CP violation due to the CP phase of the CKM matrix is generated by the long distance effect. The long distance contribution of the CKM phase arises from the interference between the tree level strangeness violating $|\Delta S| = 1$ W boson exchange process and the penguin diagram (see fig. 3), which forms the Jarlskog invariant (7). From a naive dimensional anal-

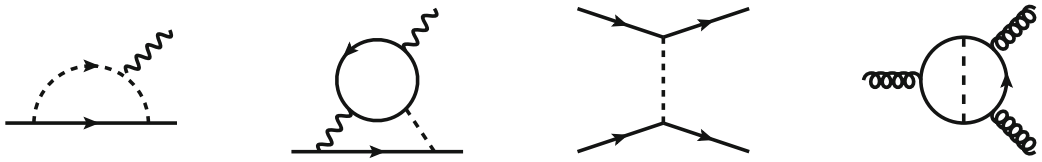

(a) (b) (c) (d)

Fig. 4. Leading contribution of the new physics of BSM to the effective interaction at the TeV scale. (a) One-loop level fermion EDM, (b) Barr-Zee–type diagram, (c) CP-odd four-fermion interaction, (d) Weinberg operator. The external wavy lines of (a) and (b) are either a photon or a gluon, and the internal one of (b) is either a photon, weak gauge bosons, or gluon.

ysis, the nucleon and nuclear EDMs are estimated as $d \sim O(\frac{\alpha_s}{4\pi} G_F^2 J \Lambda_{\rm QCD}^3) \sim 10^{-32} e\,{\rm cm}$, which is larger than the contribution from the short distance processes (quark EDM, chromo-EDM, Weinberg operator, etc.). Previous calculations of the nucleon EDM are in good agreement with this estimations [69–78].

The CP-violating effects in the SM exhibit an EDM far smaller than the experimental detectability, and large room is left for the discovery of new source of CP violation BSM.

2.3 Sources of CP violation from BSM physics

In many scenarios of BSM, large EDMs are predicted, because of higher-order contributions that can arise at the one- or two-loop levels. These contributions overwhelmingly exceed the loop suppressed SM contribution. In fig. 4, we present the typical lowest-order CP-violating processes of BSM contributing to the EDMs at the elementary level. In this subsection, we would like to elaborate several such well-motivated candidates of BSM which can generate EDMs.

2.3.1 Higgs doublet models

The Higgs boson was recently discovered [4, 5], but the detailed Higgs potential is still unknown. There are currently many well-motivated extensions of the Higgs sector BSM. The most well-known one is the two-Higgs doublet model (2HDM), and extensive studies have been performed [79–98].

As the Higgs boson has a small coupling with light fermions, the one-loop level fermion EDM and the CP-odd four-fermion interactions are suppressed in 2HDM [99, 100]. The leading contribution to the elementary level CP violation contributing to the EDM is the two-loop level Barr-Zee–type diagram [79] (fig. 4(b)), enhanced by the large Yukawa coupling of the top quark of the inner loop. The Barr-Zee–type diagram contribution to the EDM of SM fermion can be written as [79]

$$d_f = \frac{Q_f e \alpha_{\rm em}}{48\pi^3 m_t}\left[\left(Y_f^{(+)} Y_t^{(+)}\right)(f+g) - \left(Y_f^{(-)} Y_t^{(-)}\right)(f-g)\right], \tag{8}$$

where

$$f \equiv \frac{m_t^2}{2m_H^2}\int_0^1 {\rm d}x \frac{1-2x(1-x)}{x(1-x)-m_t^2/m_H^2}\ln\frac{x(1-x)}{m_t^2/m_H^2}, \tag{9}$$

$$g \equiv \frac{m_t^2}{2m_H^2}\int_0^1 {\rm d}x \frac{1}{x(1-x)-m_t^2/m_H^2}\ln\frac{x(1-x)}{m_t^2/m_H^2}, \tag{10}$$

and $Y_f^{(\pm)}$ and $Y_t^{(\pm)}$ are the Yukawa couplings relating the lightest Higgs boson ($m_H = 125\,{\rm GeV}$) with the fermion $f = e, u, d$ and the top quark, respectively. The first (second) term of eq. (8) is generated by the vacuum expectation value $\langle \phi_i^0 \phi_1^{0*}\rangle$ ($\langle \phi_i^0 \phi_1^0\rangle$), where ϕ_i is the Higgs doublet interacting with the up-type quark ($i = 1$) or the down-type fermion ($i = 2$, for the electron or down-type quarks). These vacuum expectation values strongly depend on the Higgs potential. Those couplings are obtained from the diagonalization of the Higgs doublets.

In diamagnetic atoms, the most important CP-violating process is the quark chromo-EDM:

$$d_q^c = \frac{g_s \alpha_s}{32\pi^3 m_t}\left[\left(Y_q^{(+)} Y_t^{(+)}\right)(f+g) - \left(Y_q^{(-)} Y_t^{(-)}\right)(f-g)\right]. \tag{11}$$

With $Y_q^{(\pm)} \sim 10^{-6}$, we have $d_f^c \sim Y_t^{(+)} \times 10^{-25}\,{\rm cm}$. We must note that the Weinberg operator (4) is also generated in the 2HDM (see fig. 4(d)) [80, 81]. Its typical value is $w \sim 10^{-10}\,{\rm GeV}^{-2}$, with $m_H = 125\,{\rm GeV}$. We will see in later sections that this contribution is subleading for the nucleon EDM.

2.3.2 Supersymmetric (SUSY) models

As the next attractive model for BSM physics, we have the minimal supersymmetric standard model (MSSM) [101–103]. The MSSM contains several phenomenological interactions which generically possess CP phases. In the most simplified parametrization, the Higgs bilinear μ-term

$$\mathcal{L}_\mu = e^{i\theta_\mu}\mu^2 H_u \cdot H_d, \tag{12}$$

from the superpotential, which is required to give mass to higgsinos, and the supersymmetry-breaking sfermion trilinear interactions

$$\begin{aligned}\mathcal{L}_A = {} & e^{i\theta_A} A_u \tilde{u}_R H_u \cdot \tilde{Q}_L + e^{i\theta_A} A_d \tilde{d}_R H_d \cdot \tilde{Q}_L \\ & + e^{i\theta_A} A_e \tilde{e}_R H_d \cdot \tilde{L}_L + {\rm h.c.},\end{aligned} \tag{13}$$

are CP violating. Here the dot denotes the $SU(2)_L$ inner product. For the sfermion trilinear interactions, we often assume a flavor diagonal one, with a common CP phase θ_A. This assumption is due to the strong constraints on

flavor changing neutral current from phenomenology [37, 104].

Under this MSSM Lagrangian, the fermion EDM appears at the one-loop level [99, 105–116] (see fig. 4(a)). The electron EDM and the quark EDM, in the simplified parametrization of MSSM where masses of all the supersymmetric particles as well as $|\mu|$ are given by $M_{\rm SUSY}$, are given by [36]

$$d_e \approx \frac{em_f}{16\pi^2 M_{\rm SUSY}^2}\left(\frac{5g_2^2+g_1^2}{24}\sin\theta_\mu\tan\beta+\frac{g_1^2}{12}\sin\theta_A\right), \tag{14}$$

$$d_q \approx \frac{Q_q em_f}{16\pi^2 M_{\rm SUSY}^2}\frac{2g_s^2}{9}\left(\sin\theta_\mu[\tan\beta]^{-2Q_q+\frac{1}{3}}-\sin\theta_A\right), \tag{15}$$

respectively, with Q_q is the electric charge of the quark q, and g_1, g_2 and g_s are the couplings of the $U(1)_Y$ and $SU(2)_L$ gauge theories and QCD, respectively. The quark chromo-EDM is similarly given by

$$d_q^c \approx \frac{g_s m_f}{16\pi^2 M_{\rm SUSY}^2}\frac{5g_s^2}{18}\left(\sin\theta_\mu[\tan\beta]^{-2Q_q+\frac{1}{3}}-\sin\theta_A\right), \tag{16}$$

where $\tan\beta \equiv \frac{v_d}{v_u}$ is the ratio between the vacuum expectation values of the up-type and down-type Higgs fields. As for the Higgs doublet models, we also see here a dependence on $\tan\beta$. By assuming $M_{\rm SUSY} = O(\text{TeV})$ and θ_μ, θ_A, $\beta = O(1)$, the MSSM contribution to the EDMs of the fermions and the chromo-EDMs of quarks at the scale $\mu = 1\,\text{TeV}$ [$\alpha_s(\mu = 1\,\text{TeV}) \approx 0.09$] become $d_e = O(10^{-27})e\,\text{cm}$, $d_q = O(10^{-25})e\,\text{cm}$ and $d_f^c = O(10^{-25})\,\text{cm}$ (see footnote[1]).

To conceive natural scenarios in MSSM, it is often assumed that the first and the second generations have no sfermion trilinear interactions. In such a case, the leading-order CP violation are given by the two-loop level effect, namely the Barr-Zee–type diagrams (fig. 4(b)) [118–130] and the Weinberg operator (fig. 4(d)) [131–133]. We must note that the Barr-Zee–type diagram and the four-fermion interaction are enhanced when $\tan\beta$ is large [124, 134–137]. Global analyses with constrained supersymmetric parameters by the Grand unification theory (GUT) strongly constrain CP phases [138–143].

Another natural supersymmetric scenario is the split SUSY model [144, 145], relying on the GUT. In this case, the sfermions are much heavier than the gauginos, and one-loop level diagrams, which must contain sfermions, are suppressed. The Barr-Zee–type diagram with chargino inner loop therefore becomes dominant [146–149].

The SUSY model can be extended with additional interactions, with several motivations. The first possibility is to take into account additional soft supersymmetry-breaking terms, in particular the flavor-violating ones which are not forbidden by any symmetries or by other experimental constraints. The flavor non-diagonal soft breaking terms can generically have CP phases. This extension was motivated by the deviation of the CP-violating $B \to \phi K_s$ decay [150,151] suggested by Belle experiment [152]. The effects of those flavor-violating terms on the EDM are however large, and it was found that the EDM experimental data can strongly constrain their CP phases [153–160].

Another possible way to extend the MSSM is to add new interactions in the superpotential. The scenario on these lines is the next-to-minimal supersymmetric standard model (NMSSM) which considers an additional scalar superfield in the Higgs sector [161]. This model can dynamically generate the μ-term (12) and circumvent the problem of μ-term. It is also motivated by the difficulty to explain the appearance of the light Higgs boson in the simple parametrization of the MSSM. In the NMSSM, the EDMs of fermions do not become large [162]. If we further enlarge the superpotential by adding new local gauged terms (BLMSSM) [163, 164], the fermion EDMs can become large, and the CP phases will be strongly constrained by the current experimental data [165]. The EDM is even more enhanced if we also allow the R-parity violation, where baryon and lepton numbers are not conserved [166–169]. If we neglect the one-loop level fermion EDM which is only generated in the presence of soft breaking bilinear R-parity–violating interaction [170–173], the leading CP violation processes are the Barr-Zee–type diagram [174–180] and the CP-odd four-fermion interaction [177, 181–183]. The majority of CP phases of the R-parity–violating couplings are strongly constrained by the current EDM experimental data.

Obviously, the SUSY extensions allow larger observable EDMs as the number of parameters increases. This fact does not depend on whether we have extended the superpotential or the soft supersymmetry-breaking interaction. The supersymmetric SM is an excellent example of new physics which contributes to the EDM of composite systems through various elementary level CP-odd operators. Current EDM experimental data strongly constrain the CP phases of models with large degree of freedom. In the analysis of theories and models which have a large parameter space, it was often assumed that only a small numbers of couplings are active, and the effect of the others were neglected. We however have to note that cancellations may occur among supersymmetric CP phases [184–198]. In that case, still large CP phases may be allowed, and they may be relevant in the ongoing EDM experiments.

2.3.3 Left-right symmetric models

The left-right symmetric models contain an additional gauge theory which couples to the right-handed fermions of SM [199–201]. An $SU(3)_c \times SU(2)_L \times SU(2)_R \times U(1)_{B-L}$ gauge group is assumed to be spontaneously broken at

[1] Unfortunately such models, except for the few predictive ones, have so many undetermined parameters and we should be careful about under what assumptions such and such predictions have been made. On this point one can refer to ref. [117] for more detailed clarification.

some high-energy scale, and gives the SM as an effective theory below it. Phenomenologically, a mixing of W boson with a heavier W_R boson is possible. The mass of additional weak gauge boson is constrained by LHC experiment, and the current lower bound is a few TeV [202–206].

In low-energy effective theory, we obtain a 4-quark interaction with the structure $(V-A)\times(V+A)$:

$$\begin{aligned}\mathcal{L}_{LR} &= i\,\mathrm{Im}(\Xi)\left[\bar{u}_R\gamma_\mu d_R\cdot\bar{d}_L\gamma^\mu u_L-\bar{d}_R\gamma_\mu u_R\cdot\bar{u}_L\gamma^\mu d_L\right]\\ &= \frac{\mathrm{Im}(\Xi)}{12}[2(\bar{q}q\cdot\bar{q}i\gamma_5\tau_z q-\bar{q}\tau_z q\cdot\bar{q}i\gamma_5 q)\\ &\quad+3(\bar{q}t_a q\cdot\bar{q}i\gamma_5\tau_z t_a q-\bar{q}t_a\tau_z q\cdot\bar{q}i\gamma_5 t_a q)],\end{aligned}\tag{17}$$

where the coupling constant Ξ scales as $O(m_{W_R}^{-2})$. The terms in the last line are the color octet four-quark interaction, with t_a the generator of the $SU(3)_c$ group. If Ξ has a CP phase, the EDM is induced in hadronic systems [207–215]. It is important to note that the above four-quark interaction breaks both the chiral and isospin symmetries [213]. This property is useful in estimating the leading CP-odd hadron level effective interaction generated by it [216]. Moreover, the effective interaction (17) is generated at the scale $\mu = m_W$, where the W boson is integrated out.

2.3.4 Models with vectorlike fermion

The vectorlike fermions are spin $\frac{1}{2}$ particles which have the same gauge charges for their left- and right-handed components [217]. They are not constrained by the analysis of the Higgs boson in collider experiments, as it was for extensions with extra generations of chiral fermions [218]. This class of models are attractive since those particles are often relevant in extensions of SM with composite sectors [219–221] or extradimensions [222, 223].

As a model-independent feature, the vectorlike fermions may mix with SM fermions, but those processes are strongly constrained by the flavor changing neutral current [217, 224–234]. Regarding more model-dependent aspects, additional dynamically generated bosons may accompany vectorlike fermions, such as the Higgs bosons, Kaluza-Klein particles, or higher-energy resonances, and their interactions with SM fermions may generate EDM at the one-loop level. This process is also strongly constrained by phenomenology [231, 235–240]. Under those constraints, the vectorlike fermions may appear in the intermediate states connected only by the exchange of gauge bosons [241]. The leading CP-violating process is therefore the Weinberg operator [242].

The contribution of the Weinberg operator in the vectorlike fermion models can be written as

$$w_{\mathrm{VF}} = -\sum_i^{N_F}\frac{g_s\alpha_s Y_i Y_{Pi}}{(4\pi)^3 M_i^2}h(M_i,m_{H'}),\tag{18}$$

with $h(M,m_{H'})\equiv\frac{M^4}{2}\int_0^1\mathrm{d}x\int_0^1\mathrm{d}u\frac{u^3x^3(1-x)}{[M^2x(1-ux)+m_{H'}^2(1-u)(1-x)]^2}$.

Here we have assumed a boson H' which couples to N_F vectorlike fermions with mass M_i $(i=1,\cdots,N_F)$. In the limiting case $M\gg m_{H'}$, we have $h(M,m_{H'})\approx\frac{1}{16}$ [115]. In technicolor theories, an effective $WW\gamma$ interaction is generated by a similar mechanism [243].

2.3.5 Leptoquark models

The leptoquarks are bosons which couple to both leptons and baryons, and often appears in scenarios with GUT. Those which violate the baryon number are strongly constrained by the proton decay, but those which conserve lepton and baryon numbers are allowed up to the constraints from the LHC experiments [244–249], and their interaction can be probed using low-energy precision tests [250]. The simplest interaction of the scalar leptoquark is given as

$$\mathcal{L}_{\mathrm{LQ}} = \sum_{i,j}\varphi(\lambda_{ij}\bar{Q}_{Li}\cdot e_{Rj}+\lambda'_{ij}\bar{u}_{Ri}\cdot L_{Lj})+\mathrm{h.c.},\tag{19}$$

where φ is the leptoquark field, and the indices i, j denote the flavor.

If the couplings λ and λ' have relative CP phases, the EDM will be induced in atomic systems. The leading CP violation is given by the one-loop level fermion EDM [99, 251] and the CP-odd e-q interaction (see eq. (6)) [100,252,253]. For the atomic system, the latter is especially important, since it contributes to the tree level. The leptoquark model is one of the rare models which contribute to the T-PT CP-odd e-N interaction (the term with C_{T} in eq. (6)).

2.4 Renormalization group evolution (RGE)

In the usual discussion of particle physics, the effect of BSM physics is calculated at some high-energy scale, much higher than that of the strong interaction $\mu\gg\Lambda_{\mathrm{QCD}}\sim 200\,\mathrm{MeV}$. On the other hand, their matching with the hadronic effective interaction is done at the hadron scale, we must evolve the Wilson coefficients of elementary level interactions down to the hadronic scale. In this subsection, we first present the RGE of purely hadronic CP-odd operators, and then that of CP-odd e-q interactions, which do not mix with each other.

2.4.1 RGE of strong CP-odd operators

The effective CP-odd Lagrangian and their Wilson coefficients are given as

$$\begin{aligned}\mathcal{L}_{eff} &= \sum_{i=1,2,4,5}\sum_q C_i^q(\mu)O_i^q(\mu)+C_3(\mu)O_3(\mu)\\ &\quad+\sum_{i=1,2}\sum_{q\neq q'}C_i^{q'q}(\mu)\tilde{O}_i^{q'q}(\mu)\\ &\quad+\frac{1}{2}\sum_{i=3,4}\sum_{q\neq q'}C_i^{q'q}(\mu)\tilde{O}_i^{q'q}(\mu),\end{aligned}\tag{20}$$

with

$$O_1^q = -\frac{i}{2} m_q \bar{q} Q_q e \sigma_{\mu\nu} F^{\mu\nu} \gamma_5 q, \tag{21}$$

$$O_2^q = -\frac{i}{2} m_q \bar{q} g_s \sigma_{\mu\nu} G_a^{\mu\nu} t_a \gamma_5 q, \tag{22}$$

$$O_3 = -\frac{1}{6} g_s f_{abc} G_{\mu\nu,a} G^{\nu}{}_{\rho,b} G_{\alpha\beta,c} \epsilon^{\rho\mu\alpha\beta}, \tag{23}$$

$$O_4^q = \bar{q} q \, \bar{q} i \gamma_5 q, \tag{24}$$

$$O_5^q = \bar{q} \sigma^{\mu\nu} q \, \bar{q} i \sigma_{\mu\nu} \gamma_5 q, \tag{25}$$

$$\tilde{O}_1^{q'q} = \bar{q}' q' \, \bar{q} i \gamma_5 q, \tag{26}$$

$$\tilde{O}_2^{q'q} = \bar{q}'_\alpha q'_\beta \, \bar{q}_\beta i \gamma_5 q_\alpha, \tag{27}$$

$$\tilde{O}_3^{q'q} = \bar{q}' \sigma^{\mu\nu} q' \, \bar{q} i \sigma_{\mu\nu} \gamma_5 q, \tag{28}$$

$$\tilde{O}_4^{q'q} = \bar{q}'_\alpha \sigma^{\mu\nu} q'_\beta \, \bar{q}_\beta i \sigma_{\mu\nu} \gamma_5 q_\alpha, \tag{29}$$

where the color indices α and β were explicitly written when the color contraction is not taken in the same fermion bilinear. The summation of the quark q for the above operators must be taken for the relevant flavor at the renormalization scale chosen (*e.g.*, $q = u, d, s$ for $\mu = 1\,\mathrm{GeV}$).

We note that the above CP-odd operators are defined in a scale where the Higgs boson, massive electroweak gauge bosons and the top quark are integrated out. Their Wilson coefficients therefore also involve the BSM CP-odd effect related with those particles at a higher-energy scale through the RGE [90,254–257]. In this section, we do not treat them explicitly, but consider their effects through the renormalized Wilson coefficients at the electroweak scale as the initial condition.

The evolution of the Wilson coefficients is dictated by the renormalization group equation, which mixes the CP-odd operators when the scale is changed. It is given by the following differential equation:

$$\frac{\mathrm{d}}{\mathrm{d}\ln\mu} \mathbf{C}(\mu) = \hat{\gamma}^T(\alpha_s) \mathbf{C}(\mu). \tag{30}$$

The anomalous dimension matrix is given by

$$\hat{\gamma} = \hat{Z}^{-1} \frac{\mathrm{d}}{\mathrm{d}\ln\mu} \hat{Z}, \tag{31}$$

with $\hat{Z}$ the renormalization matrix. By integrating (30) with the initial condition at the scale of new physics $\mu' = M_{\mathrm{NP}}$, we have

$$\mathbf{C}(\mu) = \hat{U}(\mu, \mu' = M_{\mathrm{NP}}) \mathbf{C}(\mu' = M_{\mathrm{NP}}), \tag{32}$$

where

$$\hat{U}(\mu, \mu' = M_{\mathrm{NP}}) = T_g \exp \int_{g(M_{\mathrm{NP}})}^{g(\mu)} \mathrm{d}g' \frac{\hat{\gamma}^T(g')}{\beta(g')}, \tag{33}$$

with the strong coupling $g \equiv \sqrt{4\pi\alpha_s}$, and the coupling ordered product operator T_g. The anomalous dimension matrix and the beta function $\beta(g)$ are expanded in terms of the QCD coupling as

$$\hat{\gamma}(g) = \hat{\gamma}^{(0)} + \hat{\gamma}^{(1)} + \cdots, \tag{34}$$

$$\beta(g) = -\beta_0 \frac{g^3}{16\pi^2} - \beta_1 \frac{g^5}{(16\pi^2)^2} + \cdots. \tag{35}$$

Let us see the leading logarithmic order contribution. The leading-order coefficient of the beta function is $\beta_0 = \frac{11}{3} n_c - \frac{2}{3} n_f$ with the color number $n_c = 3$. The anomalous dimension matrix $\hat{\gamma}^{(0)}$, depending on n_f, is expressed in terms of submatrices as [254, 258–265]

$$\hat{\gamma}^{(0)} = \begin{pmatrix} \frac{\alpha_s}{4\pi}\hat{\gamma}_s & \hat{0} & \hat{0} \\ \frac{\alpha_s}{(4\pi)^2}\hat{\gamma}_{sf} & \frac{\alpha_s}{4\pi}\hat{\gamma}_f & \hat{0} \\ \frac{\alpha_s}{(4\pi)^2}\hat{\gamma}'_{sf} & \hat{0} & \frac{\alpha_s}{4\pi}\hat{\gamma}_f \end{pmatrix}, \tag{36}$$

where $\hat{0}$ is the null matrix with arbitrary dimension, and

$$\hat{\gamma}_s = \begin{pmatrix} 8C_F & 0 & 0 \\ 8C_F & 16C_F - 4n_c & 0 \\ 0 & 2n_c & n_c + 2n_f + \beta_0 \end{pmatrix}, \tag{37}$$

$$\hat{\gamma}_f = \begin{pmatrix} -12C_F + 6 & \frac{1}{n_c} - \frac{1}{2} \\ \frac{48}{n_c} + 24 & 4C_F + 6 \end{pmatrix}, \tag{38}$$

$$\hat{\gamma}'_f = \begin{pmatrix} -12C_F & 0 & 0 & 0 & \frac{1}{n_c} & -1 \\ -6 & \frac{6}{n_c} & 0 & 0 & -\frac{1}{2} & c_1 \\ 0 & 0 & -12C_F & 0 & \frac{1}{n_c} & -1 \\ 0 & 0 & -6 & \frac{6}{n_c} & -\frac{1}{2} & c_2 \\ \frac{24}{n_c} & -24 & \frac{24}{n_c} & -24 & 4C_F & 0 \\ -12 & c_3 & -12 & c_4 & 6 & c_5 \end{pmatrix}, \tag{39}$$

$$\hat{\gamma}_{sf} = \begin{pmatrix} 4 & 4 & 0 \\ -32n_c - 16 & -16 & 0 \end{pmatrix}, \tag{40}$$

$$\hat{\gamma}'_{sf} = \begin{pmatrix} 0 & 0 & 0 \\ 0 & 0 & 0 \\ 0 & 0 & 0 \\ 0 & 0 & 0 \\ -16n_c \frac{m_{q'}}{m_q} \frac{Q_{q'}}{Q_q} & 0 & 0 \\ -16 \frac{m_{q'}}{m_q} \frac{Q_{q'}}{Q_q} & -16 \frac{m_{q'}}{m_q} & 0 \end{pmatrix}, \tag{41}$$

where $C_F = 4/3$, $c_1 = -C_F + \frac{1}{2n_c}$, $c_2 = -C_F + \frac{1}{2n_c}$, $c_3 = -24C_F + \frac{12}{n_c}$, $c_4 = -24C_F + \frac{12}{n_c}$, and $c_5 = -8C_F - \frac{6}{n_c}$.

Let us show the results for three explicit cases with the initial condition $\mu = M_{\rm NP} = 1\,{\rm TeV}$. For the quark EDM, there is no mixing with other operators. If only the quark EDM is dominant at the initial scale, we have

$$\frac{d_q(\mu=\mu_{\rm had})}{d_q(\mu=M_{\rm NP})} = \frac{C_1^q(\mu=\mu_{\rm had})m_q(\mu=\mu_{\rm had})}{C_1^q(\mu=M_{\rm NP})m_q(\mu=M_{\rm NP})} = 0.79, \tag{42}$$

for $\mu_{\rm had} = 1\,{\rm GeV}$. The running of the quark mass is

$$m_q(\mu=\mu_{\rm had})/m_q(\mu=M_{\rm NP}) = 2.0. \tag{43}$$

We have used the quark masses $m_t(\mu=m_t) = 160\,{\rm GeV}$, $m_b(\mu=m_b) = 4.18\,{\rm GeV}$, and $m_c(\mu=m_c) = 1.27\,{\rm GeV}$ as input [266].

If the quark chromo-EDM is dominant at $\mu = M_{\rm NP}$, the Wilson coefficients at the hadronic scale mixes with the quark EDM:

$$\frac{d_q(\mu=\mu_{\rm had})}{d_q^c(\mu=M_{\rm NP})} = \frac{C_1^q(\mu=\mu_{\rm had})m_q(\mu=\mu_{\rm had})}{C_2^q(\mu=M_{\rm NP})m_q(\mu=M_{\rm NP})} = -0.80, \tag{44}$$

$$\frac{d_q^c(\mu=\mu_{\rm had})}{d_q^c(\mu=M_{\rm NP})} = \frac{C_2^q(\mu=\mu_{\rm had})m_q(\mu=\mu_{\rm had})}{C_2^q(\mu=M_{\rm NP})m_q(\mu=M_{\rm NP})} = 0.89. \tag{45}$$

Note that the flavor of the quark q is conserved during the running in the leading logarithmic order. It is also to be noted that the running of the quark EDM in eq. (42) and the chromo-EDM in eq. (45) are additionally affected by the integration of the Higgs boson, heavy electroweak gauge bosons and the top quark, if those particles have CP-violating interactions in the BSM physics [215].

In the case where only the Weinberg operator is present at $\mu = M_{\rm NP}$, we have

$$C_1^q(\mu=\mu_{\rm had})/C_3(\mu=M_{\rm NP}) = 7.7\times10^{-2}, \tag{46}$$
$$C_2^q(\mu=\mu_{\rm had})/C_3(\mu=M_{\rm NP}) = -0.14, \tag{47}$$
$$C_3(\mu=\mu_{\rm had})/C_3(\mu=M_{\rm NP}) = 0.16. \tag{48}$$

Here the Wilson coefficients C_1^q and C_2^q are generated for all relevant quark flavors ($q = u, d, s$). It is also important to note that C_3 is sizably suppressed after the running. By comparing eqs. (45) and (48), we see that the chromo-EDM becomes large at the hadronic scale, even if the Wilson coefficients of the Weinberg operator and the chromo-EDM are of the same order of magnitude. This is the case for 2HDM, where the contribution from Barr-Zee–type diagrams are the most important.

We also show the evolution of the four-quark operator of the left-right symmetric model (see sect. 2.3.3). The CP-odd four-quark coupling of eq. (17), renormalized at the electroweak scale $\mu = m_W$, is evolved down to the hadronic scale as [254]

$$\frac{C_4^u(\mu=\mu_{\rm had})}{{\rm Im}(\Xi)(\mu=m_W)} = \frac{C_4^d(\mu=\mu_{\rm had})}{{\rm Im}(\Xi)(\mu=m_W)} = -\frac{C_1^{ud}(\mu=\mu_{\rm had})}{2\,{\rm Im}(\Xi)(\mu=m_W)} = -\frac{C_1^{du}(\mu=\mu_{\rm had})}{2\,{\rm Im}(\Xi)(\mu=m_W)} = 4.8 \quad (\mu_{\rm had}=1\,{\rm GeV}). \tag{49}$$

Although we obtain several other Wilson coefficients at the hadronic scale, here we focus on C_4^u, C_4^d, C_1^{du} and C_1^{ud}, since their corresponding operators are the components of the operator $\bar{q}q\,\bar{q}i\gamma_5\tau_z q$, which is suggested to be the leading contribution of the isovector pion-nucleon interaction (see sect. 3.3). We also note again that the running of the Wilson coefficient ${\rm Im}(\Xi)$ begins at the electroweak scale $\mu = m_W$, since the W boson has to be integrated out to generate the four-quark operator in the left-right symmetric model. At the scale above $\mu = m_W$, the coupling of the right-handed W_R boson with quarks does not run. In running from $\mu = m_W$ to $\mu_{\rm had}$, the left-right four-quark operator mixes with several other four-quark operators, but it is interesting to note that it does not mix with the quark EDM, the quark chromo-EDM, and the Weinberg operator.

In the case where several CP-odd processes are simultaneously relevant at the TeV scale, the RGE of them down to the hadronic scale is just given by the linear combination of Wilson coefficients seen above. This is because the RGE is calculated only in QCD and the effect of CP-odd interactions on the running is negligible.

Finally, let us also briefly present the running of SM contribution, although we do not discuss the detail. The SM contribution at the electroweak scale is expressed by ten $|\Delta S| = 1$ four-quark operators [267]. The next-to-next-to-leading logarithmic order evolution of the SM contribution enhances one of the penguin operator (see fig. 3) by a factor of about 40 when the scale is varied from $\mu = m_W$ to $\mu = 1\,{\rm GeV}$ [267–269]. This effect is nontrivial and enhances the SM contribution to the nucleon level CP-odd processes from the naive estimation.

Note that the RGE of this subsection is calculated in the perturbative framework, and systematics due to non-perturbative effects may be important at the hadronic scale $\mu = 1\,{\rm GeV}$.

2.4.2 RGE of CP-odd e-q interaction

We now present the QCD RGE of the CP-odd e-q interactions. The change of the Wilson coefficients of the CP-odd e-q interactions depends on the Lorentz structure of the quark bilinears. For the S-PS– and PS-S–type ones (terms with $C_{\rm SP}$ and $C_{\rm PS}$ of eq. (6), respectively), the renormalization is the same as that of the quark mass. We therefore have

$$\frac{C_{eq}^{\rm SP}(\mu=\mu_{\rm had})}{C_{eq}^{\rm SP}(\mu=M_{\rm NP})} = \frac{C_{eq}^{\rm PS}(\mu=\mu_{\rm had})}{C_{eq}^{\rm PS}(\mu=M_{\rm NP})} = \frac{m_q(\mu=\mu_{\rm had})}{m_q(\mu=M_{\rm NP})} = \begin{cases} 2.0 & (\mu_{\rm had}=1\,{\rm GeV}), \\ 1.8 & (\mu_{\rm had}=2\,{\rm GeV}), \end{cases} \tag{50}$$

with $M_{\rm NP} = 1\,{\rm TeV}$. Here we also show the ratio for $\mu_{\rm had} = 2\,{\rm GeV}$, for which we have less theoretical uncertainty due to the non-perturbative effect of QCD. This renormalization point is often used in the lattice QCD calculations of nucleon matrix elements.

For the T-PT CP-odd e-q interaction (the term with $C_{\rm T}$ of eq. (6)), the renormalization is the same as that of the quark EDM. The renormalization group evolution is then

$$\frac{C_{eq}^{\rm T}(\mu=\mu_{\rm had})}{C_{eq}^{\rm T}(\mu=M_{\rm NP})} = \frac{d_q(\mu=\mu_{\rm had})}{d_q(\mu=M_{\rm NP})} = \frac{C_1^q(\mu=\mu_{\rm had})m_q(\mu=\mu_{\rm had})}{C_1^q(\mu=M_{\rm NP})m_q(\mu=M_{\rm NP})} = \begin{cases} 0.79 & (\mu_{\rm had}=1\,{\rm GeV}), \\ 0.83 & (\mu_{\rm had}=2\,{\rm GeV}). \end{cases} \tag{51}$$

The S-PS– and S-PS–type P,CP-odd e-q interactions with heavy quarks are integrated out at scale below the quark masses, but their effects remain relevant through the P,CP-odd electron-gluon (e-g) interaction. The P,CP-odd e-g interaction is defined as

$$\mathcal{L}_{eg} = -\frac{G_F}{\sqrt{2}}\left[C_{eg}^{\rm SP} G^a_{\mu\nu}G_a^{\mu\nu}\,\bar{e}i\gamma_5 e + C_{eg}^{\rm PS}\tilde{G}^a_{\mu\nu}G_a^{\mu\nu}\,\bar{e}e\right]. \tag{52}$$

The matching of the couplings at each quark mass threshold works as

$$C_{eg}^{\rm SP}(\mu=m_Q-\epsilon) = C_{eg}^{\rm SP}(\mu=m_Q+\epsilon) + \frac{\alpha_s(\mu=m_Q)}{12\pi m_Q}C_{eQ}^{\rm SP}(\mu=m_Q+\epsilon), \tag{53}$$

$$C_{eg}^{\rm PS}(\mu=m_Q-\epsilon) = C_{eg}^{\rm PS}(\mu=m_Q+\epsilon) + \frac{\alpha_s(\mu=m_Q)}{8\pi m_Q}C_{eQ}^{\rm PS}(\mu=m_Q+\epsilon), \tag{54}$$

where ϵ is the infinitesimal shift of energy scale. As $\alpha_s G^a_{\mu\nu}G_a^{\mu\nu}$ is invariant under the RGE, the couplings $C_{eg}^{\rm SP}$ and $C_{eg}^{\rm PS}$ run in the same way as the strong coupling $\alpha_s(\mu)$.

If there is only one type of CP-odd e-q interaction $C_{eQ}^{\rm SP}$ $(Q=t,b)$ at the scale $\mu=1\,{\rm TeV}$, the running of its effect down to the hadronic scale is given by

$$12\pi m_t\frac{C_{eg}^{\rm SP}(\mu=\mu_{\rm had})}{C_{et}^{\rm SP}(\mu=M_{\rm NP})} = \frac{\alpha_s(\mu=\mu_{\rm had})m_q(\mu=m_t)}{\alpha_s(\mu=m_t)m_q(\mu=M_{\rm NP})} = \begin{cases} 3.7 & (\mu_{\rm had}=1\,{\rm GeV}), \\ 2.8 & (\mu_{\rm had}=2\,{\rm GeV}), \end{cases} \tag{55}$$

$$12\pi m_b\frac{C_{eg}^{\rm SP}(\mu=\mu_{\rm had})}{C_{eb}^{\rm SP}(\mu=M_{\rm NP})} = \frac{\alpha_s(\mu=\mu_{\rm had})m_q(\mu=m_b)}{\alpha_s(\mu=m_b)m_q(\mu=M_{\rm NP})} = \begin{cases} 2.7 & (\mu_{\rm had}=1\,{\rm GeV}), \\ 2.0 & (\mu_{\rm had}=2\,{\rm GeV}). \end{cases} \tag{56}$$

If we consider a hadronic scale lower than the charm quark mass, the charm quark is also integrated out. The CP-odd e-g coupling generated by $C_{ec}^{\rm SP}$ is then

$$12\pi m_c\frac{C_{eg}^{\rm SP}(\mu=\mu_{\rm had})}{C_{ec}^{\rm SP}(\mu=M_{\rm NP})} = \frac{\alpha_s(\mu=\mu_{\rm had})m_q(\mu=m_c)}{\alpha_s(\mu=m_c)m_q(\mu=M_{\rm NP})} = 2.2 \quad (\mu_{\rm had}=1\,{\rm GeV}). \tag{57}$$

Obviously, the contributions of the CP-odd electron-heavy quark interactions are suppressed as the quark mass increases. This additional damping is because the CP-odd e-g operator has one mass dimension higher than that of the CP-odd electron-quark interaction. We reiterate that the same running of the Wilson coefficients of eqs. (55), (56) and (57) also applies for $C_{eg}^{\rm PS}$ (we must replace $12\pi m_Q$ by $8\pi m_Q$ in the right-hand side of the equalities).

2.5 θ-term and Peccei-Quinn mechanism

The QCD θ-term is a dimension-4, P- and CP-violating interaction (see eq. (1)), which is not constrained by symmetries in the SM. In the point of view of the naturalness, $\bar{\theta}\sim O(1)$, but it is known to generate a too large EDM of neutron. The contribution of $\bar{\theta}$ to the neutron EDM was extensively studied [36,270–287], and the most recent analysis based on the chiral effective field theory (EFT) is giving [288–293]

$$d_n = -(2.7\pm1.2)\times10^{-16}\bar{\theta}\,e\,{\rm cm}, \tag{58}$$

$$d_p = (2.1\pm1.2)\times10^{-16}\bar{\theta}\,e\,{\rm cm}. \tag{59}$$

From the experimental data [24,30]

$$d_n < 3.0\times10^{-26}e\,{\rm cm}, \tag{60}$$

we therefore have

$$\bar{\theta} < 10^{-10}, \tag{61}$$

which is a too strong constraint to the θ-term, which should naturally be of the same order of magnitude as the CP-even QCD Lagrangian. This problem is known as the *Strong CP Problem*. This problem is also accentuated in the context of new sources of CP violation of BSM. A large θ-term is also generated in many models of new physics such as SUSY models [36,105,106,110], and this gives rise to a serious fine-tuning problem, as their effects must cancel to fulfill the constraint (61). If we want to extend the SM to a theory with large source of CP violation, a mechanism which makes the θ-term irrelevant to observables are at least mandatory.

A natural solution to the strong CP problem was proposed by Peccei and Quinn [294]. Their mechanism forces the θ-term to have a zero expectation value by adding a new scalar field, the *axion*. The newly introduced Lagrangian of the axion is

$$\mathcal{L}_a = \frac{1}{2}\partial_\mu a\partial^\mu a + \frac{a(x)}{f_a}\frac{\alpha_s}{8\pi}G^a_{\mu\nu}\tilde{G}^{\mu\nu,a}, \tag{62}$$

where the axion field a has replaced the parameter $\bar{\theta}$ of the strong CP Lagrangian.

The effective potential of the axion will then become

$$\mathcal{L}_a^{eff} = \frac{1}{2}\partial_\mu a\partial^\mu a - K_1\left(\frac{a}{f_a}+\bar{\theta}\right) - \frac{1}{2}K\left(\frac{a}{f_a}+\bar{\theta}\right)^2 + \cdots, \tag{63}$$

where $K = -m_*\langle 0|\bar{q}q|0\rangle + O(m_*^2)$ is the topological susceptibility with

$$m_* \equiv \frac{m_u m_d m_s}{m_u m_d + m_u m_s + m_d m_s} \approx \frac{m_u m_d}{m_u + m_d}\,, \tag{64}$$

and K_1 is the correlation between the topological charge and the isoscalar CP-odd operators with high mass dimensions. The decay constant f_a is given by the spontaneous breaking of a chiral $U(1)_{\rm PQ}$ symmetry of BSM. Here the vacuum expectation value of the axion becomes the θ-term $\langle a\rangle/f_a = -\bar{\theta}$. If there are no other CP-odd operators than the θ-term, this value is zero, which means that the θ-term is dynamically canceled. This mechanism of Peccei and Quinn is the most attracting scenario to naturally resolve the strong CP problem.

In the presence of flavor $SU(3)$ singlet CP-odd operators other than the θ-term, the vacuum expectation value of the axion is not canceled, and becomes $\bar{\theta} = \bar{\theta}_{\rm ind} \equiv -K_1(O_{CP})/K$ [295]. It is controlled by the coefficient K_1, which is expressed as [296,297]

$$K_1(O_{CP}) = -i\lim_{k\to 0}\int {\rm d}^4x e^{ikx} \times\langle 0|T\left\{\frac{\alpha_s}{8\pi}G^a_{\mu\nu}\tilde{G}^{\mu\nu,a}(x)O_{CP}(0)\right\}|0\rangle. \tag{65}$$

In this review, the relevant ones are the quark chromo-EDM $\mathcal{L}_{\rm cEDM} = -\frac{i}{2}d_q^c\bar{q}g_s\sigma^{\mu\nu}G^a_{\mu\nu}t_a\gamma_5 q$ and the left-right four-quark operator $\mathcal{L}_{LR} = C_{LR}\sum_{q,q'=u,d}\bar{q}q\,\bar{q}'i\gamma_5\tau_z q'$. The coefficient of the CP-odd four-quark operator is given by $C_{LR} = C_1^u = C_1^d = -C_4^{ud} = -C_4^{du}$ (the corresponding operators are defined in eqs. (24) and (26)). In the case of the quark chromo-EDM, the evaluation of the correlator gives [296,297]

$$K_1(\mathcal{L}_{\rm cEDM}) = \frac{m_*}{2}\sum_{q=u,d,s}\frac{d_q^c}{m_q}\langle 0|\bar{q}g_s\sigma^{\mu\nu}G^a_{\mu\nu}t_a q|0\rangle, \tag{66}$$

where $m_0^2 \equiv -\frac{\langle 0|g_s\bar{q}\sigma_{\mu\nu}t_aG_a^{\mu\nu}q|0\rangle}{\langle 0|\bar{q}q|0\rangle} = (0.8\pm 0.1)\,{\rm GeV}^2$ [298, 299]. The induced θ-term is then

$$\bar{\theta}_{\rm ind}(\mathcal{L}_{\rm cEDM}) = -\frac{m_0^2}{2}\sum_{q=u,d,s}\frac{d_q^c}{m_q}\,. \tag{67}$$

For the left-right four-quark operator, the induced θ-term is given by [214,300]

$$\bar{\theta}_{\rm ind}(\mathcal{L}_{LR}) \approx -C_{LR}\frac{f_\pi^2 m_\pi^2}{m_u m_d}\,, \tag{68}$$

where the vacuum saturation approximation $\langle 0|\bar{q}q\bar{q}'i\gamma_5\tau_z q'|\pi^0\rangle \approx \langle 0|\bar{q}q|0\rangle\langle 0|\bar{q}'i\gamma_5\tau_z q'|\pi^0\rangle$ was used. From the large N_c analysis, the correction to this formula is $O(1/N_c)$.

The Weinberg operator is also a flavor $SU(3)$ singlet, but the induced θ-term is suppressed by a factor of light quark mass, so it becomes negligible for the case of interest.

3 Hadron level effective P,CP-odd interactions

The atomic EDM receives contribution from the hadron level CP violation. The effective hadronic CP-odd interaction is generated by quark and gluon level CP-odd processes, but the calculation of their relations is a highly nontrivial task due to the non-perturbative nature of QCD. Here we summarize the current situation of the derivation of the hadron level CP violation from the QCD level physics.

3.1 Hadron level effective interaction at the hadronic scale

After obtaining the QCD level operators and their Wilson coefficients at the hadronic scale, we must now match them to the hadron level effective interactions. The P,CP-odd hadronic interaction we consider is

$$\mathcal{L}_{\rm hadron} = \mathcal{L}_{eN} + \mathcal{L}_{\rm NEDM} + \mathcal{L}_{\pi NN}, \tag{69}$$

with

– The P,CP-odd e-N interaction

$$\mathcal{L}_{eN} = -\frac{G_F}{\sqrt{2}}\sum_{N=p,n}\left[C_N^{\rm SP}\bar{N}N\,\bar{e}i\gamma_5 e + C_N^{\rm PS}\bar{N}i\gamma_5 N\,\bar{e}e + \frac{1}{2}C_N^{\rm T}\epsilon^{\mu\nu\rho\sigma}\bar{N}\sigma_{\mu\nu}N\,\bar{e}\sigma_{\rho\sigma}e\right]. \tag{70}$$

– The nucleon EDM

$$\mathcal{L}_{\rm NEDM} = -\frac{i}{2}\sum_{N=p,n}d_N\bar{N}\sigma_{\mu\nu}\gamma_5 N F^{\mu\nu}, \tag{71}$$

– The P,CP-odd pion-nucleon (π-N-N) interaction [301, 302]

$$\mathcal{L}_{\pi NN} = \sum_{N=p,n}\left[\sum_{a=1}^{3}\bar{g}^{(0)}_{\pi NN}\bar{N}\tau^a N\pi^a + \bar{g}^{(1)}_{\pi NN}\bar{N}N\pi^0 + \sum_{a=1}^{3}\bar{g}^{(2)}_{\pi NN}(\bar{N}\tau^a N\pi^a - 3\bar{N}\tau^3 N\pi^0)\right], \tag{72}$$

where a denotes the isospin index.

The schematic dependences of the hadronic scale operators on the quark level operators are shown in fig. 1. In this subsection, we review the currently available results of the calculation of the hadronic effective CP violation.

We can also extend eq. (69) by adding several interactions with low chiral indices. For example we have the three-pion interaction [289]

$$\mathcal{L}_{3\pi} = m_N\Delta_{3\pi}\,\pi^z\sum_{a=1}^{3}\pi_a^2, \tag{73}$$

the CP-odd η-nucleon interaction [303, 304]

$$\mathcal{L}_{\eta NN} = \sum_{N=p,n} \left[\bar{g}^{(0)}_{\eta NN} \bar{N} N \eta + \bar{g}^{(1)}_{\eta NN} \bar{N} \tau^z N \eta \right]. \quad (74)$$

and the isoscalar CP-odd contact interaction

$$\mathcal{L}_{\rm C} = \bar{C}_1 \bar{N} N \partial_\mu (\bar{N} S^\mu N) + \sum_{a=1}^{3} \bar{C}_2 \bar{N} \tau_a N \cdot \partial_\mu (\bar{N} S^\mu \tau_a N). \quad (75)$$

It is important to note that the above interactions give the leading contribution in the power counting of the chiral EFT for several dimension-six CP-odd interactions [305]. For example, the three-pion interaction in eq. (73) receives the leading contribution from the isovector quark chromo-EDM or the left-right four-quark interaction in eq. (17). It is known to give a sizable next-to-leading–order correction to the isovector CP-odd pion-nucleon interaction coupling $\bar{g}^{(1)}_{\pi NN}$, so can be used to estimate the theoretical uncertainty. Regarding the CP-odd contact interaction in eq. (75), it receives the leading contribution from the Weinberg operator or some CP-odd four-quark interactions. Its effect is however of short range, and we can expect it to be subleading at the nuclear level, since the nuclear EDM is a low-energy phenomena dominated by the pion exchange physics. This fact is suggested by the *ab initio* analyses of the EDM of light nuclei, which have smaller sensitivities on the heavy meson exchange CP-odd nuclear forces than those with the pion exchanges [306–311].

3.2 CP-odd e-N interaction

The CP-odd e-N interaction (70) is a CP-violating effect which can specifically be probed with the atomic EDM. It is related to the CP-odd e-q interaction (6) and the CP-odd e-g interaction (52) by several nucleon matrix elements, as

$$-\frac{G_F}{\sqrt{2}} C_N^{\rm SP} \bar{N} N \, \bar{e} i\gamma_5 e = C_q^{\rm SP} \langle N|\bar{q}q|N\rangle \, \bar{e} i\gamma_5 e + C_{eg}^{\rm SP} \langle N|G^a_{\mu\nu} G_a^{\mu\nu}|N\rangle \, \bar{e} i\gamma_5 e, \quad (76)$$

$$-\frac{G_F}{\sqrt{2}} C_N^{\rm PS} \bar{N} i\gamma_5 N \, \bar{e} e = C_q^{\rm PS} \langle N|\bar{q} i\gamma_5 q|N\rangle \, \bar{e} e + C_{eg}^{\rm PS} \langle N|G^a_{\mu\nu} \tilde{G}_a^{\mu\nu}|N\rangle \, \bar{e} e, \quad (77)$$

$$-\frac{G_F}{\sqrt{2}} C_N^{\rm T} \frac{1}{2} \epsilon^{\mu\nu\rho\sigma} \bar{N} \sigma_{\mu\nu} N \, \bar{e} \sigma_{\rho\sigma} e = \frac{1}{2} C_q^{\rm T} \epsilon^{\mu\nu\rho\sigma} \times \langle N|\bar{q}\sigma_{\mu\nu} q|N\rangle \, \bar{e} \sigma_{\rho\sigma} e. \quad (78)$$

To calculate the nucleon matrix elements, evaluations of nonperturbative effects of QCD are required. Here it is an excellent opportunity to use the results of the lattice QCD, which has recently made significant progress [312, 313].

To determine the S-PS CP-odd e-N interaction (76), the nucleon scalar density matrix elements $\langle N|\bar{q}q|N\rangle$ and $\langle N|G^a_{\mu\nu} G_a^{\mu\nu}|N\rangle$ are required. To obtain the light quark contribution, we combine the isoscalar and isovector nucleon scalar densities. The isoscalar one can be derived

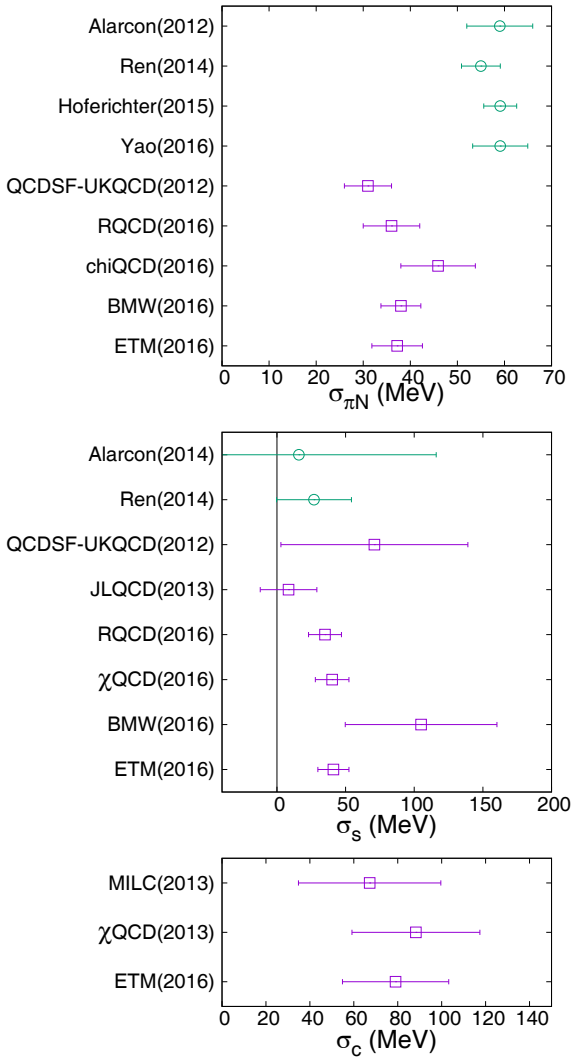

Fig. 5. Comparison of the results of several calculations of the nucleon sigma term ($\sigma_{\pi N}$) [319, 321–323, 330–334], the strange content of nucleon (σ_s) [321, 330–334, 354, 362] and the charm content of nucleon (σ_c) [333, 360, 361].

from the nucleon sigma term $\sigma_{\pi N} \equiv \frac{m_u+m_d}{2} \langle N|\bar{u}u + \bar{d}d|N\rangle$, which has extensively been discussed in phenomenology [314–323] and in lattice QCD [324–334] (see fig. 5). The result is

$$\sigma_{\pi N} = (30\text{–}60)\,\text{MeV}. \quad (79)$$

The phenomenological extractions are centered to 60 MeV, whereas the results of lattice QCD calculations are showing values around 40 MeV. We consider this deviation as a systematic error. By using the Particle data group value of up and down quark masses renormalized at $\mu = 2\,\text{GeV}$ $m_u = 2.2^{+0.6}_{-0.4}\,\text{MeV}$ and $m_d = 4.7^{+0.5}_{-0.4}\,\text{MeV}$ [266], the isoscalar nucleon scalar density is then

$$\langle N|\bar{u}u + \bar{d}d|N\rangle \sim 15 \quad (\mu = 2\,\text{GeV}), \quad (80)$$

with a theoretical uncertainty of about 30%.

The isovector nucleon scalar density can be derived in the leading order of the current quark masses in terms of the proton-neutron mass splitting $\Delta m_N^{(0)}$ as [177,197,335–338]

$$\langle p|\bar{u}u - \bar{d}d|p\rangle = \frac{\Delta m_N^{(0)}}{m_d - m_u} = 0.9 \quad (\mu = 2\,\mathrm{GeV}), \tag{81}$$

with a theoretical uncertainty of about 30%. Here $\Delta m_N^{(0)} = 2.33 \pm 0.11\,\mathrm{MeV}$ is the nucleon mass splitting without electromagnetic effects [266,339,340]. The isovector nucleon scalar density has also been studied on lattice, and consistent results with the above phenomenological value are given [341–348].

By combining eqs. (80) and (81), we obtain

$$\langle p|\bar{u}u|p\rangle = \langle n|\bar{d}d|n\rangle \sim 8, \tag{82}$$
$$\langle p|\bar{d}d|p\rangle = \langle n|\bar{u}u|n\rangle \sim 7, \tag{83}$$

at $\mu = 2\,\mathrm{GeV}$, with a theoretical uncertainty of 30%. It is important to note that this error bar is mainly due to the uncertainty of the current quark mass and to that of the determination of the nucleon sigma term. The nucleon scalar densities due to light quarks are substantially enhanced compared with the prediction of the non-relativistic quark model ($\langle p|\bar{u}u|p\rangle = 2$, $\langle p|\bar{d}d|p\rangle = 1$). This enhancement is understood by the dynamical gluon dressing effect [349–352].

For the strange and charm contents of the nucleon $\sigma_s \equiv m_s\langle N|\bar{s}s|N\rangle$ and $\sigma_c \equiv m_c\langle N|\bar{c}c|N\rangle$, there are also available data from lattice QCD calculations [325–334, 353–361] (see fig. 5). Their averaged values at the renormalization point $\mu = 2\,\mathrm{GeV}$ are

$$\langle N|\bar{s}s|N\rangle \sim 0.4, \tag{84}$$
$$\langle N|\bar{c}c|N\rangle \sim 0.07. \tag{85}$$

Here we have used $m_s = 96^{+8}_{-4}\,\mathrm{MeV}$ for the current strange quark mass [266]. For the charm quark mass, we have adopted $m_c = 1.17\,\mathrm{GeV}$, which is obtained by running $m_c = 1.27\,\mathrm{GeV}$ from the renormalization point $\mu = m_c = 1.27\,\mathrm{GeV}$ [266] to $\mu = 2\,\mathrm{GeV}$. The theoretical uncertainty is not less than 100% for the strange content. The results of phenomenological analyses have a large error bar and cannot be used in the determination of the strange content of nucleon [321,362]. Lattice QCD results also seem to have a systematic error, as some values are not consistent (see fig. 5). This situation may be improved in the future by refining lattice QCD analyses. We may also expect improvement from a new experimental approach which can constrain the strange content of nucleon through the measurement of ϕ mesons in nuclear medium [363–365].

For the charm content the uncertainty of lattice QCD data is about 30%. It agrees with the heavy quark expansion formula [350,351,366–369]

$$\langle N|\bar{c}c|N\rangle = -\frac{\alpha_s(\mu = 2\,\mathrm{GeV})}{12\pi m_c}\langle N|G^a_{\mu\nu}G^{\mu\nu}_a|N\rangle + O(1/m_c^2) \approx 0.054. \tag{86}$$

To obtain the gluonic content of the nucleon, we use the two-loop level trace anomaly formula of the nucleon mass:

$$\begin{aligned} m_N &= \frac{\beta_{\mathrm{QCD}}}{2g_s}\langle N|G^a_{\mu\nu}G^{\mu\nu}_a|N\rangle + \sum_q m_q\langle N|\bar{q}q|N\rangle \\ &\approx \frac{\alpha_s(\mu)}{8\pi}\left[\beta_0 + \beta_1\frac{\alpha_s(\mu)}{4\pi}\right]\langle N|G^a_{\mu\nu}G^{\mu\nu}_a|N\rangle \\ &\quad + 2\sigma_{\pi N} + \sigma_s + \sigma_c, \end{aligned} \tag{87}$$

with $\beta_0 = \frac{25}{3}$ and $\beta_1 = \frac{154}{3}$ ($n_f = 4$ at $\mu = 2\,\mathrm{GeV}$). By subtracting the quark contents of nucleon in eqs. (79), (84), and (85), it yields

$$\langle N|G^a_{\mu\nu}G^{\mu\nu}_a|N\rangle \approx (-6000 \pm 450)\,\mathrm{MeV}, \tag{88}$$

where we have used $\alpha_s(\mu = 2\,\mathrm{GeV}) = 0.30$ (from two-loop level renormalization group equation). Here the error bar is only due to the nucleon scalar densities, and amounts to about 8%. The error of the perturbative expansion of eq. (87) can be estimated by evaluating the three-loop level correction. The relative error is given by the ratio between the one-loop level and three-loop level term $\frac{\alpha_s^2\beta_2}{(4\pi)^2\beta_0} = 3\%$, where $\beta_2 = \frac{1}{2}[2857 - \frac{20132}{9} + \frac{5200}{27}]$ ($n_f = 4$, $\alpha_s(\mu = 2\,\mathrm{GeV}) = 0.3$). Here the most important source of theoretical uncertainty of $\langle N|G^a_{\mu\nu}G^{\mu\nu}_a|N\rangle$ is the error bars of the strange and charm contents of nucleon. To improve the accuracy of the S-PS–type CP-odd e-N interaction, continuous efforts in lattice QCD calculations are required. We also have to remark that the contributions from the light and charm quarks are determined within 30%, and quantitative discussions are becoming possible.

To know the coupling of the PS-S–type CP-odd e-N interaction (77), values of pseudoscalar nucleon matrix elements are required. Let us first evaluate the gluonic pseudoscalar nucleon matrix element $\langle N|G^a_{\mu\nu}\tilde{G}^{\mu\nu}_a|N\rangle$. It can phenomenologically be calculated as [370–372]

$$\begin{aligned} -\frac{\alpha_s}{8\pi}\langle N|G^a_{\mu\nu}\tilde{G}^{\mu\nu}_a|N\rangle &= m_N\left[\sum_q \frac{m_*}{m_q}\Delta q\right] + m_*\eta \\ &\approx -400\,\mathrm{GeV}, \end{aligned} \tag{89}$$

where the nucleon axial charges are given by $\Delta u = [0.82, 0.85]$, $\Delta d = [-0.45, -0.42]$ and $\Delta s = [-0.11, -0.08]$ (renormalized at $\sqrt{3}\,\mathrm{GeV}$) [373]. The results of lattice QCD analyses for Δs is smaller than the experimental value [355, 374]. Here η is the deviation of the relation $\sum_q\langle p|\bar{q}i\gamma_5 q|p\rangle = 0$ which is valid in the large N_c limit, and it should be considered as an $O(N_c^{-1})$ systematic error, which is negligible in this derivation [370, 372]. The largest theoretical uncertainty to $\frac{\alpha_s}{8\pi}\langle N|G^a_{\mu\nu}\tilde{G}^{\mu\nu}_a|N\rangle$ comes from the current quark mass of u and d quarks and the total error bar may not be less than 30%.

By using the anomalous Ward identity

$$m_N\Delta q = m_q\langle p|\bar{q}i\gamma_5 q|p\rangle - \frac{\alpha_s(\mu)}{8\pi}\langle N|G^a_{\mu\nu}\tilde{G}^{\mu\nu}_a|N\rangle, \tag{90}$$

the quark pseudoscalar contents of nucleon can be calculated phenomenologically as [181, 197, 338, 370–372, 375, 376]

$$\langle p|\bar{u}i\gamma_5 u|p\rangle = 180, \tag{91}$$
$$\langle p|\bar{d}i\gamma_5 d|p\rangle = -170, \tag{92}$$
$$\langle p|\bar{s}i\gamma_5 s|p\rangle = -5.1, \tag{93}$$
$$\langle p|\bar{c}i\gamma_5 c|p\rangle = -0.34. \tag{94}$$

For the charm quark contribution, we have neglected Δc and used $m_c(\mu = 2\,\mathrm{GeV}) = 1170\,\mathrm{MeV}$. We remark that the pseudoscalar nucleon matrix elements for light quarks are large. This is due to the pion pole effect [352]. This enhancement has an important impact in the evaluation of the atomic EDM, because it can counterbalance the non-relativistic suppression of the effect of PS-S CP-odd e-N interaction in eq. (77). The nucleon pseudoscalar density $\langle p|\bar{q}i\gamma_5 q|p\rangle$ receives the dominant contribution from the gluonic matrix element $\frac{\alpha_s}{8\pi}\langle N|G^a_{\mu\nu}\tilde{G}^{\mu\nu}_a|N\rangle$. The main source of its theoretical uncertainty, therefore, comes from the current quark masses. Since we do not know the higher-order correction in the chiral expansion reliably, we can conservatively estimate the total uncertainty to $\langle p|\bar{q}i\gamma_5 q|p\rangle$ is about 50%.

The T-PT CP-odd e-N couplings are given in terms of the nucleon tensor charge δq as

$$-C_p^{\mathrm{T}} = \delta u\, C_{eu}^{\mathrm{T}} + \delta d\, C_{ed}^{\mathrm{T}} \sum_{q=s(,c)} \delta q\, C_{eq}^{\mathrm{T}}, \tag{95}$$
$$-C_n^{\mathrm{T}} = \delta d\, C_{eu}^{\mathrm{T}} + \delta u\, C_{ed}^{\mathrm{T}} + \sum_{q=s(,c)} \delta q\, C_{eq}^{\mathrm{T}}, \tag{96}$$

where we have assumed the isospin symmetry and the proton tensor charge δq are defined by

$$\langle p(k,s)|\bar{q}i\sigma_{\mu\nu}\gamma_5 q|p(k,s)\rangle = 2(s_\mu k_\nu - s_\nu k_\mu)\delta q, \tag{97}$$

with s and k the 4-vector polarization and momentum of the proton, respectively. The nucleon tensor charge is the transversely polarized quark contribution to the nucleon polarization, where the nucleon is transversely polarized against its momentum k. Currently, lattice QCD is giving the most accurate data, and the results are [341–348, 355, 377–380]

$$\delta u \approx 0.8, \tag{98}$$
$$\delta d \approx -0.2, \tag{99}$$
$$|\delta s| < 0.02, \tag{100}$$

at the renormalization point $\mu = 2\,\mathrm{GeV}$, with theoretical uncertainties of roughly 10% for the up and down quark contributions. For δs, these are currently the only results consistent with zero at the physical point [378, 379]. In the literature, the non-relativistic quark model predictions $\delta u = \frac{4}{3}$ and $\delta d = -\frac{1}{3}$ were often quoted. The suppression of the nucleon tensor charges in eqs. (98) and (99) from the non-relativistic quark model prediction is partially understood by the gluon dressing effect, which superposes spin flipped states of spin 1/2 quarks due to the emission and absorption of spin 1 gluons, as suggested by the Schwinger-Dyson analyses [381, 382]. The nucleon tensor charges can also be extracted from the experimental data, but the analysis may have sizable systematics due to the functional form used in the analysis [383–388].

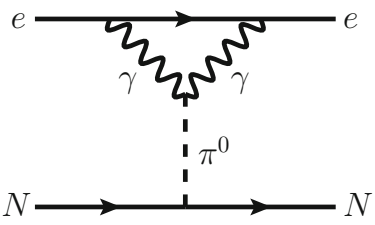

Fig. 6. SM contribution to the CP-odd e-N interaction.

Let us also discuss the SM contribution to the CP-odd e-N interaction, generated by the CKM matrix elements. The leading contribution is given by the S-PS–type interaction C_N^{SP} (see fig. 6) [61, 252]. We estimate this effect as

$$C_N^{\mathrm{SP}} \sim \bar{g}^{(1)}_{\pi NN,\mathrm{SM}} \frac{3\alpha_{\mathrm{em}}^2 m_e}{2\pi^2 f_\pi} \frac{\sqrt{2}}{m_\pi^2 G_F} \ln\frac{m_\pi}{m_e} = O(10^{-17}), \tag{101}$$

where we have estimated the effective $\pi^0\bar{e}i\gamma_5 e$ vertex by solving the one-loop level renormalization group equation with the non-renormalizable Wess-Zumino-Witten term $\frac{\pi^0}{4\pi f_\pi}F_{\mu\nu}\tilde{F}^{\mu\nu}$ [389]. The CP-odd π-N-N coupling in SM $\bar{g}^{(1)}_{\pi NN,\mathrm{SM}} = O(10^{-17})$ which was given in the factorization approach with the $|\Delta S| = 1$ four-quark interaction calculated obtained from the two-loop level renormailzation group evolution (see also the end of sect. 3.3) [269]. The CP-odd e-N interaction generated by the exchange of the Higgs boson in the SM is negligibly small [390]. In the SM, the PS-S and T-PT CP-odd e-N interactions are generated at higher order than for the S-PS one, so we neglect them.

3.3 The CP-odd π-N-N interaction

Now let us present the calculation of the hadron level CP violation. The most important CP-odd interaction is the CP-odd π-N-N interaction, which is the base of hadronic effective CP-odd interaction.

Let us first see the θ-term contribution to the CP-odd π-N-N interaction in eq. (72). Using the partially conserved axial current relation (PCAC), the isoscalar CP-odd π-N-N coupling is given as

$$\bar{g}^{(0)}_{\pi NN} \approx \frac{\bar{\theta} m_*}{f_\pi}\langle N|\bar{u}u - \bar{d}d|N\rangle, \tag{102}$$

where m_* is defined in eq. (64). A more refined calculation in chiral EFT yields [292]

$$\bar{g}^{(0)}_{\pi NN} = (15.5 \pm 2.5) \times 10^{-3}\bar{\theta}. \tag{103}$$

The θ-term contribution to the isovector coupling was also estimated in ref. [391], as

$$\bar{g}^{(1)}_{\pi NN} = -(3.4 \pm 2.4) \times 10^{-3} \bar{\theta}. \tag{104}$$

The large error bar is due to the uncertainty of the low-energy constants as well as higher-order corrections. It can be noted that the $\bar{\theta}$ contribution to the CP-odd π-N-N couplings is important even in the case when the Peccei-Quinn mechanism is active, since the quark chromo-EDM induces $\bar{\theta}_{\rm ind}$ (see eq. (67)).

Let us now see the contribution of the quark chromo-EDM to the CP-odd π-N-N couplings. The chromo-EDM contributes to the CP-odd π-N-N interaction through two leading processes. The first one is the short distance contribution, which can be obtained by applying the PCAC relation to the π-N-N matrix element

$$\langle B_a \pi^c | \mathcal{L}_{\rm cEDM} | B_b \rangle \approx \frac{d^c_q}{f_\pi} \langle B_a | \bar{q} g_s \sigma_{\mu\nu} G^{\mu\nu}_a t_a T_c q | B_b \rangle. \tag{105}$$

The nucleon matrix element in the right-hand side of the above equation cannot be reduced further, and we have to quote the result of calculations using phenomenological models. Here we use the result of QCD sum rules [36,392, 393]:

$$D_u \equiv \langle p | \bar{u} g_s \sigma_{\mu\nu} G^{\mu\nu}_a t_a u | p \rangle = -0.26\,{\rm GeV}^2, \tag{106}$$
$$D_d \equiv \langle p | \bar{d} g_s \sigma_{\mu\nu} G^{\mu\nu}_a t_a d | p \rangle = -0.17\,{\rm GeV}^2, \tag{107}$$

at the renormalization point $\mu = 1\,{\rm GeV}$. These matrix elements have an uncontrolled systematic uncertainty which is certainly not less than $O(100\%)$.

The quark chromo-EDM also contributes to the CP-odd π-N-N interaction through the pion pole [394]. Combining the second-order term of the chiral Lagrangian with the pion tadpole generated by the chromo-EDM, we have

$$\begin{aligned}\bar{g}^{(0)}_{\pi NN} \approx & -\frac{D_u - D_d}{4 f_\pi}(d^c_u + d^c_d) \\ & - \frac{m_*}{2 f_\pi} \langle p | \bar{u} u - \bar{d} d | p \rangle \left[2\bar{\theta} + \frac{m_0^2}{2} \left(\frac{m_u - m_d}{m_u m_d}(d^c_u - d^c_d) \right.\right. \\ & \left.\left. + \frac{d^c_u + d^c_d - 2 d^c_s}{m_s} \right) \right], \end{aligned} \tag{108}$$

$$\bar{g}^{(1)}_{\pi NN} \approx -\frac{d^c_u - d^c_d}{4 f_\pi} \left[D_u + D_d + m_* \langle p | \bar{u} u + \bar{d} d | p \rangle m_0^2 \right], \tag{109}$$

where $m_* \equiv \frac{m_u m_d m_s}{m_u m_d + m_d m_s + m_u m_s}$. Here we have also written the θ-term contribution to take into account the induced θ-term for the case where the Peccei-Quinn mechanism is active [294]. By substituting the induced θ-term in eq. (67), the isoscalar CP-odd π-N-N coupling becomes

$$\bar{g}^{(0)}_{\pi NN,{\rm PQ}} \approx -\frac{d^c_u + d^c_d}{4 f_\pi} \left[D_u - D_d + m_* \langle p | \bar{u} u - \bar{d} d | p \rangle m_0^2 \right]. \tag{110}$$

The total quark chromo-EDM contribution to $\bar{g}^{(0)}_{\pi NN,{\rm PQ}}$ and $\bar{g}^{(1)}_{\pi NN}$ is then [36, 392]

$$\bar{g}^{(0)}_{\pi NN,{\rm PQ}}(d^c_q) = \tilde{\omega}^{(0)}_{\rm PQ} \frac{d^c_u + d^c_d}{10^{-26}\,{\rm cm}}, \tag{111}$$
$$\bar{g}^{(1)}_{\pi NN}(d^c_q) = \tilde{\omega}^{(1)} \frac{d^c_u - d^c_d}{10^{-26}\,{\rm cm}}, \tag{112}$$

with

$$\tilde{\omega}^{(0)}_{\rm PQ} = -6.9 \times 10^{-13} \times \frac{|\langle 0 | \bar{q} q | 0 \rangle|}{(265\,{\rm MeV})^3} \frac{|m_0^2|}{0.8\,{\rm GeV}^2}, \tag{113}$$
$$\tilde{\omega}^{(1)} = -1.0 \times 10^{-11} \times \frac{|\langle 0 | \bar{q} q | 0 \rangle|}{(265\,{\rm MeV})^3} \frac{|m_0^2|}{0.8\,{\rm GeV}^2}. \tag{114}$$

Here the coefficient of the isovector component of the quark chromo-EDM is enhanced, due to the large value of the isoscalar nucleon scalar density $\langle p | \bar{u} u + \bar{d} d | p \rangle$ ($\sim O(10)$ at $\mu = 2\,{\rm GeV}$) (see eq. (80)). It is also important to note that the dominant contribution comes from the pion pole effect (or the vacuum alignment). The short distance effect, due to the matrix elements $\langle N | \bar{q} g_s \sigma_{\mu\nu} G^{\mu\nu}_a t_a q | N \rangle$, is less than 20% for $\bar{g}^{(0)}_{\pi NN,{\rm PQ}}$, and less than 10% for $\bar{g}^{(1)}_{\pi NN}$. From this fact, we can estimate the theoretical uncertainty of the quark chromo-EDM contribution to the CP-odd π-N-N interaction. The pion pole effect depends on the light quark mass, scalar densities and the mixed condensate m_0^2, which have all sizable error bars. The largest should be the light quark masses, which is about $O(30\%)$. We also have keep in mind that the above analysis was performed at the leading order of the chiral expansion. There are also substantial uncertainties due to the unknown higher-order contributions, which are expected to be quantifiable in the next-to-leading–order analysis [292, 395]. Being optimistic, the error bars of the coefficients given by eqs. (113) and (114) are expected to be about 50%.

The last important contribution to the CP-odd π-N-N interaction to be investigated is the P,CP-odd 4-quark interactions. Here let us see the effect of the left-right four-quark interaction

$$\begin{aligned}\mathcal{L}'_{LR} = & C'_{LR1} \bar{d} \gamma^\mu P_L u \bar{u} \gamma^\mu P_R d + C'_{LR2} \bar{d}_\alpha \gamma^\mu P_L u_\beta \bar{u}_\beta \gamma^\mu P_R d_\alpha \\ & + {\rm h.c.}, \end{aligned} \tag{115}$$

which gives the leading contribution to the isovector π-N-N interaction ($\bar{g}^{(1)}_{\pi NN}$). Here we use the operator basis of ref. [396], where it is pointed that the isovector CP-odd pion-nucleon coupling is generated by the vacuum alignment effect (pion pole effect). We have

$$\begin{aligned}\bar{g}^{(1)}_{\pi NN} \approx & -{\rm Im}(C'_{LR1}) \times 0.63\,{\rm GeV}^2 \\ & - {\rm Im}(C'_{LR2}) \times 2.9\,{\rm GeV}^2, \end{aligned} \tag{116}$$

where the renormalization scale is set to $\mu = 3\,{\rm GeV}$. Here we note that the direct contribution to the CP-odd pion-nucleon vertex, which is given by the short distance physics, is not considered.

The direct contribution is not easy to evaluate, and we have to use model calculations which will give us the theoretical uncertainty. In the estimation of the direct contribution of the CP-odd four-quark interaction, the vacuum

saturation approximation is often used [300,397–400]. The contribution of the left-right four-quark interaction (see eq. (17)) to the isovector CP-odd π-N-N coupling can be calculated as

$$\begin{aligned}\bar{g}^{(1)}_{\pi NN} &= \langle \pi^0 N|\mathcal{L}'_{LR}|N\rangle \\ &\approx \left[\frac{1}{3}\,\mathrm{Im}(C'_{LR1}) + \frac{1}{2}\,\mathrm{Im}(C'_{LR2})\right] \\ &\quad\times\langle \pi^0 N|\bar{q}i\gamma_5\tau_z q\,(\bar{u}u+\bar{d}d)|N\rangle \\ &\approx \left[\frac{1}{3}\,\mathrm{Im}(C'_{LR1}) + \frac{1}{2}\,\mathrm{Im}(C'_{LR2})\right] \\ &\quad\times\langle \pi^0|\bar{q}i\gamma_5\tau_z q|0\rangle\langle N|\bar{u}u+\bar{d}d|N\rangle \\ &= -\left[\frac{2}{3}\,\mathrm{Im}(C'_{LR1}) + \mathrm{Im}(C'_{LR2})\right] \\ &\quad\times\frac{\langle 0|\bar{q}q|0\rangle}{f_\pi}\langle N|\bar{u}u+\bar{d}d|N\rangle \\ &= \mathrm{Im}(C'_{LR1})\times 4\,\mathrm{GeV}^2 \\ &\quad + \mathrm{Im}(C'_{LR2})\times 5\,\mathrm{GeV}^2, \end{aligned} \tag{117}$$

where we have used the PCAC assertion in the fourth equality, and $\langle 0|\bar{q}q|0\rangle \approx -\frac{m_\pi^2 f_\pi^2}{m_u+m_d}$. Here it is important to remark that the direct contribution is enhanced by the scalar density of the light quarks $\langle N|\bar{u}u+\bar{d}d|N\rangle \sim O(10)$, and is as large as that of the pion pole (116). The renormalization scale of $\langle 0|\bar{q}q|0\rangle$ and $\langle N|\bar{q}q|N\rangle$ is taken as $\mu = 3\,\mathrm{GeV}$. This feature is suggested by the model analysis where the scalar density is enhanced by the constructive interference due to dynamical gluon emissions and absorptions [352]. In the large N_c analysis, the error bar of the direct contribution is estimated as $O(100\%)$ due to the presence of baryons. In addition to the model dependence, higher-order correction due to the three-pion interaction (73), which is known to contribute to $\bar{g}^{(1)}_{\pi NN}$, may also be sizable [215, 292, 395]. We therefore conclude that the theoretical uncertainty of the left-right four-quark interaction to $\bar{g}^{(1)}_{\pi NN}$ is $O(100\%)$. For the strange quark contribution, the systematics due to the direct contribution is smaller, due to the small value of $\langle N|\bar{s}s|N\rangle \sim O(0.1)$ (see eq. (84) and discussion below it), and the pion pole contribution is the dominant process.

We have to note that the contribution of the Weinberg operator to the CP-odd π-N-N interaction (72) is suppressed by at least a factor of light quark, due to its chiral-symmetry–breaking nature.

The SM contribution generated by the CP phase of the CKM matrix can be estimated by using the factorization of $|\Delta S| = 1$ four-quark operators. By combining the hyperon-nucleon transition and the $|\Delta S| = 1$ meson-baryon interaction, we can calculate $\bar{g}^{(0)}_{\pi NN}$ and $\bar{g}^{(1)}_{\pi NN}$. The result is of the order of $\bar{g}^{(0)}_{\pi NN,\mathrm{SM}} \sim \bar{g}^{(1)}_{\pi NN,\mathrm{SM}} \sim 10^{-17}$ [7,269,401–404]. This estimation also involves a theoretical uncertainty of $O(100\%)$, due to the gluonic correction in the $1/N_c$ expansion.

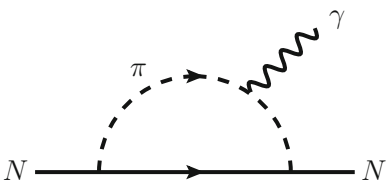

Fig. 7. Diagrammatic representation of the meson-loop contribution to the nucleon EDM. The solid line represents a baryon, the dashed line a light pseudoscalar meson, and the wavy line a photon.

3.4 The nucleon EDM

The nucleon EDM receives the leading-order contribution from the quark EDM, the quark chromo-EDM, and the Weinberg operator, without suppression by the light quark mass[2]:

$$d_N = d_N(d_q) + d_N(d_q^c) + d_N(w), \tag{118}$$

where $N = p, n$. The quark EDM contribution to the nucleon EDM $d_N(d_q)$ is simply given by the proton tensor charges (97), as

$$d_p(d_q) = \delta u\, d_u + \delta d\, d_d + \delta s\, d_s, \tag{119}$$

$$d_n(d_q) = \delta d\, d_u + \delta u\, d_d + \delta s\, d_s, \tag{120}$$

where we have assumed the isospin symmetry. Note that the quark EDM can only be probed with the nucleon EDM. It therefore plays an important role in probing the CP violation of several scenarios such as the split SUSY (see sect. 2.3.2).

The quark chromo-EDM contribution to the nucleon EDM $d_N(d_q^c)$ can be estimated in the chiral approach. As we have seen in the previous section, the quark chromo-EDM generates the CP-odd π-N-N interaction. We can therefore infer that the most important part of $d_N(d_q^c)$ is given by the long distance effect, the meson cloud diagram of fig. 7. The isoscalar and isovector nucleon EDMs defined by $d_0 \equiv d_p + d_n$ and $d_1 \equiv d_p - d_n$, respectively, are given in the leading-order chiral perturbation by the following formulae [154, 183, 197, 198, 213, 216, 270, 272, 288–293, 393, 405, 406]:

$$d_0 = \bar{d}_0 - \frac{e g_A \bar{g}^{(0)}_{\pi NN}}{4\pi f_\pi}\left(\frac{3m_\pi}{4m_N}\right) - \frac{e g_A \bar{g}^{(1)}_{\pi NN}}{16\pi f_\pi}\frac{m_\pi}{m_N}, \tag{121}$$

and

$$\begin{aligned} d_1 = \bar{d}_1 &- \frac{e g_A \bar{g}^{(0)}_{\pi NN}}{4\pi^2 f_\pi}\left(\frac{2}{4-d} - \gamma_E + \ln\frac{4\pi\mu^2}{m_\pi^2} + \frac{5\pi m_\pi}{4m_N}\right) \\ &- \frac{e g_A \bar{g}^{(1)}_{\pi NN}}{16\pi f_\pi}\frac{m_\pi}{m_N}, \end{aligned} \tag{122}$$

[2] It is to be noted that the left-right four-quark interaction also sizably contributes to the nucleon EDM through the induced θ-term when the PQ mechanism is active [214] (see sect. 2.5).

where the isovector axial coupling is given by $g_A = 1.27$ [407]. The low-energy constants $\bar{d}_0$ and $\bar{d}_1$ are the counter terms of the one-loop level diagram (fig. 7), and include the short distance effect which does not come from the meson cloud. Roughly, they originate from short distance effect (shorter than the renormalization scale, $\mu = 1\,\mathrm{GeV}$ in our case). Let us show the quark chromo-EDM contribution to the nucleon EDM by neglecting $\bar{d}_n$ and $\bar{d}_p$. The leading-order chiral analysis of the nucleon EDM generated by the quark chromo-EDM, taking into account the effect of hadrons with strange quark, was done in ref. [393]. These results are given by

$$d_n(d_q^c) = e\tilde{\rho}_n^u d_u^c + e\tilde{\rho}_n^d d_d^c + e\tilde{\rho}_n^s d_s^c, \tag{123}$$

$$d_p(d_q^c) = e\tilde{\rho}_p^u d_u^c + e\tilde{\rho}_p^d d_d^c + e\tilde{\rho}_p^s d_s^c, \tag{124}$$

so that we have $\tilde{\rho}_n^u \approx -0.76$, $\tilde{\rho}_n^d \approx -0.17$, $\tilde{\rho}_n^s \approx 0.55$, $\tilde{\rho}_p^u \approx -0.026$, $\tilde{\rho}_p^d \approx -1.1$, and $\tilde{\rho}_p^s \approx 1.3$ when there is no Peccei-Quinn mechanism, and $\tilde{\rho}_n^u \approx 1.5$, $\tilde{\rho}_n^d \approx 0.93$, $\tilde{\rho}_n^s \approx 0.60$, $\tilde{\rho}_p^u \approx 0.37$, $\tilde{\rho}_p^d \approx -0.93$, and $\tilde{\rho}_p^s \approx 1.3$ when the Peccei-Quinn mechanism is active. The neutron EDM was also evaluated using QCD sum rules [408, 409], giving smaller results. It is possible that the QCD sum rules approach could not take into account the long distance physics due to the pion loop which enhances the nucleon EDM. On the contrary, the QCD sum rules can quantify the short distance physics which is in principle impossible to treat in the calculation using the effective CP-odd meson-nucleon interaction without the knowledge of the low-energy constants. It is to be noted that the above result may be affected by a sizable theoretical uncertainty due to the effect of higher-order corrections [292, 395]. The ideal way to obtain $d_N(d_q^c)$ is to evaluate it on lattice. There are currently continuous efforts to achieve this goal [410–413].

The final important process contributing to the nucleon EDM to be discussed is the Weinberg operator. The derivation is based on the CP-violating rotation of the nucleon state evaluated using the QCD sum rules [296, 297, 414]. By quoting the calculation using the QCD sum rules, the nucleon EDM generated by the Weinberg operator constant w is

$$\begin{aligned} d_N(w) &\sim \frac{a_N}{2m_N} w \frac{3g_s m_0^2}{32\pi^2} \ln\frac{M_b^2}{\mu_{\mathrm{IR}}^2} \\ &\approx \begin{cases} -w \times 20\, e\,\mathrm{MeV} & (N=n), \\ w \times 5\, e\,\mathrm{MeV} & (N=p), \end{cases} \end{aligned} \tag{125}$$

where $\frac{M_b^2}{\mu_{\mathrm{IR}}^2} = 2$ and $g_s = 2.1$. The anomalous magnetic moment $(g-2)$ of the nucleon N is given by a_N ($a_n = -3.91$, $a_p = 0.79$). As we have seen previously, the Weinberg operator also induces a θ-term when the Peccei-Quinn mechanism is relevant, but its contribution is suppressed by a factor of light quark mass. The theoretical uncertainty of eq. (125) is large due to the model dependence, and certainly exceeds $O(100\%)$.

As mentioned in sect. 2.2, the nucleon EDM in the SM is of order $O(10^{-(31-32)})e\,\mathrm{cm}$. It is estimated by the long distance effect generated by the chiral loop diagram (see fig. 7) with $|\Delta S| = 1$ interactions [69–76, 78]. A loopless process with high mass dimension operator was also pointed out to contribute to the nucleon EDM with the same order of magnitude [77]. Like the other CP-violating processes, the nucleon EDM in the SM is much smaller than that generated by typical models of new physics with TeV scale parameters.

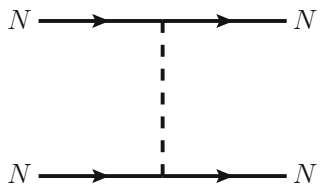

Fig. 8. Diagrammatic representation of one-meson exchange CP-odd nuclear force. The solid line represents the nucleon and the dashed line a light pseudoscalar meson (π, η).

3.5 CP-odd nuclear force

The CP-odd nuclear force is the leading CP-violating process in generating CP-odd nuclear moments. The most general CP-odd nuclear force is given by

$$\begin{aligned} H_{\not P \not T} = \Big\{ & \boldsymbol{\sigma}_- V_1(r) + \boldsymbol{\tau}_1 \cdot \boldsymbol{\tau}_2\, \boldsymbol{\sigma}_- V_2(r) \\ & + \frac{1}{2}(\tau_+^z \boldsymbol{\sigma}_- + \tau_-^z \boldsymbol{\sigma}_+) V_3(r) + \frac{1}{2}(\tau_+^z \boldsymbol{\sigma}_- - \tau_-^z \boldsymbol{\sigma}_+) V_4(r) \\ & + (3\tau_1^z \tau_2^z - \boldsymbol{\tau}_1 \cdot \boldsymbol{\tau}_2)\, \boldsymbol{\sigma}_- V_5(r) \Big\} \cdot \hat{\boldsymbol{r}}, \end{aligned} \tag{126}$$

where $\hat{\boldsymbol{r}} \equiv \frac{\boldsymbol{r}_1 - \boldsymbol{r}_2}{|\boldsymbol{r}_1 - \boldsymbol{r}_2|}$ with $\boldsymbol{r}_1$ and $\boldsymbol{r}_2$ are the coordinates of the interacting two nucleons. The spin and isospin matrices are given by $\boldsymbol{\sigma}_- \equiv \boldsymbol{\sigma}_1 - \boldsymbol{\sigma}_2$, $\boldsymbol{\sigma}_+ \equiv \boldsymbol{\sigma}_1 + \boldsymbol{\sigma}_2$, $\boldsymbol{\tau}_- \equiv \boldsymbol{\tau}_1 - \boldsymbol{\tau}_2$, and $\boldsymbol{\tau}_+ \equiv \boldsymbol{\tau}_1 + \boldsymbol{\tau}_2$. As we can see, the CP-odd nuclear force is a spin-dependent interaction, so the CP-odd nuclear polarization arises only for systems with nonzero angular momenta.

At the scale of nuclear physics, with the cutoff scale $\mu = 500\,\mathrm{MeV}$, the pion exchange CP-odd nuclear force provides the leading contribution to the CP-odd nuclear moment. At the leading order, the CP-odd nuclear force is a one-pion exchange process made by combining the CP-even and CP-odd pion-nucleon interactions (see fig. 8). Its non-relativistic potential is given by [302, 415, 416]

$$V_2^\pi(r)\hat{\boldsymbol{r}} = -\frac{g_{\pi NN}\bar{g}_{\pi NN}^{(0)}}{2m_N} \nabla \mathcal{Y}(m_\pi, r), \tag{127}$$

$$V_3^\pi(r)\hat{\boldsymbol{r}} = -\frac{g_{\pi NN}\bar{g}_{\pi NN}^{(1)}}{2m_N} \nabla \mathcal{Y}(m_\pi, r), \tag{128}$$

$$V_5^\pi(r)\hat{\boldsymbol{r}} = \frac{g_{\pi NN}\bar{g}_{\pi NN}^{(2)}}{2m_N} \nabla \mathcal{Y}(m_\pi, r), \tag{129}$$

where $\mathcal{Y}(m_\pi, r) \equiv \frac{e^{-m_\pi r}}{4\pi r}$, and $g_{\pi NN} \equiv \frac{g_A m_N}{f_\pi}$. Note the sign change for the isoscalar and isovector couplings which is due to the difference of conventions [36,417].

We should also present some subleading processes. The first one is the contact interaction (terms with $\bar{C}_1$ and $\bar{C}_2$ of eq. (75)), which can be written as

$$V_1^C(r)\hat{\boldsymbol{r}} = -m_N \bar{C}_1 \nabla\delta(r), \tag{130}$$

$$V_2^C(r)\hat{\boldsymbol{r}} = -m_N \bar{C}_2 \nabla\delta(r), \tag{131}$$

where the delta function is valid up to the cutoff (renormalization) scale. In practice, it is smeared with a Gaussian or a Yukawa function with the cutoff scale as their range. An example of the effect contributing to the contact interaction is the CP-odd nuclear force with η meson exchange (see fig. 8). It can be matched with the isoscalar CP-odd N-N interaction as [418]

$$g_{\eta NN}\bar{g}^{(0)}_{\eta NN} \approx -m_N m_\eta^2 \bar{C}_1, \tag{132}$$

where $g_{\eta NN} = 2.24$ [419] is the CP-even η-nucleon coupling. Quantifying the effect of the CP-odd contact interaction is potentially important since it receives contributions from the Weinberg operator. Unfortunately, there are currently no hadron level evaluations available.

Another possible subleading contribution is the CP-odd three-nucleon interaction [213]. This interaction is generated by the three-pion interaction (terms with Δ of eq. (73)). This process however interacts with the spin and isospin of all the three relevant nucleons. This kind of configurations is suppressed in nuclei due to the pairing of nucleons, so the effect of the CP-odd three-nucleon interaction is not important. Neglecting this interaction should therefore be a good approximation.

Before going to the nuclear physics, we have to point out that the renormalization scale where the CP-odd nuclear force eq. (126) was defined is not the same as that used in the calculational approach adopted for heavy nuclei. If we respect the "bare" CP-odd nuclear force, the model space of many-body nuclear systems becomes too large, with exponentially growing calculational cost. To treat the CP-odd nuclear force in some many-body approaches, we actually have to construct an effective theory for heavy nuclei, respecting the model space. We can expect that the long-range pion exchange is not much affected by this change of model space, since the pion exchange is the most relevant interaction in low-energy nuclear physics. We must however note that the contact interaction which contains the short-range physics suffers from the renormalization in the reduction of the model space, required in the construction of the effective interaction in heavy nuclei.

In the context of the change of model space, a notable CP-odd contribution is the isotensor CP-odd nuclear force. At the scale of the hadron level effective theory (renormalization scale of eq. (126), *e.g.*, $\mu = 500\,\mathrm{MeV}$), this interaction is suppressed by the isospin splitting of the quark mass. The situation may however change in heavy nuclei, where the CP-odd nuclear force must be renormalized into an effective theory with a reduced model space. As heavy nuclei have a medium with large isospin breaking, they certainly induce an isotensor CP-odd nuclear force through the renormalization of isovector CP-odd interaction. There are currently no evaluations of the effective CP-odd nuclear forces for heavy nuclei, but this is an important subject to be discussed in the future. At the same time, the evaluation of the effect of the isotensor CP-odd nuclear force to the CP-odd nuclear moments are almost mandatory in quantifying the EDM of heavy atoms.

The leading SM contribution to the CP-odd nuclear force is generated by the pion-exchange process, which is just the combination of the CP-even and CP-odd pion-nucleon interactions (see sect. 3.3). In SM, we can also consider additional effects due to the exchange of K and η mesons, which contribute to all terms of eq. (126) [269].

4 Nuclear structure calculation

In this section we first give the definition of the NSM and then review how it is evaluated in framework of the nuclear shell model and other calculations based on the mean-field theories.

4.1 Definition of NSM

The effective electric field $\Phi(\boldsymbol{r})$ which an electron at position $\boldsymbol{r}$ feels can be expressed as [420]

$$\langle\Psi|\, e\Phi(\boldsymbol{r}) - \frac{1}{Z}\langle \boldsymbol{d}_N\rangle \cdot \boldsymbol{\nabla}\Phi(\boldsymbol{r})\,|\Psi\rangle = -\frac{Ze^2}{|r|} + 4\pi e\mathbf{S}\cdot\boldsymbol{\nabla}\delta(\boldsymbol{r}) + \cdots, \tag{133}$$

where $|\Psi\rangle$ indicates the nuclear ground state, $\langle \boldsymbol{d}_N\rangle$ is the nuclear electric dipole moment of the nuclear ground state and Z is the number of protons. Here the k-th component ($k = x, y, z$) of the NSM S_k may be given as

$$S_k = S_{\mathrm{ch},k} + S_{\mathrm{int},k}. \tag{134}$$

The $S_{\mathrm{ch},k}$ is caused by the charge asymmetry of a nucleus and is given as

$$S_{\mathrm{ch},k} = \frac{1}{10}\int\left(r^2 r_k - \frac{5}{3}\langle r^2\rangle_{\mathrm{ch}} r_k - \frac{2}{3}\langle Q_{kk'}\rangle r_{k'}\right)\rho(\boldsymbol{r})\mathrm{d}\boldsymbol{r}, \tag{135}$$

where r_k represents position of a nucleon, $\rho(\boldsymbol{r})$ nuclear charge density, $\langle Q_{kk'}\rangle$ nuclear quadrupole moment of the nuclear ground state, which can be dropped for the spin $I = 1/2$ nuclear state. $\langle r^2\rangle_{\mathrm{ch}}$ is the charge mean square radius.

Then the NSM is defined as the maximum projection of the NSM operator on the nuclear axis, $S = \langle \hat{S}_z\rangle$ and is calculated as

$$S_{\mathrm{ch}} = \left\langle \Psi \left| \hat{S}_{\mathrm{ch},z} \right| \Psi, \right\rangle, \tag{136}$$

where $|\Psi\rangle$ is the PT-violating ground state, which is usually evaluated by the nuclear mean-field theories. The operator $\hat{\mathbf{S}}_{\rm ch}$ is expressed in terms of nucleon's degree of freedom as

$$\hat{\mathbf{S}}_{\rm ch} = \frac{1}{10}\sum_{i=1}^{A} e_i \left(r_i^2 - \frac{5}{3}\left\langle r^2 \right\rangle_{\rm ch} \right) \boldsymbol{r}_i. \tag{137}$$

Here A is the mass number of a specific nucleus, and e_i is the charge for the ith nucleon. We take $e_i = 0$ for a neutron and $e_i = e$ for a proton. As inclusion of the relativistic effects, Flambaum *et al.* had pointed out the contribution to the NSM operator as [421]

$$\mathbf{S}' = \frac{Ze}{10}\frac{1}{1-\frac{5}{14}Z^2\alpha^2}\left\{ \left[\left\langle \mathbf{r} r^2 \right\rangle - \frac{5}{3}\left\langle \mathbf{r} \right\rangle \left\langle r^2 \right\rangle - \frac{2}{3}\left\langle r_i \right\rangle \left\langle q_{ij} \right\rangle \right] - \frac{5}{28}\frac{Z^2\alpha^2}{R_N^2}\left[\left\langle \mathbf{r} r^4 \right\rangle - \frac{7}{3}\left\langle \mathbf{r} \right\rangle \left\langle r^4 \right\rangle - \frac{2}{3}\left\langle r_i \right\rangle \left\langle q_{ij} r^2 \right\rangle \right] \right\}, \tag{138}$$

where R_N is the nuclear radius, q_{ij} is the nuclear quadrupole moment operator and Z is the atomic number of the nucleus.

If P, T-odd, which is equivalent to P, CP-odd, interaction $\hat{V}^{PT}_{\pi(T)}$ exists in the total Hamiltonian, we have

$$H = H_0 + \hat{V}^{PT}_{\pi(T)}, \tag{139}$$

where H_0 does not break P and T. Here $\hat{V}^{\pi}_{PT}$ is the pion-exchange CP-odd nuclear force, given by the sum of the isoscalar ($T = 0$, defined in eq. (127)), isovector ($T = 1$, defined in eq. (128)) and isotensor ($T = 2$, defined in eq. (129)) terms. The coupling constants can be rewritten as

$$\bar{g}^{(0)}g = -g_{\pi NN}\bar{g}^{(0)}_{\pi NN}, \tag{140}$$

$$\bar{g}^{(1)}g = -g_{\pi NN}\bar{g}^{(1)}_{\pi NN}, \tag{141}$$

$$\bar{g}^{(2)}g = g_{\pi NN}\bar{g}^{(2)}_{\pi NN}, \tag{142}$$

to respect the convention often adopted in the nuclear structure calculations. We note again that the bare CP-odd nuclear force obtained at the hadron scale and that used in the calculations of the CP-odd moments of heavy nuclei (that of this section) are not the same, since the model spaces where they are defined are different. The nuclear forces in the media are usually calculated in terms of the Brueckner-Bethe-Goldstone (BBG) many-body theory [422]. Another complexity comes in from the shell model calculation. In the shell model calculation we divide the model space into the core and valence spaces. The effective interaction in the valence shell should be modified by taking into account the core excitations. Since the treatment of both of them is rather involved, we do not take into account these effects in this paper.

Since $\hat{V}^{PT}_{\pi(T)}$ is very weak, the NSM which is P,T-odd is calculated perturbatively as

$$S_{\rm ch} = \sum_{k=1} \frac{\langle I_1^+ | \hat{S}_{{\rm ch},z} | I_k^- \rangle \langle I_k^- | \hat{V}^{PT}_{\pi(T)} | I_1^+ \rangle}{E_1^+ - E_k^-} + \text{c.c.} \tag{143}$$

Here $|I_1^+\rangle$ represents the lowest state with spin I and positive parity (parity of the nuclear ground state is assumed to positive here) and $|I_k^-\rangle$, the k-th state with spin I and negative parity. The energy E_k^{π} of the k-th state with parity π, is obtained by diagonalizing the original shell model Hamiltonian H_0, *i.e.*

$$H_0 \left| I_k^{\pi} \right\rangle = E_k^{\pi} \left| I_k^{\pi} \right\rangle .$$

Then the NSM is expressed in terms of $\bar{g}^{(T)}$ as

$$S_{\rm ch} = a_0\, \bar{g}^{(0)}g + a_1\, \bar{g}^{(1)}g + a_2\, \bar{g}^{(2)}g, \tag{144}$$

where coefficients a_T with $T = 1, 2, 3$ in front of $\bar{g}^{(T)}g$'s are given in units of e fm^3. Coefficients a_T are tabulated in the following.

Another contribution to $\hat{\mathbf{S}}_{\rm int}$ coming from the nucleon intrinsic EDM is given by as [423]

$$\hat{\mathbf{S}}_{\rm int} = \frac{1}{6}\sum_{i=1}^{A} \mathbf{d}_i \left(r_i^2 - \left\langle r^2 \right\rangle_{\rm ch} \right) + \frac{1}{5}\sum_{i=1}^{A} \left[\mathbf{r}_i \left(\mathbf{r}_i \cdot \mathbf{d}_i \right) - \mathbf{d}_i r_i^2/3 \right], \tag{145}$$

where $\mathbf{d}_i$ is the i-th nucleon intrinsic dipole moment (either proton or neutron). Then the intrinsic component of NSM is expressed as

$$S_{\rm int} = s_p d_p + s_n d_n, \tag{146}$$

where d_p and d_n are EDMs of the proton and the neutron, respectively. Here s_p and s_n are the unknown coefficients that have to be calculated using nuclear many-body methods.

4.2 Evaluation of NSMs

4.2.1 Simple shell model approaches

As a simple shell model estimate, an odd-mass nucleus is expressed as a one-particle (either neutron or proton) plus the core (even-even part of the nucleus). In ref. [424] NSMs were calculated for a set of nuclei (^{199}Hg, ^{129}Xe, ^{211}Rn, ^{213}Ra, ^{225}Ra, ^{133}Cs, and ^{223}Fr) with full account of core polarization effects (namely from the even-even part of the nucleus). Their results are given in table 1 without core polarization and in table 2 with core polarization effects. The effects of core polarization are found to have in general a large effect on the reduction of the Schiff moments (ten to hundred times reduction). It is also found that the dominant contribution comes from the isovector ($T = 1$) term for ^{199}Hg.

In ref. [425], the Skyrme-Hartree-Fock method is used to calculate the NSM for the octupole deformed nucleus ^{225}Ra. ^{225}Ra is known as a possible candidate which has a large Schiff moment. The first $I^{\pi} = \frac{1}{2}^-$ state is located at 55 keV above the ground state with spin $I^{\pi}_{g.s.} = \frac{1}{2}^+$ and the energy denominator in eq. (143) becomes large. As intermediate states in perturbation theory, they took only the first $I^{\pi} = \frac{1}{2}^-$ state with excitation energy of $\Delta E = 55$ keV.

Table 1. Coefficients a_T in ref. [424] in units of e fm^3. The bare values of the Schiff moment in eq. (144), without core polarization, are calculated. Note that the sign of tensor-type interaction is changed from the original paper in accordance with the definition in the present paper.

	a_0	a_1	a_2
^{199}Hg	−0.09	−0.09	−0.18
^{129}Xe	0.06	0.06	0.12
^{211}Rn	−0.12	−0.12	−0.24
^{213}Ra	−0.012	−0.021	−0.016
^{225}Ra	0.08	0.08	0.16
^{133}Cs	0.08	−0.02	0.21
^{223}Fr	−0.122	−0.052	−0.300

Table 2. Coefficients a_T in ref. [424] with core polarization in units of e fm^3.

	a_0	a_1	a_2
^{199}Hg	−0.00004	−0.055	−0.009
^{129}Xe	0.008	0.006	0.009
^{211}Rn	−0.019	0.061	−0.053
^{213}Ra	−0.012	−0.021	−0.016
^{225}Ra	0.033	−0.037	0.046
^{133}Cs	0.006	−0.02	0.04
^{223}Fr	−0.009	−0.016	−0.030

Table 3. Coefficients a_T in ref. [425] for ^{225}Ra in units of e fm^3.

	a_0	a_1	a_2
^{225}Ra	−5.06	10.4	−10.1

Then, to a very good approximation, we have

$$S = -\frac{\langle 1/2^+|\hat{S}_z|1/2^-\rangle\langle 1/2^-|\hat{V}^{PT}|1/2^+\rangle}{\Delta E} + \text{c.c.} \quad (147)$$

This is further simplified as

$$S = -2\frac{J}{J+1}\frac{\langle\hat{S}_z\rangle\langle\hat{V}^{PT}\rangle}{\Delta E}\,, \quad (148)$$

where $J = 1/2$ and $\langle\hat{S}_z\rangle$ and $\langle\hat{V}^{PT}\rangle$ are expectation values in terms of mean fields (intrinsic-states). Their result is summarized in table 3.

The effect of the intrinsic nucleon EDM to the Schiff moment can also be estimated in the simple shell model. It is given by [7, 49, 197]

$$S_{\rm int} = \begin{cases} d_N\left[\frac{1}{10}\frac{2+j}{1+j}\langle r^2\rangle_{\rm val} - \frac{1}{6}\langle r^2\rangle_{\rm ch}\right] & (j = l+1/2), \\ d_N\left[\frac{1}{10}\frac{1-j}{1+j}\langle r^2\rangle_{\rm val} + \frac{1}{6}\frac{j}{1+j}\langle r^2\rangle_{\rm ch}\right] & (j = l-1/2), \end{cases} \quad (149)$$

where $\langle r^2\rangle_{\rm val}$ is the mean square radius of the valence nucleon N. The nuclear angular momentum and the orbital angular momentum of the single valence nucleon are denoted by j and l, respectively. In ordinary nuclei, $\langle r^2\rangle_{\rm val} \approx \langle r^2\rangle_{\rm ch} \approx A^{\frac{2}{3}}(1.1\,\text{fm})^2$ with A the nucleon number. In the simple shell model, $\frac{1}{2}^+$ nuclei have an s-wave valence nucleon (*e.g.*, ^{129}Xe, ^{225}Ra). From eq. (149), $S_{\rm int}$ of those nuclei vanishes. In reality, the single valence nucleon approximation does not hold due to the configuration mixing, and the intrinsic nucleon EDM contribution does not cancel. We note that the effect of intrinsic nucleon EDM is not enhanced, since the relativistic effect is weak in nuclei, in contrast to that for the electrons in atoms [426–428]. For $\frac{1}{2}^+$ nuclei, we should consider that $|S_{\rm int}| \sim \frac{d_N}{6}\langle r^2\rangle_{\rm ch}$ is an upper limit.

4.2.2 Mean-field framework

In ref. [429], the NSM of the nucleus ^{199}Hg is calculated by π-N-N interaction vertices that are P,T-odd. Their approach, formulated in diagrammatic perturbation theory with important core-polarization diagrams summed to all orders, gives a close approximation to the expectation value of the Schiff operator in the odd-A Hartree-Fock-Bogoliubov ground state generated by a Skyrme interaction and a weak P,T-odd pion-exchange potential. In the following their method is reviewed in short.

The NSM is approximately expressed as the expectation value of the Schiff operator S_z in the completely self-consistent one-quasiparticle ground state of ^{199}Hg, constructed from a two-body interaction that includes both a Skyrme potential and the P,T-odd potential V^{PT}. It is an approximation because V^{PT} is not treated in a completely self-consistent way. The mean-field calculation in ^{199}Hg itself is not carried out. Instead, the HF+BCS ground state of the even-even nucleus ^{198}Hg is first calculated and add a neutron in the $2p_{1/2}$ level. The core-polarizing effects of this neutron are treated in the QRPA framework.

Following a spherical HF+BCS calculation in ^{198}Hg, the Hamiltonian is divided into unperturbed and residual parts. The unperturbed part, expressed in the quasiparticle basis, is

$$H_0 = T + V_{00} + V_{11}, \quad (150)$$

where T is the kinetic energy and V the Skyrme interaction, with subscripts referring to the numbers of quasiparticles which the interaction creates and destroys. The perturbed part is

$$H_{res} = V^{PT} + V_{22} + V_{13} + V_{31} + V_{04} + V_{40}. \quad (151)$$

The interaction V^{PT} can also be expanded in terms of quasiparticle creation and annihilation operators. The model space of effective operator theory is one-dimensional: a quasiparticle in the $a \equiv (2p_{1/2}, m = 1/2)$ level. The unperturbed ground state $|\Phi_a\rangle$ is simply this one-quasiparticle state. Then the expectation value of S^z,

Table 4. Coefficients a_T in ref. [429] in ^{199}Hg for the five different Skyrme interactions in units of e fm^3.

	a_0	a_1	a_2
SkM	0.009	0.070	0.022
SkP	0.002	0.065	0.011
SIII	0.010	0.057	0.025
SLy4	0.003	0.090	0.013
SkO′	0.010	0.074	0.018

in the full correlated ground state is given by

$$\langle \Psi_a | S_z | \Psi_a \rangle = N^{-1} \langle \Phi_a | \left[1 + H_{res} \left(\frac{Q}{\varepsilon_a - H_0} \right) + \cdots \right] S_z \times \left[1 + \left(\frac{Q}{\varepsilon_a - H_0} \right) H_{res} + \cdots \right] | \Phi_a \rangle \,. \quad (152)$$

Here ε_a is the single-quasiparticle energy of the valence nucleon, the operator Q projects onto all other single-quasiparticle states, N is the normalization factor.

The terms that are first order in H_{res} do not include the strong interaction V because it has a different parity from the Schiff operator. Thus the lowest-order contribution to the NSM is

$$\langle \Psi_a | S^z | \Psi_a \rangle^{LO} = \langle - | \, c_a \left[V^{PT} \left(\frac{Q}{\varepsilon_a - H_0} \right) S^z \right] c_a^\dagger | - \rangle + \text{c.c.}, \quad (153)$$

where $c_a^\dagger$ is the creation operator for a quasiparticle in the valence level a and $|-\rangle$ is the no-quasiparticle BCS vacuum describing the even-even core, so that $|\Phi_a\rangle$ is just $c_a^\dagger |-\rangle$. The core polarization is also considered, implemented through a certain QRPA method. To assess the uncertainty in the results, they carried out the calculation with several Skyrme interactions, the quality of which is tested by checking predictions for the isoscalar-$E1$ strength distribution in ^{208}Pb. Their final results are summarized in table 4.

In ref. [430] they present a comprehensive mean-field calculation of the NSM of the nucleus ^{225}Ra, the quantity that determines the static electric-dipole moment of the corresponding atom if T is violated in the nucleus. The calculation breaks all possible intrinsic symmetries of the nuclear mean-field and includes both exchange and direct terms from the full finite-range T-violating N-N interaction, and the effects of short-range correlations. The resulting NSM, which depends on three unknown T-violating π-N-N coupling constants, is much larger than in ^{199}Hg, the isotope with the best current experimental limit on its atomic EDM. In the following their work is reviewed briefly.

The asymmetric shape of ^{225}Ra implies parity doubling, namely, the existence of a very low-energy $|1/2^-\rangle$ state, in this case 55 keV above the ground state $|\Psi_0\rangle \equiv |1/2^+\rangle$ that dominates the sum in eq. (143) because of the corresponding small denominator. With the approximation that the shape deformation is rigid, the ground state and its negative-parity partner in the octupole-deformed nucleus are projections onto good parity and angular momentum of the same "intrinsic state", which represents the wave function of the nucleus in its own body-fixed frame with the total angular momentum aligned along the symmetry axis. Equation (143) then reduces to

$$S \approx -\frac{J}{J+1} \left\langle \hat{S}_z \right\rangle \frac{\langle V^{PT} \rangle}{(55\,\text{keV})}\,, \quad (154)$$

where $J = 1/2$ and the brackets indicate expectation values in the intrinsic state. The octupole deformation enhances $\langle \hat{S}_z \rangle$, making it collective, robust, and straightforward to calculate with an error of a factor of 2 or less. To evaluate $\langle V^{PT} \rangle$ they constructed a new version of the code Hartree-Fock code (HFODD). HFODD works with any Skyrme energy functional. Their results for various types of Skyrme interactions are given in table 5.

Table 5. Coefficients a_T in ref. [430] in ^{225}Ra, calculated with the different types of Skyrme interactions in units of e fm^3.

	a_0	a_1	a_2
SkO′	−1.5	6.0	−4.0
SIII	−1.0	7.3	−3.9
SkM*	−4.7	21.5	−11.0
SLy4	−3.0	16.9	−8.8

In ref. [431], they calculate the NSMs of the nuclei ^{199}Hg and ^{211}Rn in completely self-consistent odd-nucleus mean-field theory by modifying the Hartree-Fock-Bogoliubov code HFODD. They allow for arbitrary shape deformation and include the effects of nucleon dipole moments alongside those of a π-N-N interaction that violates charge-parity (CP) symmetry. The results for ^{199}Hg differ significantly from those of previous calculations when the CP-violating interaction is of isovector character.

Here they do not use perturbation theory, but instead the NSM is directly calculated, by including the PT-violating interaction. Namely they have

$$S_{\text{ch}} = \left\langle \Psi \left| \hat{S}_{\text{ch},z} \right| \Psi \right\rangle, \quad (155)$$

where $|\Psi\rangle$ is the P,T-odd ground state. Their results are given in tables 6 and 7.

They also calculate the Schiff moment coming from the Schiff moment operator due to nucleon intrinsic electric dipole moment [424] as in eq. (145) where the nucleon EDM operator in the leading chiral approximation [see also eqs. (121) and (122)] can be written as

$$\hat{\mathbf{d}}_i = \frac{eg}{4\pi^2 m_N} \ln \frac{m_N}{m_\pi} \left(\bar{g}^{(0)} - \bar{g}^{(2)} \right) \hat{\boldsymbol{\sigma}}_i (-\tau_i^z) \approx 5.2 \times 10^{-2}\,\text{GeV}^{-1}\, eg \left(\bar{g}^{(0)} - \bar{g}^{(2)} \right) \hat{\boldsymbol{\sigma}}_i (-\tau_i^z). \quad (156)$$

where i represents the i-th nucleon. Here the minus sign of the isospin matrix is due to the difference of convention.

Table 6. Coefficients a_T in ref. [431] in ^{211}Rn in units of $e\,\mathrm{fm}^3$.

	a_0	a_1	a_2	b
SLy4	0.042	−0.018	0.071	0.016
SkM*	0.042	−0.028	0.078	0.015
SIII	0.034	−0.0004	0.064	0.015

Table 7. Coefficients a_T in ref. [431] in ^{199}Hg in units of $e\,\mathrm{fm}^3$. The first three lines are in the HF approximation, and the next two are in the HFB approximation.

	a_0	a_1	a_2	b
SLy4	0.013	−0.006	0.022	0.003
SIII	0.012	0.005	0.016	0.004
SV	0.009	−0.0001	0.016	0.002
SLy4	0.013	−0.006	0.024	0.007
SkM*	0.041	−0.027	0.069	0.013

Table 8. Values of s_p and s_n for different g_s and g_s' in ^{199}Hg where g_s and g_s' are strengths for the Landau-Migdal interaction in ref. [423].

	s_p	s_n	g_s	g_s'
SIII	0.18	1.89	0.25	0.9
SV	0.19	1.86	0.25	1.0
SLy4	0.20	1.93	0.19	0.9
SkM*	0.22	1.90	0.19	1.0

In terms of the coefficient b of tables 6 and 7, eq. (146) is written as

$$S_{\mathrm{int}} = \frac{b\,d_n}{1.0\times10^{-2}e\,\mathrm{fm}}\,, \tag{157}$$

where it is assumed that only the intrinsic EDM of the neutron contributes.

In ref. [423], they calculated the contribution of internal d_N to the NSM of ^{199}Hg. The contribution of the d_p was obtained via core polarization effects that were treated in the framework of random phase approximation (RPA) with effective residual forces. Their results are given in table 8.

The NSM is predicted to be enhanced in nuclei with static quadrupole and octupole deformation. The analogous suggestion of the enhanced contribution to the NSM from the soft collective quadrupole and octupole vibrations in spherical nuclei is tested in this article in the framework of the quasi-RPA (QRPA) with separable quadrupole and octupole forces applied to the odd $^{217-221}$Ra and $^{217-221}$Rn isotopes (table 9). In this framework, we confirm the existence of the enhancement effect due to the soft modes, but only in the limit when the frequencies of quadrupole and octupole vibrations are close to zero. According to the QRPA, in realistic cases the enhancement in spherical nuclei is strongly reduced by a small weight of the corresponding "particle+phonon" component in a complicated wave function of a soft nucleus. They considered the following weak P,T-odd interaction:

Table 9. Schiff moments in units of $\eta\,10^{-8}e\,\mathrm{fm}^3$ in ref. [432].

^{217}Ra	^{217}Rn	^{219}Ra	^{219}Rn	^{221}Ra	^{221}Rn
−0.03	−0.01	0.30	−0.03	−0.07	0.06

$$W = \frac{G_F}{\sqrt{2}}\frac{1}{2m}\eta(\boldsymbol{\sigma n})\frac{1}{4\pi}\frac{\mathrm{d}\rho(r)}{\mathrm{d}r}\,, \tag{158}$$

where G_F is the Fermi constant of the weak interaction, and η is the strength of the P,T-odd interaction and $\rho(r)$ is the nuclear charge distribution.

4.2.3 Configuration mixing shell model approaches

In ref. [433], the NSMs for the lowest $1/2^+$ states of Xe isotopes are calculated. The nuclear wave functions beyond mean-field theories are calculated in terms of the nuclear shell model, which contains P, T-odd two-body interactions. In the following their approach is reviewed in detail.

For a description of the first $1/2^+$ states (the $1/2_1^+$ states) of odd-mass nuclei, the pair-truncated shell model (PTSM) [434–436] is adopted, where the gigantic shell model space is restricted to an efficient and dominant model space in terms of collective pairs. In the low-lying states angular momenta zero (S) and two (D) collective pairs are most important. The S and D pairs are defined as

$$\hat{S}^\dagger = \sum_j \alpha_j \hat{A}^\dagger{}_0^{(0)}(jj), \tag{159}$$

$$\hat{D}^\dagger_M = \sum_{j_1 j_2} \beta_{j_1 j_2} \hat{A}^\dagger{}_M^{(2)}(j_1 j_2), \tag{160}$$

where the structure coefficients α and β are determined by variation. Here the creation operator of a pair of nucleons in orbitals j_1 and j_2 with total angular momentum J, and its projection M is written by

$$\hat{A}^\dagger{}_M^{(J)}(j_1 j_2) = \sum_{m_1 m_2} (j_1 m_1 j_2 m_2 | JM)\, \hat{c}^\dagger_{j_1 m_1}\hat{c}^\dagger_{j_2 m_2}, \tag{161}$$

where $\hat{c}^\dagger_j$ is the nucleon creation operator for the j orbital.

The many-body wave functions of even-nucleon systems for neutrons or protons are created by applying the pair creation operators $\hat{S}^\dagger$ and $\hat{D}^\dagger$ to the inert core $|-\rangle$:

$$|S^{n_s} D^{n_d}\,\gamma I\rangle = \left(\hat{S}^\dagger\right)^{n_s}\left(\hat{D}^\dagger\right)^{n_d}|-\rangle, \tag{162}$$

where I is a total angular momentum of the many-body system, and γ an additional quantum number required to completely specify the states. The n_s and n_d are numbers of S and D pairs, respectively. The total number of S and D pairs ($n_s + n_d$) is restricted to half the number of valence nucleons in the even-nucleon system. For the description of odd-nucleon systems, an unpaired nucleon

in the j orbital is added to the even-nucleon system. The state is now written as

$$|jS^{n_s}D^{n_d}\,\gamma I\rangle = \hat{c}_j^\dagger\,|S^{n_s}D^{n_d}\,\gamma I'\rangle\,. \tag{163}$$

As for single-particle levels, all the relevant five orbitals, $0g_{7/2}$, $1d_{5/2}$, $1d_{3/2}$, $0h_{11/2}$, and $2s_{1/2}$, in the major shell between the magic numbers 50 and 82 are taken into account for both neutrons and protons. In addition, four orbitals with negative parity, $1f_{7/2}$, $1f_{5/2}$, $2p_{3/2}$ and $2p_{1/2}$, are considered above the closed shell $Z = 82$ for protons. This is because the shell model space is necessary to be expanded including the negative-parity states connected to the $1/2_1^+$ states in order to calculate the NSMs coming from the P,T-odd two-body interactions. For a description of those negative-parity states, introduce proton negative-parity ($N_k, k = 1, 2, 3, 4, 5$) pairs that are necessary in addition to the S and D pairs, *i.e.*

$$\hat{N}^{\dagger(K_1)}_{1\,M} = \hat{A}^{\dagger(K_1)}_M(g_{7/2}, f_{7/2}), \tag{164}$$
$$\hat{N}^{\dagger(K_2)}_{2\,M} = \hat{A}^{\dagger(K_2)}_M(d_{5/2}, f_{5/2}), \tag{165}$$
$$\hat{N}^{\dagger(K_3)}_{3\,M} = \hat{A}^{\dagger(K_3)}_M(s_{1/2}, p_{1/2}), \tag{166}$$
$$\hat{N}^{\dagger(K_4)}_{4\,M} = \hat{A}^{\dagger(K_4)}_M(g_{7/2}, f_{5/2}), \tag{167}$$
$$\hat{N}^{\dagger(K_5)}_{5\,M} = \hat{A}^{\dagger(K_5)}_M(d_{5/2}, f_{7/2}), \tag{168}$$

where the coupled angular momenta take values of $K_{1,2} = 0, 1, 2, 3, 4$, $K_3 = 0, 1$ and $K_{4,5} = 1, 2, 3, 4$. Then the wave function of the even-nucleon system with negative parity is constructed as

$$|S^{n_s}D^{n_d}N_k\,\gamma I\rangle = \left(\hat{S}^\dagger\right)^{n_s}\left(\hat{D}^\dagger\right)^{n_d}\hat{N}_k^\dagger|-\rangle, \tag{169}$$

where $n_s + n_d + 1$ gives half the number of valence protons.

The odd-mass (neutron odd and proton even) nuclear state with a total spin I and its projection M is written as a product of the above state in neutron space and that in proton space as

$$|\Phi(IM\eta)\rangle = \left[\left|j_n S^{\bar{n}_s}D^{\bar{n}_d}I_n\eta_n\right\rangle \otimes |S^{n_s}D^{n_d}N_i^{n_n}I_p\eta_p\rangle\right]^{(I)}_M, \tag{170}$$

where $2(\bar{n}_s + \bar{n}_d) + 1$ and $2(n_s + n_d + n_n)$ are numbers of valence neutron holes and proton particles, respectively. In this mass region, valence neutrons are treated as holes, and valence protons are treated as particles. The number of the proton negative-parity pairs, n_n, is limited to at most one (*i.e.*, $n_n = 0$ or 1).

As an effective two-body interaction, the monopole pairing (MP) and quadrupole pairing (QP) plus quadrupole-quadrupole (Q-Q) interaction is employed. The effective shell model Hamiltonian is written as

$$\hat{H} = \hat{H}_n + \hat{H}_p + \hat{H}_{np}, \tag{171}$$

where $\hat{H}_n$, $\hat{H}_p$, and $\hat{H}_{np}$ represent the interaction among neutrons, the interaction among protons, and the interaction between neutrons and protons, respectively. The interaction among like nucleons $\hat{H}_t$ ($t = n$ or p) consists of spherical single-particle energies, MP, QP and QQ interactions, *i.e.*

$$\hat{H}_t = \sum_{jm}\varepsilon_{jt}\hat{c}^\dagger_{jmt}\hat{c}_{jmt} - G_{0t}\hat{P}^{\dagger(0)}_t\hat{P}^{(0)}_t - G_{2t}\hat{P}^{\dagger(2)}_t\cdot\tilde{\hat{P}}^{(2)}_t - \kappa_t : \hat{Q}_t\cdot\hat{Q}_t :, \tag{172}$$

where :: denotes normal ordering. The interaction between neutrons and protons $\hat{H}_{np}$ is given by the QQ interaction,

$$\hat{H}_{np} = -\kappa_{np}\hat{Q}_n\cdot\hat{Q}_p. \tag{173}$$

As for the single-particle basis states, the harmonic-oscillator basis states with the oscillator parameter $b = \sqrt{\hbar/M\omega}$ are employed. Further details of the effective interaction are presented in refs. [434–436].

The Hamiltonian given in eq. (171) is diagonalized in terms of the many-body basis wave functions in eq. (170) as

$$\hat{H}\,|I^\pi; k\rangle = E(I^\pi; k)\,|I^\pi; k\rangle\,, \tag{174}$$

where $|I^\pi; k\rangle$ is the normalized eigenvector for the kth state with spin I and parity π, and $E(I^\pi; k)$ is the eigenenergy for the state $|I^\pi; k\rangle$.

The single-particle energies are determined by the following procedure. Since the small change of the single-particle energies hardly influences the energy levels of even-even nuclei, the single-particle energies are determined primarily to reproduce the energy levels of low-lying states for odd-mass nuclei. Using the same set of two-body interactions adopted in the previous studies [435], the single-particle energies are adjusted so as to approximately reproduce the energy levels of low-lying states for odd-mass nuclei. Next, the strengths of the two-body interactions are determined to reproduce the energy spectra of even-even nuclei. As shown later, the strengths of the two-body interactions are changed linearly with the number of the valence particles. Finally, the single-particle energies are again modified to get an improved fitting to the low-energy levels of odd-mass nuclei. The single-particle energies are thus obtained by repeating the above procedure, iteratively. Figure 9 shows model space for neutrons and protons adopted. The single-particle energy is listed for each single-particle orbital in ^{129}Xe. In order to investigate the systematics of low-lying states in the mass $A \sim 130$ region, it is assumed that the strengths of the two-body interactions change linearly with the number of the valence neutron holes $\bar{N}_n$ and the valence proton particles N_p [436].

In table 10 total dimensions of the $1/2^+$ states and the $1/2^-$ states are shown for Xe isotopes.

The partial contribution of the k-th state $|\frac{1}{2}\,{}^-_k\rangle$ to the Schiff moment is defined by

$$S_{(I)}(k) = \frac{\langle\frac{1}{2}\,{}^+_1|\hat{S}_{\mathrm{ch},z}|\frac{1}{2}\,{}^-_k\rangle\langle\frac{1}{2}\,{}^-_k|V^{PT}_{\pi(I)}|\frac{1}{2}\,{}^+_1\rangle}{E^{(+)}_1 - E^{(-)}_k} + \text{c.c.} \tag{175}$$

In fig. 10, the partial contribution $S_{(I)}(k)$ to the Schiff moment for the isovector ($I = 1$) two-body interaction

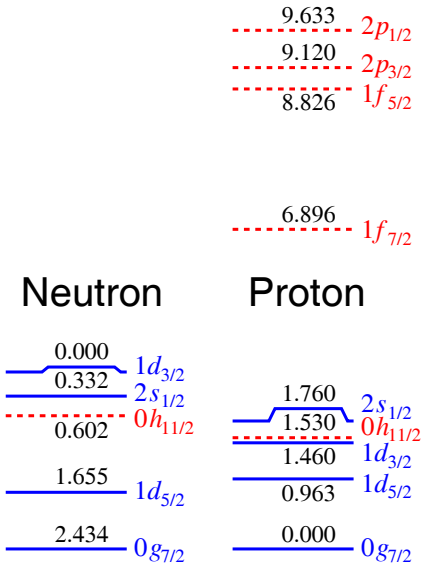

Fig. 9. (Color online) Model space for neutrons and protons adopted in the calculations. The single-particle energy is listed for each single-particle orbital in unit of MeV in the case of ^{129}Xe from ref. [433].

Table 10. Dimensions of the $1/2^+$ states of ^{129}Xe built on the neutron space with parity + and the proton space with parity −, and those of the $1/2^-$ states arising from the proton negative-parity pairs from ref. [433].

Nucleus	^{129}Xe	^{131}Xe	^{133}Xe	^{135}Xe
$1/2^+$	168	84	32	7
$1/2^-$	4077	1968	718	419

in ^{129}Xe is shown as a function of the excitation energy $E_k = E_k^{(-)} - E_1^{(+)}$. The "SUM" indicates the sum of each NSM contribution defined by

$$S_{(I)}^{\rm SUM}(k) = \sum_{i=1}^{k} S_{(I)}(i), \tag{176}$$

where the summation takes over contributions from the first state to the k-th state with spin 1/2 and parity −. There are four large contributions around $E_k = 9.0$ MeV, one positive and the others negative. Almost no contributions are seen above 12.0 MeV.

In fig. 11 the density of the $1/2^-$ states is shown

$$\rho(E_k) = \frac{{\rm d}N}{{\rm d}E} \tag{177}$$

for ^{129}Xe, where ${\rm d}E = 0.2$ MeV is taken and ${\rm d}N$ is the number of the $1/2^-$ states in the range ${\rm d}E$. It is seen from the figure that the ρ has a Gaussian shape and increases exponentially between 8 and 12 MeV. Around 13 MeV it becomes maximum, but the contribution of each state to the NSM is marginal above 12 MeV as seen from fig. 10. The density of the $1/2^-$ states presented in fig. 11 is actually large enough to accommodate the most contribution to the NSMs.

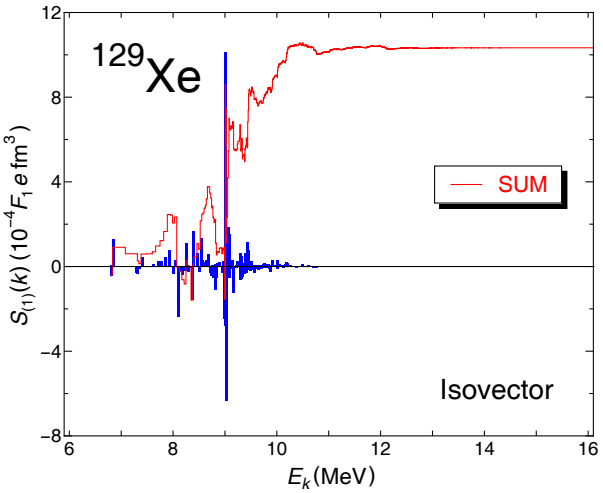

Fig. 10. (Color online) Partial contribution to the Schiff moment for the isovector-type two-body interaction in ^{129}Xe as a function of excitation energies of $1/2^-$ states from ref. [433].

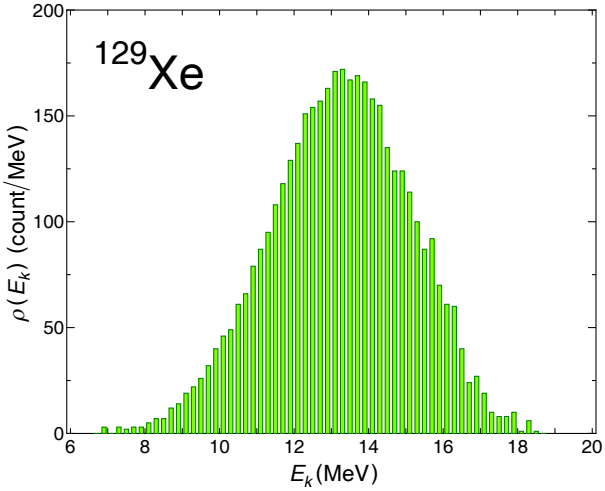

Fig. 11. (Color online) Density of the $1/2^-$ states $\rho(E_k)$ for ^{129}Xe from ref. [433].

To investigate the components of the Schiff moment, the strength function is evaluated for the NSM operator defined by

$$S(k) = \left\langle \frac{1}{2}^+_1 \middle| \hat{S}_{{\rm ch},z} \middle| \frac{1}{2}^-_k \right\rangle, \tag{178}$$

which is shown for ^{129}Xe in fig. 12. There are several strengths in the range between 9 MeV and 10 MeV, but four large strengths around 9.0 MeV contribute to the Schiff moment.

In fig. 13, the off-diagonal potential matrix elements is shown for the isovector ($I = 1$) part

$$V_{(I)}(k) = \left\langle \frac{1}{2}^-_k \middle| V^{PT}_{\pi(I)} \middle| \frac{1}{2}^+_1 \right\rangle. \tag{179}$$

In contrast to the strength function for the NSM, there are now two large contributions just above 6.8 MeV in enlarged scale. However, they do not contribute to the total

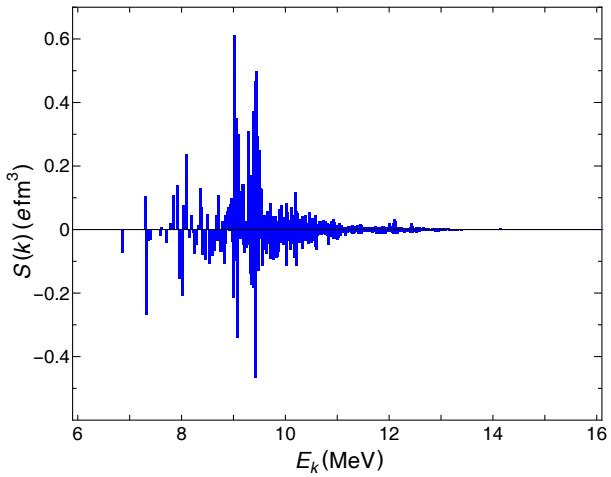

Fig. 12. (Color online) Strength function for the Schiff moment operator in ^{129}Xe from ref. [433].

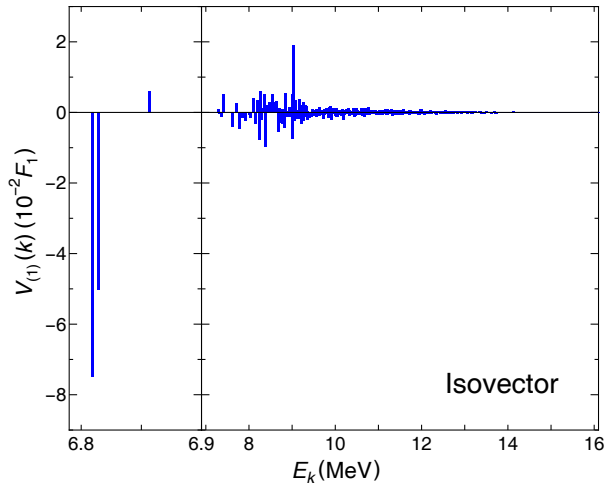

Fig. 13. (Color online) Off-diagonal potential matrix elements between $1/2^+_1$ state and $1/2^-_k$ state within the energy ranges below 6.9 MeV (left panel) and above 6.9 MeV (right panel) from ref. [433].

NSM at all since there are no strong NSM strength functions in that corresponding regime. In fig. 14 the partial contributions to the NSMs are shown and their total sums, respectively for isoscalar ($I = 0$) and isotensor ($I = 2$) two-body interactions. All the three isospin NSMs resemble to one another, but especially isovector and isotensor moments look quite similar to each other besides absolute values.

The contribution to the NSM also comes from the intrinsic d_N. By assuming the intrinsic nucleon EDM, the NSMs are evaluated for the $1/2^+_1$ states in Xe isotopes, which are shown in fig. 15. These factors for neutrons are positively large for ^{135}Xe, and negative for ^{129}Xe. For all the nuclei, the factors for protons are almost zero. $s^p_{\rm int} = +0.00156\,{\rm fm}^2$ and $s^n_{\rm int} = -0.09420\,{\rm fm}^2$ are obtained for ^{129}Xe.

There is one limitation which requires better discussion, namely, limitations of the model space used in the

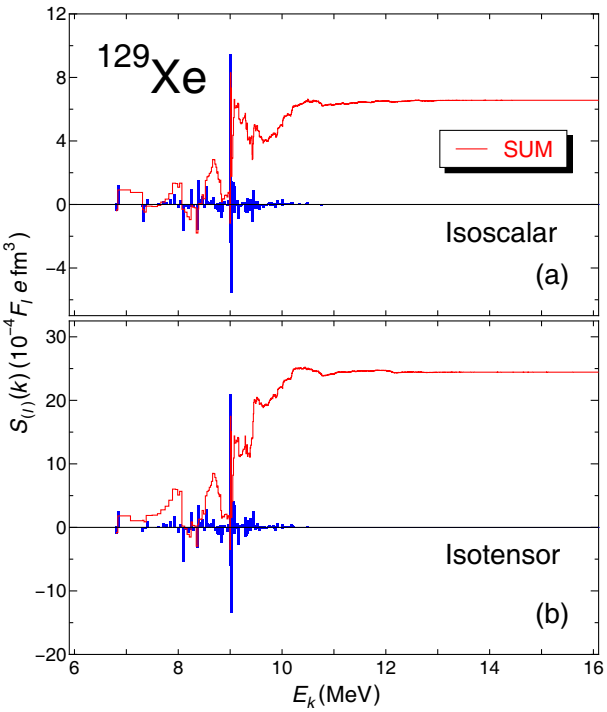

Fig. 14. (Color online) Same as in fig. 10, but for the (a) isoscalar ($I = 0$) and (b) isotensor ($I = 2$) type two-body interactions from ref. [433].

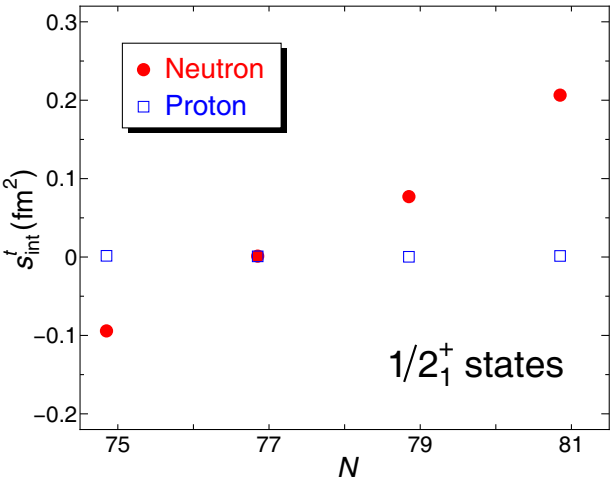

Fig. 15. (Color online) The factors $s^t_{\rm int}$ ($t = p$ or n) for the Xe isotopes. The circles and squares represent the $s^n_{\rm int}$ and $s^p_{\rm int}$ values, respectively from ref. [433].

shell model. The density of the $1/2^-$ states after 12 MeV, presented in fig. 11, is a result of the model space cutoff. It is a question whether the model space is rich enough for the converged determination of the NSMs.

Only one negative parity pair with different kinds are considered as in eq. (169). It should be examined how the bell-shape density of the $1/2^-$ states, presented in fig. 11 is large enough to accommodate the most contribution to the NSMs.

In order to consider all the intermediate states in eq. (175), the summation is carried out using the closure

Table 11. Coefficients a_T in units of $10^{-3}\,e\,\mathrm{fm}^3$ $(I=0,1,2)$ obtained by the closure approximation from ref. [433].

Nucleus	^{129}Xe	^{131}Xe	^{133}Xe	^{135}Xe
Isoscalar $(I=0)$	0.701	0.691	0.666	0.733
Isovector $(I=1)$	0.501	0.448	0.394	0.379
Isotensor $(I=2)$	2.30	2.00	1.70	1.54

Table 12. Coefficients a_T in units of $10^{-3}\,e\,\mathrm{fm}^3$ $(I=0,1,2)$ from ref. [433].

Nucleus	^{129}Xe	^{131}Xe	^{133}Xe	^{135}Xe
Isoscalar $(I=0)$	0.507	0.514	0.464	0.630
Isovector $(I=1)$	0.399	0.352	0.285	0.323
Isotensor $(I=2)$	1.89	1.60	1.24	1.31

approximation. Here the denominator $E_1^{(+)}-E_k^{(-)}$ is set constant as a representative value $\langle E\rangle=\langle E_1^{(+)}-E_k^{(-)}\rangle$. Using this approximation, the NSM is expressed as

$$S^{\mathrm{clo}}_{\mathrm{ch}(I)}=\sum_{k=1}\frac{\langle\frac{1}{2}\,1^+|\hat{S}_{\mathrm{ch},z}|\frac{1}{2}\,k^-\rangle\langle\frac{1}{2}\,k^-|V^{PT}_{\pi(I)}|\frac{1}{2}\,1^+\rangle}{\langle E\rangle}+\mathrm{c.c.}$$
$$=\frac{\langle\frac{1}{2}\,1^+|\hat{S}_{\mathrm{ch},z}V^{PT}_{\pi(I)}|\frac{1}{2}\,1^+\rangle}{\langle E\rangle}+\mathrm{c.c.}, \tag{180}$$

where the identity $\sum_{k=1}|\frac{1}{2}\,k^-\rangle\langle\frac{1}{2}\,k^-|=1$ is used. As shown in figs. 10 and 14, the contribution to the NSM $S_{(I)}(k)$ is dominant around the excitation energy $E_k(=E_k^{(-)}-E_1^{(+)})=9.0\,\mathrm{MeV}$. Thus $\langle E\rangle=-9.0\,\mathrm{MeV}$ is adopted.

The NSMs using the closure approximation are shown in table 11. Each value is consistently about 1.3 times larger than the corresponding one shown in table 12, which validates their discussion that the model space is rich enough to accommodate the most contribution to the NSMs.

4.2.4 Recent shell model calculation with configuration mixing

In a recent paper [437] any intermediate state given in eq. (143) is represented as a one-particle and one-hole excited state ($1p1h$-state) from the state $|I_1^+\rangle$. Since the NSM operator is a one-body operator working only on protons, it is enough to consider proton excited $1p1h$-states. To evaluate the NSM in eq. (143), the k-th intermediate $1p1h$-state is approximately given as

$$\left|I_k^-\right\rangle\sim\left|(ij)K;I^-\right\rangle=N_{ij}^{(K)}\left[\left[c^\dagger_{i\pi}\tilde{c}_{j\pi}\right]^{(K)}\otimes\left|I_1^+\right\rangle\right]^{(I)}, \tag{181}$$

where $c^\dagger_{i\pi}$ $(c_{j\pi})$ represents the proton creation (annihilation) operator in the orbital i (j), with $\tilde{c}_{jm}=(-1)^{j-m}c_{j-m}$. Namely, a $1p1h$-state with spin K, in which one proton excites from orbital j to orbital i by the NSM operator, is coupled with the nuclear ground state $|I_1^+\rangle$ to form an excited state $|(ij)K;I^-\rangle$. $N_{ij}^{(K)}$ is the normalization constant determined as

$$\langle(ij)K;I^-|(ij)K;I^-\rangle=1.$$

Here K can take 1 or 0 for $I=1/2$.

Originally an intermediate state should satisfy $H|I_k^-\rangle=E_k^-|I_k^-\rangle$, where H is the original shell model Hamiltonian. Here it is approximately assumed that $H|(ij)K;I^-\rangle=(\varepsilon_i-\varepsilon_j+E_1^+)|(ij)K;I^-\rangle$, where ε_j (ε_i) represents the single-particle energy in the orbital j (i). With this approximation in mind, eq. (143) is written as

$$S_{(T)}=\sum_{Kij}\frac{\langle I_1^+|S_0^{(1)}|(ij)K;I^-\rangle\langle(ij)K;I^-|V^{PT}_{\pi(T)}|I_1^+\rangle}{\Delta E_{ij}}+\mathrm{c.c.} \tag{182}$$

Here the denominator ΔE_{ij} is explicitly written as $\Delta E_{ij}\equiv\varepsilon_j-\varepsilon_i$.

Here three types of $1p1h$-excitations are considered. The first type is a set of excitations from an orbital between 50 and 82 to an orbital over 82. These excitations are called *type-I* excitations. The second type is a set of excitations from an orbital under 50 to an orbital between 50 and 82. These excitations are called *type-II* excitations. The third type is a set of excitations from an orbital under 50 to an orbital over 82. These excitations are called *type-III* excitations. Note that excitations among orbitals between 50 and 82 are vanished since these orbitals are not connected by the NSM operator.

For the type-I excitation, an intermediate state is explicitly written as

$$\left|(ph)K;I^-\right\rangle_{\text{type-I}}=N_{ph}^{(K)}\left[\left[a^\dagger_{p\pi}\tilde{c}_{h\pi}\right]^{(K)}\otimes\left|I_1^+\right\rangle\right]^{(I)}. \tag{183}$$

Here $a^\dagger_{p\pi}$ represents the proton creation operator in the orbital p, where p indicates an orbital over 82. $\tilde{c}_{h\pi}$ represents the proton annihilation operator in the orbital h, where h indicates an orbital between 50 and 82. For the type-II excitation, an intermediate state is written as

$$\left|(ph)K;I^-\right\rangle_{\text{type-II}}=N_{ph}^{(K)}\left[\left[c^\dagger_{p\pi}\tilde{b}_{h\pi}\right]^{(K)}\otimes\left|I_1^+\right\rangle\right]^{(I)}. \tag{184}$$

Here $c^\dagger_{p\pi}$ represents the proton creation operator in an orbital p, where p indicates an orbital between 50 and 82. $\tilde{b}_{h\pi}$ represents the proton annihilation operator in the orbital h, where h indicates an orbital below 50. For the type-III excitation, an intermediate state is written as

$$\left|(ph)K;I^-\right\rangle_{\text{type-III}}=N_{ph}^{(K)}\left[\left[a^\dagger_{p\pi}\tilde{b}_{h\pi}\right]^{(K)}\otimes\left|I_1^+\right\rangle\right]^{(I)}. \tag{185}$$

Here $a^\dagger_{p\pi}$ represents the proton creation operator in an orbital p, where p indicates an orbital over 82. $\tilde{b}_{h\pi}$ represents the proton annihilation operator in the orbital h, where h indicates an orbital below 50.

In the study, all orbitals below the magic number 50 are considered for core orbitals. However, $0d_{3/2}$, $1s_{1/2}$, and $0s_{1/2}$ orbitals are not connected by the NSM operator. For over-shell orbitals over the magic number 82, all orbitals up to $8\,\hbar\omega$ from the bottom are considered. However, $2d_{5/2}$, $0j_{15/2}$, $0j_{13/2}$, $1h_{11/2}$, $0k_{15/2}$, $0k_{17/2}$, $2g_{7/2}$, $3d_{3/2}$, $3d_{5/2}$, and $4s_{1/2}$ orbitals are also not connected by the Schiff moment operator. Orbitals over $8\,\hbar\omega$ have less contributions to the NSM because the NSM operator proportionals to the r-square radius and these orbitals are not connected to low-lying orbitals by the NSM operator.

The energy of each single-particle orbital is taken from the Nillson energy as

$$\epsilon_{n\ell j} = \left(2n + \ell + \frac{3}{2}\right)\hbar\omega - \kappa\left(2\boldsymbol{\ell}\cdot\boldsymbol{s} + \mu\left(\boldsymbol{\ell}^2 - \left\langle\boldsymbol{\ell}^2\right\rangle_N\right)\right)\hbar\omega, \tag{186}$$

with $\kappa = 0.0637$ and $\mu = 0.60$, where $\langle\boldsymbol{\ell}^2\rangle_N = \frac{1}{2}N(N+3)$ with the primary quantum number N and $\hbar\omega = 41A^{-1/3}\,\mathrm{MeV}$.

To analyze contributions to the NSMs from each orbital, a partial contribution of the NSM from any orbital (h) between 50 and 82 to a specific orbital (p) over 82 (type-I excitations) is defined in terms of $\bar{g}^{(T)}g$ as

$$s^{\text{type-I}}_{(T)}(p) = a^{\text{type-I}}_{(T)}(p)\,\bar{g}^{(T)}g, \tag{187}$$

where

$$s^{\text{type-I}}_{(T)}(p) = \sum_{Kh}\frac{\langle I_1^+|S_0^{(1)}|(ph)K;I^-\rangle\langle(ph)K;I^-|V^{PT}_{\pi(T)}|I_1^+\rangle}{\Delta E_{ph}} + \text{c.c.}, \tag{188}$$

and $a^{\text{type-I}}_{(T)}(p)$'s are coefficients so determined in evaluating the partial NSM $s^{\text{type-I}}_{(T)}(p)$.

A partial contribution to any orbital (p) between 50 and 82 from the specific orbital (h) below 50 (type-II excitations) is defined as

$$s^{\text{type-II}}_{(T)}(h) = a^{\text{type-II}}_{(T)}(h)\,\bar{g}^{(T)}g, \tag{189}$$

where

$$s^{\text{type-II}}_{(T)}(h) = \sum_{Kp}\frac{\langle I_1^+|S_0^{(1)}|(ph)K;I^-\rangle\langle(ph)K;I^-|V^{PT}_{\pi(T)}|I_1^+\rangle}{\Delta E_{ph}} + \text{c.c.} \tag{190}$$

A partial contribution from the specific orbital (h) below 50 to any orbital (p) over 82 (type-III excitations) is also defined as

$$s^{\text{type-III}}_{(T)}(h) = a^{\text{type-III}}_{(T)}(h)\,\bar{g}^{(T)}g, \tag{191}$$

Table 13. Calculated results of $a_{(T)}$ for the nuclear ground state $1/2^+$ state (in units of $10^{-3}e\,\mathrm{fm}^3$) from ref. [437]. Previous results ($a^{\text{prev}}_{(T)}$) are taken from ref. [433].

	T	$a^{\text{type-I}}_{(T)}$	$a^{\text{type-II}}_{(T)}$	$a^{\text{type-III}}_{(T)}$	$a_{(T)}$	$a^{\text{prev}}_{(T)}$
	0	2.357	0.670	−1.057	1.969	0.630
^{135}Xe	1	1.297	1.693	−0.602	2.389	0.323
	2	5.427	9.490	−2.554	12.363	1.31
	0	1.812	1.716	−1.047	2.481	0.464
^{133}Xe	1	0.949	1.510	−0.578	1.882	0.285
	2	3.982	7.343	−2.419	8.906	1.24
	0	1.575	2.097	−0.968	2.704	0.514
^{131}Xe	1	0.787	1.282	−0.530	1.539	0.352
	2	3.145	5.596	−2.177	6.564	1.60
	0	1.322	2.897	−0.978	3.242	0.507
^{129}Xe	1	0.586	1.140	−0.522	1.204	0.399
	2	2.192	3.940	−1.961	4.172	1.89

where

$$s^{\text{type-III}}_{(T)}(h) = \sum_{Kp}\frac{\langle I_1^+|S_0^{(1)}|(ph)K;I^-\rangle\langle(ph)K;I^-|V^{PT}_{\pi(T)}|I_1^+\rangle}{\Delta E_{ph}} + \text{c.c.} \tag{192}$$

Using these definitions, the NSM is given as

$$S = \sum_T\left(s^{\text{type-I}}_{(T)} + s^{\text{type-II}}_{(T)} + s^{\text{type-III}}_{(T)}\right), \tag{193}$$

with

$$s^{\text{type-I}}_{(T)} = \sum_p s^{\text{type-I}}_{(T)}(p), \tag{194}$$

$$s^{\text{type-II}}_{(T)} = \sum_h s^{\text{type-II}}_{(T)}(h), \tag{195}$$

$$s^{\text{type-III}}_{(T)} = \sum_h s^{\text{type-III}}_{(T)}(h). \tag{196}$$

Table 13 shows the calculated results of $a_{(T)}$ for the lowest $I = 1/2$ states of Xe isotopes. Here, using eqs. (187), (189), and (191), $a_{(T)}$ is given as

$$a_{(T)} = a^{\text{type-I}}_{(T)} + a^{\text{type-II}}_{(T)} + a^{\text{type-III}}_{(T)}, \tag{197}$$

with

$$a^{\text{type-I}}_{(T)} = \sum_p a^{\text{type-I}}_{(T)}(p), \tag{198}$$

$$a^{\text{type-II}}_{(T)} = \sum_h a^{\text{type-II}}_{(T)}(h), \tag{199}$$

and

$$a^{\text{type-III}}_{(T)} = \sum_h a^{\text{type-III}}_{(T)}(h). \tag{200}$$

The contributions of the core excitations are a few times larger than those from the over-shell excitations for most of the components. The isotensor ($T = 2$) components are largest for all nuclei.

As a more elaborate configuration mixing framework of the shell model [438], NSMs for the ground $1/2^+$ states around the mass 130 are calculated in terms of the nuclear shell model. The intrinsic NSM is evaluated as

$$S = s_p d_p + s_n d_n, \tag{201}$$

where d_p and d_n are the electric dipole moments of the proton and the neutron, respectively. The factors s_p and s_n for the intrinsic NSM of ^{129}Xe are calculated as $s_p = +0.0061$ and $s_n = -0.3169$ (in fm^2).

4.2.5 Reliability, accuracy and uncertainty of the NSM calculations

In this subsection we discuss the accuracy, reliability and uncertainty of the theoretical calculations on the NSM.

First of all, it is noted that the atoms considered in this article are closed-shell atoms, whereas the corresponding nucleus is no more closed for both neutrons and protons. Therefore the treatment in nuclear physics is expected to be different from atomic physics even if many-body problems should be solved in both physics.

The accurate estimation of the NSM is very tough in nuclear physics. There are various things we have to consider when arguing the accuracy and the reliability of the calculations on the NSM.

We start from the following nuclear Hamiltonian (139):

$$H = H_0 + \hat{V}^{PT}_{\pi(T)},$$

where H_0 is the nuclear strong interaction which conserves P and T.

i) One major problem here is how to derive (calculate) the nuclear strong interaction H_0 in a nucleus, namely in the nuclear media. Firstly the difference between the atom and the nucleus is in that we do not know precisely the interactions between nucleons. For atoms the interaction is the Coulomb force, but the nuclear force is considered to be a Van der Waals force derived from the fundamental QCD interaction among quarks and gluons. Secondly we cannot use the bare interaction between free nucleons because the nuclear interaction should be modified according to the medium effects. This medium effect is taken into account by the Brueckner-Bethe-Goldstone (BBG) many-body theory [422]. However, for nuclei in the medium and heavy region such as ^{129}Xe and ^{199}Hg, it is a hard task to obtain the effective interaction through BBG theory. Thus we have to utilize some kinds of phenomenological interactions such as the Skyrme interactions, surface delta interaction or pairing and quadrupole ($P + QQ$) interactions. Usually for the mean-field theories such as HF or HFB, the Skyrme interactions are often used, but there are many kinds of Skyrme interactions. For more elaborate calculations, the surface delta interaction and the $P + QQ$ interaction are often used in the nuclear shell model. The uncertainty on the NSM coming from these phenomenological interactions are supposed to be not so large because the results calculated by using these interactions are tested by comparing them with the experimental data, such as nuclear energy spectra, electro-magnetic moments and transitions. On the other hand, in some simple mean-field theories the binding energy is the only experimental source to be compared with theory and the reliability is relatively small compared to the nuclear shell model.

ii) The second problem is related to the CP-odd nuclear force $\hat{V}^{PT}_{\pi(T)}$ appearing in eq. (139) obtained at the hadron scale. The strength of the interaction used in the calculations of the CP-odd moments of heavy nuclei should not be the same with the bare CP-odd nuclear force. This is the same problem discussed above. For the actual strength of the CP-odd nuclear force uncertainty is expected to be large and we have no method to estimate its strength at present.

Since the PT-violating interaction is so weak compared to the nuclear force, the formula (143) by perturbation theory is good enough in the evaluation of the NSM,

$$S_{\rm ch} = \sum_{k=1} \frac{\langle I_1^+|\hat{S}_{{\rm ch},z}|I_k^-\rangle\langle I_k^-|\hat{V}^{PT}_{\pi(T)}|I_1^+\rangle}{E_1^+ - E_k^-} + \text{c.c.}$$

iii) The third problem is related to the ground-state wave functions $|I_1^+\rangle$ and the intermediate states $|I_k^-\rangle$. In order to obtain accurate eigenfunctions, Hamiltonian (139) should be diagonalized assuming a suitable set of basis states. This cannot be done exactly due to the huge dimension of the configurations. Therefore the eigenfunctions can be obtained only approximately. There are basically two ways to calculate the ground-state wave functions. One is to use mean-field theories such as HF or HFB theories. Another is to use theories beyond the mean-field (BMF) theories. In mean-field theories the wave functions are obtained with comparative ease by breaking symmetries of rotation and the particle-number, but the wave functions do not have specific spin and parity or particle-number, which are essential in a solitary system like a nucleus. It is necessary to restore these symmetries.

In the following we discuss the accuracy of the results in the cases of ^{199}Hg and ^{129}Xe. For ^{199}Hg, the results in table 1 and 2 are given by the same group [424]. The results in table 1 are calculated using a simple shell model, where the whole nuclear state is determined by the last neutron in the orbital $p_{1/2}$ in the major shell of 50 and 82 without considering other nucleon's effects. The results in table 2 are calculated by considering other nucleon's effects and as can be seen in the tables ten times difference is present between them. Certainly, the results in table 2 are more reliable in comparison with those in table 1. The results in table 4 are the most elaborate ones up to date for the ^{199}Hg, but the method is based on the mean-field theories and analyses using BMF theories are expected. The results in table 7 are given by mean-field theories [431].

Table 14. The neutron quenching factor $\langle\hat{\sigma}_z^n\rangle$ for each nuclear $1/2_1^+$ state from ref. [440].

Nucleus	$\langle\hat{\sigma}_z^n\rangle$
^{129}Xe	0.2306
^{131}Xe	0.4644
^{133}Xe	0.6546
^{135}Xe	0.9777
^{129}Ba	0.1090
^{131}Ba	0.3537
^{133}Ba	0.4360
^{135}Ba	0.9811

Even signs of the isovector components are different according to the various usage of the Skyrme interactions.

For ^{129}Xe the results in tables 11, 12 and 13 are calculated by the same group [433, 437] based on the shell model. The results in table 12 are given in terms of the PTSM calculations [433] using the effective $P + QQ$ interaction. The results in table 11 are given by the closure approximation where intermediate energies E_k^- are set constant as $\langle E_k^-\rangle$. Then the summation over intermediate states are exactly evaluated as in eq. (180). The results in table 13 are the most elaborate ones using one-particle one-hole states for intermediate states $|I_k^-\rangle$. The results are most reliable up to now and only a factor of two or three times difference compared to the results in table 2.

4.3 Nuclear spin matrix elements

To evaluate the effect of the nucleon spin-dependent CP-odd e-N interaction, namely $C_N^{\rm T}$ and $C_N^{\rm PS}$, on the atomic EDM, the values of the nuclear spin matrix elements $\langle\Psi|\sigma^p|\Psi\rangle$ and $\langle\Psi|\sigma^n|\Psi\rangle$ are required. In the simple shell model, they are given as [197]

$$\left\langle \left(l\frac{1}{2}\right)j,\ m=j\,|\sigma_z|\,\left(l\frac{1}{2}\right)j,\ m=j\right\rangle = \begin{cases} 1 & (j=l+1/2), \\ -\dfrac{j}{j+1} & (j=l-1/2), \end{cases} \tag{202}$$

where σ_z is the single valence nucleon spin-operator. The nuclear spin matrix element is also useful in evaluating the nucleon EDM effect to the nuclear EDM. An extension of the above formula using the magnetic moment are also available [439].

In refs. [438,440], the nuclear spin matrix elements for the lowest $1/2^+$ states of Xe and Ba isotopes are calculated in terms of the nuclear shell model with configuration mixing. Values for several Xe and Ba isotopes (calculated in the context of the nuclear EDM) are given in table 14 taken from ref. [440]. We see that the quenching of the nucleon spin becomes important in the nucleus as the nucleon number goes away from the magic number. This is due to the superposition of configurations where the nucleon spin interferes destructively, due to the mixing with the orbital angular momentum. This suppression means that the effect of $C_N^{\rm T}$ and $C_N^{\rm PS}$ are attenuated in nuclei far from magic numbers. The nuclear spin matrix elements are still unknown for many nuclei, although their evaluation is easier than the nuclear Schiff moment. It is therefore an important future subject to discuss for reducing the theoretical uncertainty of the atomic EDM.

4.4 Enhancement due to octupole deformation

A charged particle, residing outside of the nucleus at distance r like an electron, can see the potential due to electromagnetic interactions within the nucleus as [49, 441]

$$\phi(r) = \int \mathrm{d}^3 r_N \frac{\rho(r_N)}{|r - r_N|}\,. \tag{203}$$

Carrying out the multipole expansion of $\frac{1}{|r-r_N|}$ can give rise to both P,T-odd and even potential terms. The first and dominant P,T-odd term can arise as

$$\phi(r) = -\int \mathrm{d}^3 r_N \rho(r_N) \left(\boldsymbol{r}_N \cdot \boldsymbol{\nabla}_r \frac{1}{r}\right). \tag{204}$$

As per the Schiff theorem, this term will exactly cancel out with the NSM contribution for a point-like nucleus. In order to obtain the P,T-odd interaction term from here, it is therefore necessary to account the next leading-order term, which yields

$$\phi_{oct}(r) \simeq -\frac{1}{6}\int \mathrm{d}^3 r_N \rho(r_N) r_i r_j r_k \nabla_i \nabla_j \nabla_k \frac{1}{r}\,, \tag{205}$$

where the subscript *oct* implies that it corresponds to contribution from the electric octupole moment (EOM) for which the EOM tensor is given by

$$O_{ijk} = \int \mathrm{d}^3 r_N \rho(r_N) \times \left[r_i r_j r_k - \frac{1}{5}(\delta_{ij} r_k + \delta_{jk} r_i + \delta_{ki} r_j)\right]. \tag{206}$$

The EOM tensor O_{ijk} has three units of angular momentum, hence it can only exist in nuclei with spin $I \geq 3/2$, whereas the NSM can arise in nuclei with spin $I \geq 1/2$. Without the P,T-odd interactions the average value of the EOM for a rotational state in the laboratory system is zero. However, in the presence of such an interaction, the odd- and even-parity mixing of rotational doublet states gives rise to a finite value of the EOM. In particular for atoms with nuclei that have almost degenerate rotational doublets, there is a large enhancement of the EOM leading to an increase in the size of the observable EDMs of the atoms. This contribution needs to be extracted before estimating limits on various nuclear and particle physics parameters from the observed atomic EDMs. From preliminary investigations it has been found that the EOM enhances the EDMs in ^{223}Ra, ^{225}Ra and ^{223}Rn atoms by 400, 300 and 1000 times more than due to the other P,T-odd interactions [49, 441, 442].

5 Atomic structure calculations

5.1 P,T-odd sources in atoms

As has been discussed before, the dominant P,T-odd interactions in an atomic system can come from three important sources [36,37,52,392]. They are i) EDMs of constituent particles such as the d_e, d_n and d_p, ii) P,T-odd e-N and N-N interactions, and iii) P,T-odd pion exchange interactions.

Considering the dominant P,T-odd interactions in the diamagnetic atoms, the interaction Hamiltonian due to the NSM for the exchange of pions is given by [49,443]

$$H_{at}^{N} = \frac{3\mathbf{S}\cdot\mathbf{r}}{B_4}\rho(r), \tag{207}$$

where $B_4 = \int_0^\infty \mathrm{d}r r^4\rho(r)$, and similarly by adding the coherent contributions from the individual nucleons the net electron-nucleus T-PT interaction Hamiltonian is given by

$$H_{at}^{T} = i\sqrt{2}G_F C_{at}^{T}\sum_e \sigma_N\cdot\boldsymbol{\gamma}\rho(r), \tag{208}$$

where C_{at}^{T} is the T-PT electron-nucleus and $\sigma_N = \langle\sigma_N\rangle\mathbf{I}/I$ is the Pauli spinor of the nucleus.

Nevertheless, in the diamagnetic atoms the d_e and the P,T-odd or P,CP-odd–type S-PS–type e-N interaction corresponding to term with the coupling C_N^{SP} of eq. (70) can also contribute to the atomic EDM to some extent, mainly through the hyperfine-induced interaction. Since these are not the dominant contributions in these atoms, we estimate their contributions using analytical formulas known in the literature instead of performing rigorous numerical calculations.

The contribution of the electron EDM can analytically be related to the T-PT–type P,T-odd e-N interaction (*i.e.*, the term with the coupling C_N^{T} of eq. (70)) as [7,49,444]

$$d_e \leftrightarrow \frac{3m_N e}{7\pi\alpha_{\mathrm{em}}\mu}\frac{R}{R-1}\frac{G_F}{\sqrt{2}} \times\left(C_p^{\mathrm{T}}\sum_p\langle\Psi|\boldsymbol{\sigma}_p|\Psi\rangle + C_n^{\mathrm{T}}\sum_n\langle\Psi|\boldsymbol{\sigma}_n|\Psi\rangle\right), \tag{209}$$

where $\mathcal{R}$ is the atomic enhancement factor to the atomic EDM due to T-PT e-N interaction and μ_I is the nuclear magnetic moment in unit of nuclear magneton μ_N. The nuclear spin matrix elements $\langle\Psi|\boldsymbol{\sigma}_N|\Psi\rangle$ $(N = p, n)$ is the expectation value of the nucleon spin polarized in the z-direction.

Analogously, the contribution of C_N^{SP} is analytically related to C_N^{T} by

$$\left(\frac{Z}{A}C_p^{\mathrm{SP}} + \frac{A-Z}{A}C_n^{\mathrm{SP}}\right) \leftrightarrow \frac{1.9\times10^3}{(1+0.3Z^2\alpha_{\mathrm{em}}^2)A^{-2/3}\mu} \times\left(C_p^{\mathrm{T}}\sum_p\langle\Psi|\boldsymbol{\sigma}_p|\Psi\rangle + C_n^{\mathrm{T}}\sum_n\langle\Psi|\boldsymbol{\sigma}_n|\Psi\rangle\right). \tag{210}$$

Assuming same number of protons and neutrons in the atom and their interaction strengths are of similar order, we can conveniently express [443]

$$C_{at}^{P} \leftrightarrow 3.8\times10^3\times\frac{A^{1/3}}{Z}C_{at}^{T}, \tag{211}$$

where C_{at}^{P} is the corresponding P,T-odd S-PS coupling constant for the electron-nucleus interaction. Thus, with the knowledge of C_{at}^{T} and its enhancement factor, we can estimate contributions due to C_{at}^{P} and d_e in the diamagnetic atoms. Hence, we only intend to estimate the C_{at}^{T} coupling coefficient by accounting the interaction Hamiltonian given by eq. (208).

Again, the magnetic quadrupole moment (MQM) of the nucleus can also contribute to the EDM of diamagnetic atoms through hyperfine-induced interaction, but that contribution will be extremely small and has been neglected here.

5.2 Atomic many-body methods

The EDM of the ground-state wave function ($|\Psi_0\rangle$) in an atom is given by

$$d_{at} = \frac{\langle\Psi_0|D|\Psi_0\rangle}{\langle\Psi_0|\Psi_0\rangle}, \tag{212}$$

where D is the electric dipole moment operator. The evaluation of $|\Psi_0\rangle$ should take into consideration the electromagnetic and weak interactions in the atomic systems. In actual practice, the dominant one-photon electromagnetic interactions are included in the first step followed by if necessary higher-order relativistic effects and the basic quantum electrodynamics (QED) corrections. The much weaker P,T-odd interactions are added subsequently only to first order either in a perturbative or non-perturbative framework. Such an approach is computationally simpler than including the P and T violating in the zeroth order Hamiltonian as it would would involve atomic wave functions of a definite parity in the calculations as opposed to wave functions of mixed parity which would result from the latter approach.

The starting point of the relativistic atomic many-body calculations is the Dirac-Coulomb (DC) Hamiltonian which is

$$H^{DC} = \sum_i\left[c\boldsymbol{\alpha}_i\cdot\mathbf{p}_i + (\beta_i-1)c^2 + V_n(r_i) + \sum_{j>i}\frac{1}{r_{ij}}\right], \tag{213}$$

where $\boldsymbol{\alpha}$ and β are the usual Dirac matrices and $V_n(r)$ represents for the nuclear potential. We evaluate the nuclear potential considering the Fermi-charge distribution defined by

$$\rho(r) = \frac{\rho_0}{1+e^{(r-b)/a}}, \tag{214}$$

for the normalization factor ρ_0, the half-charge radius b and $a = 2.3/4(\ln 3)$ is related to the skin thickness. The

half-charge radius is determined using the relation

$$b = \sqrt{\frac{5}{3}r_{rms}^2 - \frac{7}{3}a^2\pi^2} \tag{215}$$

and the root mean square (rms) charge radius of the nucleus is evaluated by

$$r_{rms} = 0.836A^{1/3} + 0.570. \tag{216}$$

in fm.

The contribution from the frequency-independent Breit interaction is estimated by adding the term

$$V_B = -\sum i,j > i\frac{1}{2r_{ij}}\{\boldsymbol{\alpha}_i\cdot\boldsymbol{\alpha}_j + (\boldsymbol{\alpha}_i\cdot\hat{\mathbf{r}}_{ij})(\boldsymbol{\alpha}_j\cdot\hat{\mathbf{r}}_{ij})\}, \tag{217}$$

to the DC Hamiltonian; *i.e.* $H^{at} \equiv H^{DC} + V_B$.

We have also estimated the lower-order quantum electrodynamic corrections by considering the following QED potentials in the atomic Hamiltonian; *i.e.* $H^{at} \equiv H^{DC} + V_B + V_{QED}$ with $V_{QED} = \sum_i (V_U(r_i) + V_{WK}(r_i) + V_{SE}^{ef}(r_i) + V_{SE}^{mg}(r_i))$ in a manner similar to that described in refs. [445, 446] but for the above nuclear Fermi-charge distribution. In this approximate approach, the lower-order vacuum polarization (VP) effects are taken as the sum of the Uehling ($V_U(r)$) and the Wichmann-Kroll ($V_{WK}(r)$) potentials, which are given by

$$V_U(r) = -\frac{2\alpha^2}{3r}\int_0^\infty \mathrm{d}x\, x\,\rho(x)\int_1^\infty \mathrm{d}t\sqrt{t^2-1} \times\left(\frac{1}{t^3}+\frac{1}{2t^5}\right)\left[e^{-2ct|r-x|} - e^{-2ct(r+x)}\right] \tag{218}$$

and

$$\begin{aligned} V_{WK}(r) = -\frac{8Z^2\alpha^4}{9r}(0.092)\int_0^\infty \mathrm{d}x\, x\,\rho(x) \\ \times\big(0.22\big\{\arctan[1.15(-0.87+2c|r-x|)] \\ -\arctan[1.15(-0.87+2c(r+x))]\big\} \\ +0.22\big\{\arctan[1.15(0.87+2c|r-x|)] \\ -\arctan[1.15(0.87+2c(r+x))]\big\} \\ -0.11\big\{\ln[0.38-0.87c|r-x|+c^2(r-x)^2] \\ -\ln[0.38-0.87c(r+x)+c^2(r+x)^2]\big\} \\ +0.11\big\{\ln[0.38+0.87c|r-x|+c^2(r-x)^2] \\ -\ln[0.38+0.87c(r+x)+c^2(r+x)^2]\big\}\big). \end{aligned} \tag{219}$$

The contributions from the self-energy (SE) interaction are evaluated by considering the contributions due to the electric form-factor given by

$$\begin{aligned} V_{SE}^{ef}(r) = -A(Z)(Z\alpha)^4 e^{-Zr} + \frac{B(Z,r)\alpha^2}{r}\int_0^\infty \mathrm{d}x x\rho(x) \\ \times\int_1^\infty \mathrm{d}t\frac{1}{\sqrt{t^2-1}}\left\{\left(\frac{1}{t}-\frac{1}{2t^3}\right)\right. \\ \left.\times\left[\ln(t^2-1)+4\ln\left(\frac{1}{Z\alpha}+\frac{1}{2}\right)\right]-\frac{3}{2}+\frac{1}{t^2}\right\} \\ \times\left[e^{-2ct|r-x|}-e^{-2ct(r+x)}\right] \end{aligned} \tag{220}$$

and from the magnetic form-factor given by

$$\begin{aligned} V_{SE}^{mg}(r) = \frac{i\alpha}{4\pi c}\boldsymbol{\gamma}\cdot\boldsymbol{\nabla}_r\int_0^\infty \mathrm{d}^3x\,\rho(x) \\ \times\left[\left(\int_1^\infty \mathrm{d}t\frac{e^{-2tcR}}{Rt^2\sqrt{t^2-1}}\right)-\frac{1}{R}\right], \end{aligned} \tag{221}$$

where $A(Z) = 0.074 + 0.35Z\alpha$, $B(Z,r) = [1.071 - 1.97((Z-80)\alpha)^2 - 2.128((Z-80)\alpha)^3 + 0.169((Z-80)\alpha)^4]cr/(cr + 0.07(Z\alpha)^2)$ and $R = |\mathbf{r}-\mathbf{x}|$.

To incorporate the first-order corrections due to the P,T-odd weak interactions, we express the total Hamiltonian of the atom as

$$H = H^{at} + \lambda H^{PT}, \tag{222}$$

where H^{at} represents the atomic Hamiltonian; *i.e.* the DC Hamiltonian supplemented by higher-order relativistic corrections if necessary and λH^{PT} corresponds to either of the P,T-odd Hamiltonians given by eqs. (207) and (208). Here λ can be S or C_{at}^T for the respective Hamiltonian. The atomic wave function can be expressed as

$$|\Psi_0\rangle \approx \left|\Psi_0^{(0)}\right\rangle + \lambda\left|\Psi_0^{(1)}\right\rangle, \tag{223}$$

where nonlinear terms in λ have been neglected, and $|\Psi_0^{(0)}\rangle$ and $|\Psi_0^{(1)}\rangle$ are the wave functions of H^{at} and its first-order correction due to the P,T-odd interaction Hamiltonian, respectively. Hence eq. (212) is approximated as

$$d_{at} \simeq 2\lambda\frac{\langle\Psi_0^{(0)}|D|\Psi_0^{(1)}\rangle}{\langle\Psi_0^{(0)}|\Psi_0^{(0)}\rangle}. \tag{224}$$

The actual quantity that is relevant for the calculation is

$$\mathcal{R} = d_{at}/\lambda = 2\frac{\langle\Psi_0^{(0)}|D|\Psi_0^{(1)}\rangle}{\langle\Psi_0^{(0)}|\Psi_0^{(0)}\rangle} \tag{225}$$

and it can be combined with the experimentally measured d_{at} values to determine λ.

The first-order perturbed wave function $|\Psi^{(1)}\rangle$ can be calculated by two different approaches. One is the sum-over-states approach, where we express

$$\left|\Psi_0^{(1)}\right\rangle = \sum_{I\neq 0}\left|\Psi_I^{(0)}\right\rangle\frac{\langle\Psi_I^{(0)}|H^{PT}|\Psi_0^{(0)}\rangle}{E_I^{(0)}-E_0^{(0)}}, \tag{226}$$

where $|\Psi_I^{(0)}\rangle$'s are the states other than $|\Psi_0^{(0)}\rangle$ of H^{at} with the energies $E_I^{(0)}$ and $E_0^{(0)}$, which are the intermediate state and the ground-state energies, respectively. The advantage of this approach is that one can include only the dominant contributions which come from the low-lying states. However, this method cannot account for contributions from the core, the high-lying excited states including the continuum which can be significant in heavy atomic

systems. The other approach, which is often more desirable is to determine the first-order perturbed wave function by solving the following inhomogeneous equation:

$$\left(H^{at} - E_0^{(0)}\right)\left|\Psi_0^{(1)}\right\rangle = \left(E_0^{(1)} - H^{PT}\right)\left|\Psi_0^{(0)}\right\rangle = -H^{PT}\left|\Psi_0^{(0)}\right\rangle, \quad (227)$$

where the first-order perturbed energy vanishes as H^{PT} is an odd-parity operator. It is well known that the accurate calculation of $|\Psi_0^{(0)}\rangle$ in heavy atomic systems is challenging owing to the presence of the two-body Coulomb and Breit interactions. So establishing suitable many-body methods to determine $|\Psi_0^{(0)}\rangle$ and its correction $|\Psi_0^{(1)}\rangle$ with the simultaneously inclusion of electromagnetic and weak interactions are of immense interest.

We discuss some of the all-order relativistic many-body methods that have been employed to determine $\mathcal{R}$ in some of the atoms of experimental interest such as ^{129}Xe, ^{199}Hg, ^{223}Rn, and ^{225}Ra. Earlier, only simpler approximated many-body methods such as the relativistic third-order many-body perturbation theory (MBPT(3)) and the relativistic RPA were employed to determine these quantities in ^{129}Xe and ^{223}Rn [443,447,448]. These methods cannot accurately determine the values of $\mathcal{R}$ in other atoms like ^{199}Hg and ^{225}Ra, where pair-correlation effects contribute significantly. Two calculations, where important classes of correlation effects were included using a perturbed relativistic coupled-cluster (PRCC) method [449] and a hybrid approach of configuration interaction with finite-order many-body perturbation theory (CI+MBPT) [443] were employed to calculate the above quantities in ^{199}Hg the results were fairly close. In the combined CI+MBPT method, the initial single-particle wave functions were determined using the V^{N_c-2} potential with N_c as the total number of electrons and the electron correlation effects are accounted for by dividing the electrons into valence and core electrons. For ^{225}Ra, calculations using the CI+MBPT method with RPA corrections by Dzuba and coworkers [443,450] were performed. We shall discuss some of these methods below. It is also worth mentioning here that the PRCC method and a relativistic coupled-cluster method that will be described subsequently are similar; the difference between them lies in the treatment of the normalization of the wave function in the two theoretical approaches [451].

To obtain both $|\Psi_0^{(0)}\rangle$ and $|\Psi_0^{(1)}\rangle$, we first calculate the Dirac-Hartree-Fock (DF) wave function $|\Phi_0\rangle$ using the DF Hamiltonian

$$H_{DF}^{at} = \sum_i \left[c\boldsymbol{\alpha}_i \cdot \mathbf{p}_i + (\beta_i - 1)c^2 + V_{nuc}(r_i) + U_{DF}(r_i)\right] = \sum_i [h_0(r_i) + U_{DF}(r_i)], \quad (228)$$

with an average DF potential $U_{DF}(r)$, disregarding contributions from the residual interaction

$$V_{es} = \sum_{j>i}^{N} V(r_{ij}) - \sum_i U_{DF}(r_i). \quad (229)$$

where $V(r_{ij})$ is(are) the two-body interaction (Coulomb or Coulomb with Breit) interaction operator(s).

The DF potential and the single-particle wave function $|\phi_i^{(0)}\rangle$ of $|\Phi_0\rangle$ are obtained by solving the following equations:

$$\left\langle \phi_i^{(0)}\right| U_{DF}\left|\phi_j^{(0)}\right\rangle = \sum_b^{N_c}\left[\left\langle \phi_i^{(0)}\phi_b^{(0)}\right| V(r_{ij})\left|\phi_b^{(0)}\phi_j^{(0)}\right\rangle - \left\langle \phi_i^{(0)}\phi_b^{(0)}\right| V(r_{ij})\left|\phi_j^{(0)}\phi_b^{(0)}\right\rangle\right] \quad (230)$$

and

$$(h_0 + U_{DF})\left|\phi_i^{(0)}\right\rangle = \epsilon_i^{(0)}\left|\phi_i^{(0)}\right\rangle \quad (231)$$

simultaneously in a self-consistent procedure. In the above expression, when the sum is considered up to $N_c - M$, for M number of valence electrons M, this particular kind of DF potential is referred to as the V^{N_c-M} potential in the literature.

We now focus on the similarities and differences between some of the many-body methods that have been widely employed to treat V_{es} in order to calculate atomic properties. In particular, we present the pertinent details of certain methods that consider V_{es} to all orders. There are several ways to deal with this, but different approaches will capture various correlation effects corresponding to approximations in the levels of particle-hole excitations. For a comprehensive understanding of these theories, we take recourse to an approach based on the Bloch equation [452] in which one expresses

$$\left|\Psi_0^{(0)}\right\rangle = \Omega^{(0)}|\Phi_0\rangle = \sum_k^n \Omega^{(k,0)}|\Phi_0\rangle, \quad (232)$$

where $\Omega^{(0)}$ is known as the wave operator in the MBPT(n) method that accounts only up to n (say) orders of Coulomb interactions and k represents the order of V_{es} associated with each wave operator in a perturbative expansion of $\Omega^{(0)}$. In the presence of another external interaction, like the operator H^{PT}, the exact state can be written as

$$|\Psi_0\rangle = \Omega|\Phi_0\rangle = \sum_\beta^n \sum_\delta^m \Omega^{(\beta,\delta)}|\Phi_0\rangle, \quad (233)$$

where the perturbation expansion is described by n orders of V_{es} and m orders of H^{PT}. For our requirement of obtaining the first-order wave function due to H^{PT}, we have

$$\left|\Psi_0^{(1)}\right\rangle = \sum_\beta^n \Omega^{(\beta,1)}|\Phi_0\rangle. \quad (234)$$

To obtain the solutions for the wave operators, we use the following generalized Bloch equations:

$$\left[\Omega^{(\beta,0)}, H_{DF}^{at}\right]P = QV_{es}\Omega^{(\beta-1,0)}P - \sum_{m=1}^{\beta-1}\Omega^{(\beta-m,0)}PV_{es}\Omega^{(m-1,l)}P \quad (235)$$

and

$$\left[\Omega^{(\beta,1)}, H_{DF}^{at}\right] P = QV_{es}\Omega^{(\beta-1,1)}P + QD\Omega^{(\beta,0)}P - \sum_{m=1}^{\beta-1}\Big(\Omega^{(\beta-m,1)}PV_{es}\Omega^{(m-1,0)}P - \Omega^{(\beta-m,1)}PD\Omega^{(m,0)}P\Big), \quad (236)$$

where $P = |\Phi_0\rangle\langle\Phi_0|$ and $Q = 1 - P$. It implies that $\Omega^{(0,0)} = 1$, $\Omega^{(1,0)} = \sum_I \frac{\langle\Phi_I|V_{es}|\Phi_0\rangle}{E_I^{DF}-E_0^{DF}} = 0$ and $\Omega^{(0,1)} = \sum_I \frac{\langle\Phi_I|H^{PT}|\Phi_0\rangle}{E_I^{DF}-E_0^{DF}}$. Here $|\Phi_I\rangle$ with DF energy E_I^{DF} is an excited state with respect to $|\Phi_0\rangle$ and E_0^{DF} is the sum of DF single-particle energies.

In the case of the V^{N_c-M} potential, it requires a slightly different formalism to account for the electron correlation effects. In this approach, electrons are divided into a closed core and M valence electrons which are expected to play the major role in describing the dominant part of the electron correlation effects. The wave operator in such a scenario can be expressed as

$$\Omega = 1 + \chi_c + \chi_v, \quad (237)$$

where χ_c and χ_v are the operators that are responsible for excitations within the closed-core (say $|\Phi_c\rangle$) and among the valence orbitals (say $|\Phi_v\rangle$), respectively. It is necessary to solve a set of equations similar to those above by expanding the wave operators as

$$\chi_c = \sum_{\beta}^{n}\sum_{\delta}^{m}\chi_c^{(\beta,\delta)} \quad (238)$$

and

$$\chi_v = \sum_{\beta}^{n}\sum_{\delta}^{m}\chi_v^{(\beta,\delta)}. \quad (239)$$

Core-valence correlations must also be taken into account in this approach. The other demerit of this approach is that the orbitals and all the correlation effects are not treated on equal footing. In particular, the correlations among the valence electrons are estimated ambiguously. This may not be appropriate for the heavier atoms when the core correlations are quite significant.

Below we discuss a few many-body methods starting with a common DF wave function $|\Phi_0\rangle$ constructed using the V^N potential. Later we shall present results from these methods to demonstrate the gradual inclusion of the electron correlation effects from lower to higher order in a variety of all-order perturbative methods.

5.2.1 The DF method

Following eqs. (212) and (236), we can obtain the lowest-order contribution to $\mathcal{R}$, the DF result, as

$$\mathcal{R} = 2\langle\Phi_0|{\Omega^{(0,0)}}^\dagger D\Omega^{(0,1)}|\Phi_0\rangle = 2\langle\Phi_0|D\Omega^{(0,1)}|\Phi_0\rangle = 2\sum_I \frac{\langle\Phi_0|D|\Phi_I\rangle\langle\Phi_I|H^{PT}|\Phi_0\rangle}{E_I^{DF}-E_0^{DF}}. \quad (240)$$

5.2.2 The MBPT(k) method

In this approximation, we assume $(k-1)$ orders of Coulomb and one order H^{PT}. Thus, it corresponds to

$$\mathcal{R} = 2\frac{\sum_{\beta=0}^{k-1}\langle\Phi_0|{\Omega^{(k-\beta,0)}}^\dagger D\Omega^{(\beta,1)}|\Phi_0\rangle}{\sum_{\beta=0}^{k-1}\langle\Phi_0|{\Omega^{(k-\beta,0)}}^\dagger\Omega^{(\beta,0)}|\Phi_0\rangle}. \quad (241)$$

This quantity can be expressed at the MBPT(2) as

$$\begin{aligned}\mathcal{R} &= \frac{2}{\mathcal{N}_2}\langle\Phi_0|\left[\Omega^{(0,0)}+\Omega^{(1,0)}\right]^\dagger D \times\left[\Omega^{(0,1)}+\Omega^{(1,1)}\right]|\Phi_0\rangle \\ &= \frac{2}{\mathcal{N}_2}\langle\Phi_0|D\Omega^{(0,1)}+D\Omega^{(1,1)}+{\Omega^{(1,0)}}^\dagger D\Omega^{(0,1)} \\ &\quad +{\Omega^{(1,0)}}^\dagger D\Omega^{(1,1)}|\Phi_0\rangle, \end{aligned} \quad (242)$$

and similarly in the MBPT(3) method it is

$$\begin{aligned}\mathcal{R} &= \frac{2}{\mathcal{N}_3}\langle\Phi_0|\left[\Omega^{(0,0)}+\Omega^{(1,0)}+\Omega^{(2,0)}\right]^\dagger D \times\left[\Omega^{(0,1)}+\Omega^{(1,1)}+\Omega^{(2,1)}\right]|\Phi_0\rangle \\ &= \frac{2}{\mathcal{N}_3}\langle\Phi_0|D\Omega^{(0,1)}+D\Omega^{(1,1)}+D\Omega^{(2,1)} \\ &\quad +{\Omega^{(1,0)}}^\dagger D\Omega^{(0,1)}+{\Omega^{(1,0)}}^\dagger D\Omega^{(1,1)} \\ &\quad +{\Omega^{(2,0)}}^\dagger D\Omega^{(0,1)}|\Phi_0\rangle, \end{aligned} \quad (243)$$

with the respective normalization constants $\mathcal{N}_2 = \langle\Phi_0|1+{\Omega^{(1,0)}}^\dagger\Omega^{(1,0)}|\Phi_0\rangle$ and $\mathcal{N}_3 = \langle\Phi_0|1+{\Omega^{(1,0)}}^\dagger\Omega^{(1,0)}+{\Omega^{(1,0)}}^\dagger\Omega^{(2,0)}+{\Omega^{(2,0)}}^\dagger\Omega^{(1,0)}+{\Omega^{(2,0)}}^\dagger\Omega^{(2,0)}|\Phi_0\rangle$.

The above expressions clearly indicate that the complexity of the calculations grows steadily as the order of perturbation increases. We describe two all-order perturbative methods to describe the electron correlation effects on the properties of the closed-shell atoms.

5.2.3 The RPA method

To arrive at the final working equation for the RPA method, we start by perturbing the DF orbitals and the single-particle energies due to the perturbation H^{PT}, *i.e.*

$$\left|\phi_i^{(0)}\right\rangle \to \left|\phi_i^{(0)}\right\rangle + \lambda\left|\phi_i^{(1)}\right\rangle \quad (244)$$

and

$$\epsilon_i^{(0)} \to \epsilon_i^{(0)} + \lambda\epsilon_i^{(1)}, \quad (245)$$

where $|\phi_i^{(1)}\rangle$ and $\epsilon_i^{(1)}$ are the first-order corrections to the particle wave function and energy, respectively. Owing to the fact that H^{PT} is an odd-parity operator, $\epsilon_i^{(1)} = 0$. In

the presence of a perturbation, the modified DF equation for the single-particle wave function yields

$$\begin{aligned}&\left(h_0+\lambda H^{PT}\right)\left(\left|\phi_i^{(0)}\right\rangle+\lambda\left|\phi_i^{(1)}\right\rangle\right)\\&+\sum_b^{N_c}\left(\left\langle\phi_b^{(0)}+\lambda\phi_b^{(1)}\right|V(r_{ij})\left|\phi_b^{(0)}+\lambda\phi_b^{(1)}\right\rangle\left|\phi_i^{(0)}+\lambda\phi_i^{(1)}\right\rangle\right.\\&\left.-\left\langle\phi_b^{(0)}+\lambda\phi_b^{(1)}\right|V(r_{ij})\left|\phi_i^{(0)}+\lambda\phi_i^{(1)}\right\rangle\left|\phi_b^{(0)}+\lambda\phi_b^{(1)}\right\rangle\right)=\\&\epsilon_i^{(0)}\left(\left|\phi_i^{(0)}\right\rangle+\lambda\left|\phi_i^{(1)}\right\rangle\right).\end{aligned}\tag{246}$$

Collecting only the terms that are linear in λ, we get

$$\left(h_0+U_{DF}-\epsilon_i^{(0)}\right)\left|\phi_i^{(1)}\right\rangle=\left(-H^{PT}-U_{DF}^{(1)}\right)\left|\phi_i^{(0)}\right\rangle,\tag{247}$$

where we use the notation $U_{DF}^{(1)}$ for

$$\begin{aligned}U_{DF}^{(1)}\left|\phi_i^{(0)}\right\rangle=\sum_b^{N_c}&\left[\left\langle\phi_b^{(0)}\right|V(r_{ij})\left|\phi_b^{(1)}\right\rangle\left|\phi_i^{(0)}\right\rangle\right.\\&-\left\langle\phi_b^{(0)}\right|V(r_{ij})\left|\phi_i^{(0)}\right\rangle\left|\phi_b^{(1)}\right\rangle\\&+\left\langle\phi_b^{(1)}\right|V(r_{ij})\left|\phi_b^{(0)}\right\rangle\left|\phi_i^{(0)}\right\rangle\\&\left.-\left\langle\phi_b^{(1)}\right|V(r_{ij})\left|\phi_i^{(0)}\right\rangle\left|\phi_b^{(0)}\right\rangle\right].\end{aligned}\tag{248}$$

We express the single-particle perturbed wave function in terms of the unperturbed single-particle wave functions as

$$\left|\phi_i^{(1)}\right\rangle=\sum_{j\neq i}C_i^j\left|\phi_j^{(0)}\right\rangle,\tag{249}$$

where C_i^js are the expansion coefficients. In the RPA approach, we write

$$\sum_{j\neq i}C_i^j\left(h_0+U_{DF}-\epsilon_j^{(0)}\right)\left|\phi_j^{(0)}\right\rangle=\left(-H^{PT}-U_{DF}^{(1)}\right)\left|\phi_i^{(0)}\right\rangle,\tag{250}$$

and solve this equation self-consistently to obtain the C_i^j coefficients to all orders in the Coulomb interaction.

The RPA wave operator can be expressed as

$$\begin{aligned}&\Omega_{RPA}^{(1)}=\sum_k^\infty\sum_{p,a}\Omega_{a\to p}^{(k,1)}=\\&\sum_{\beta=1}^\infty\sum_{pq,ab}\left\{\frac{[\langle pb|V(r_{ij})|aq\rangle-\langle pb|V(r_{ij})|qa\rangle]\Omega_{b\to q}^{(\beta-1,1)}}{\epsilon_p-\epsilon_a}\right.\\&\left.+\frac{\Omega_{b\to q}^{(\beta-1,1)^\dagger}[\langle pq|V(r_{ij})|ab\rangle-\langle pq|V(r_{ij})|ba\rangle]}{\epsilon_p-\epsilon_a}\right\},\end{aligned}\tag{251}$$

where $a\to p$ means replacement of an occupied orbital a from $|\Phi_0\rangle$ by a virtual orbital p which alternatively refers to a singly excited state with respect to $|\Phi_0\rangle$. It can be shown in the above formulation that the RPA method subsumes a certain class of singly excited configurations corresponding to the core-polarization effects to all orders.

Using the above RPA wave operator, we evaluate $\mathcal{R}$ by

$$\begin{aligned}\mathcal{R}&=2\langle\Phi_0|\Omega^{(0,0)^\dagger}D\Omega_{RPA}^{(1)}|\Phi_0\rangle\\&=2\langle\Phi_0|D\Omega_{RPA}^{(1)}|\Phi_0\rangle.\end{aligned}\tag{252}$$

5.2.4 The RCC theory

In the RCC method, we express the unperturbed atomic wave function as

$$\begin{aligned}\left|\Psi_0^{(0)}\right\rangle&=\Omega_{RCC}^{(0)}|\Phi_0\rangle=\sum_k^\infty\Omega_{RCC}^{(k,0)}|\Phi_0\rangle\\&=e^{T^{(0)}}|\Phi_0\rangle\end{aligned}\tag{253}$$

and the first order perturbed wave function as

$$\begin{aligned}\left|\Psi_0^{(1)}\right\rangle&=\Omega_{RCC}^{(1)}|\Phi_0\rangle=\sum_k^\infty\Omega_{RCC}^{(k,1)}|\Phi_0\rangle\\&=e^{T^{(0)}}T^{(1)}|\Phi_0\rangle,\end{aligned}\tag{254}$$

where $T^{(0)}$ and $T^{(1)}$ are the excitation operators from the reference state $|\Phi_0\rangle$ that take care of contributions from V_{es} and V_{es} along with the perturbed H^{PT} operator, respectively.

The amplitudes of the excitation $T^{(0)}$ and $T^{(1)}$ operators are determined using the equations

$$\langle\Phi_0^\tau|\overline{H_N^{at}}|\Phi_0\rangle=0\tag{255}$$

and

$$\langle\Phi_0^\tau|\overline{H_N^{at}}T^{(1)}|\Phi_0\rangle=-\langle\Phi_0^\tau|\overline{H}_N^{PT}|\Phi_0\rangle,\tag{256}$$

where the subscript N represents the normal-ordered form of the Hamiltonian, $\overline{O}=(Oe^{T^{(0)}})_{con}$, where *con* means only the connected terms and $|\Phi_0^\tau\rangle$ corresponds to the excited configurations with τ referring to level of excitations from $|\Phi_0\rangle$. In our calculations, we only consider the singly and doubly excited configurations ($\tau=1,2$) by defining

$$T^{(0)}=T_1^{(0)}+T_2^{(0)}\quad\text{and}\quad T^{(1)}=T_1^{(1)}+T_2^{(1)},\tag{257}$$

which is known as the CCSD method in the literature. When we consider the approximation $\overline{O}\simeq O+OT$, we refer it as the LCCSD method.

We have adopted an optimal computational strategy by constructing the intermediate diagrams in the RCC method. In this approach, we divide the effective $\overline{H_N^{at}}$ and $\overline{H}_N^{PT}$ operators containing the nonlinear CC terms into effective one-body, two-body etc. terms using the Wick's generalized theorem [452]. The intermediate diagrams for the computation of the $T^{(0)}$ amplitudes are described at length in our previous work [453,454]. We define intermediate diagrams for the evaluation of the $T^{(1)}$ amplitudes in a slightly different way. As can be seen from eq. (256), $\overline{H_N^{at}}$

contains all the nonlinear terms while for solving eq. (255) it is required to express it as $\overline{H}_N^{at} = \overline{H}_N^{at\prime} \otimes T_\tau$. Thus the intermediate diagrams in the latter case comprise terms from $\overline{H}_N^{at\prime}$ which require special scrutiny of the diagrams to avoid repetition in the single and double amplitude calculations of $T^{(0)}$. These effective diagrams are finally connected with the respective T operators to obtain the amplitudes of the single and double excitations. Contributions from the terms of $\overline{H}_N^{PT}$ are evaluated directly in the $T^{(1)}$ amplitude calculations.

$\mathcal{R}$ is evaluated by

$$\mathcal{R} = 2\frac{\langle\Phi_0|e^{T^{\dagger(0)}} D e^{T^{(0)}} T^{(1)}|\Phi_0\rangle}{\langle\Phi_0|e^{T^{\dagger(0)}} e^{T^{(0)}}|\Phi_0\rangle}\,. \tag{258}$$

Since all the operators in the above expression are in normal-order form and $e^{T^{\dagger(0)}} D e^{T^{(0)}}$ is a non-terminating series, we can express $e^{T^{\dagger(0)}} D e^{T^{(0)}} = (e^{T^{\dagger(0)}} e^{T^{(0)}})_{cl} (e^{T^{\dagger(0)}} D e^{T^{(0)}})_{cc}$ where the subscript cl and cc mean closed and closed with connected terms, respectively [455,456]. We can then show that

$$\begin{aligned}\mathcal{R} &= 2\frac{\langle\Phi_0|(e^{T^{\dagger(0)}} e^{T^{(0)}})_{cl}(e^{T^{\dagger(0)}} D e^{T^{(0)}} T^{(1)})_{cc}|\Phi_0\rangle}{\langle\Phi_0|(e^{T^{\dagger(0)}} e^{T^{(0)}})_{cl}|\Phi_0\rangle} \\ &= 2\frac{\langle\Phi_0|(e^{T^{\dagger(0)}} e^{T^{(0)}})_{cl}|\Phi_0\rangle\langle\Phi_0|(e^{T^{\dagger(0)}} D e^{T^{(0)}} T^{(1)})_{cc}|\Phi_0\rangle}{\langle\Phi_0|(e^{T^{\dagger(0)}} e^{T^{(0)}})_{cl}|\Phi_0\rangle} \\ &= 2\langle\Phi_0|(\overline{D}^{(0)} T^{(1)})_{cc}|\Phi_0\rangle, \end{aligned} \tag{259}$$

with $\overline{D}^{(0)} = e^{T^{\dagger(0)}} D e^{T^{(0)}}$, which is a non-terminating series. Note that its $(e^{T^{\dagger(0)}} e^{T^{(0)}} T^{(1)})_{cl}$ part will vanish owing to odd-parity of $T^{(1)}$. In the LCCSD method, we get $\overline{D}^{(0)} = D + DT^{(0)} + T^{\dagger(0)}D + T^{\dagger(0)}DT^{(0)}$. To account for contributions from $\overline{D}^{(0)}$ in the CCSD method, we first evaluate terms from $\overline{D}^{(0)}$ that are very unique in the sense that they will not be repeated after connecting with another $T^{(0)}$ or $T^{\dagger(0)}$ operator. Then, the contributions from the other nonlinear terms are considered by contracting with another $T^{(0)}$ and $T^{\dagger(0)}$ operators till self-consistent results were achieved. We present these contributions with k numbers of $T^{(0)}$ and/or $T^{\dagger(0)}$ as the CCSD$^{(k)}$ method to demonstrate convergence of the results with $k \to \infty$.

In order to estimate the dominant contributions from the neglected triple excitations in the CCSD method, we define an excitation operator by appealing to perturbation theory in the RCC framework as follows:

$$T_3^{(0),pert} = \frac{1}{3!}\sum_{abc,pqr}\frac{(\overline{H}_a T_2^{(0)})_{abc}^{pqr}}{\epsilon_a + \epsilon_b + \epsilon_c - \epsilon_p - \epsilon_q - \epsilon_r}\,, \tag{260}$$

where ϵ's are the energies of the occupied (denoted by a, b, c) and unoccupied (denoted by p, q, r) orbitals. From the differences between the results from the CCSD method and from the calculations carried out including the $T_3^{(0),pert}$ operator with $T^{(0)}$ in the expression given by eq. (259), we find typical order of magnitude estimates from the triple excitations. Note that the contributions of the counterparts of these excitations coming through the $T^{(1)}$ RCC operators will be extremely small.

The multi-configuration Dirac-Fock (MCDF) method has recently been used to calculate $\mathcal{R}$ for diamagnetic atoms [457]. This is an extension of the DF method, in which the wave function of an atomic state is expressed as a linear combination of the wave functions corresponding to appropriate configurations which are built from the occupied and virtual orbitals. The orbitals and the mixing coefficients are determined simultaneously in a self-consistent manner by using the variational principle. The P,T-odd Hamiltonian has been considered as a first-order perturbation and $\mathcal{R}$ is calculated by explicitly summing over many of the important odd-parity intermediate atomic states.

5.3 Atomic results

In table 15, we present the calculated $\mathcal{R}$ values from T-PT and NSM interactions for ^{129}Xe and ^{223}Rn noble gas atoms using the methods that we have described in this review, and also from previously reported calculations. From a theoretical point of view, it would be instructive to compare the correlation trends for both the atoms as they belong to the same periodic table of elements. As can be seen from the results quoted from different methods with the lower- to higher-order approximations, the magnitudes first decrease, then increase and the final results increase marginally from their DF values for both the atoms and for both the interactions. However, on close scrutiny it is evident that correlation effects are stronger in ^{223}Rn due to its larger size. The previous calculations, referred to in table 15, carried out using the DF, MBPT(3) and RPA methods [443, 447, 448, 450] cannot capture some of the correlation effects in $\mathcal{R}$ for the ground states of heavy inert gases in an efficient manner. The RPA method ignores pair correlation contributions, but takes into account the core-polarization effects to all orders. It is therefore not surprising that the results of the RPA and CCSD methods differ significantly. In fact, there are large cancellations between the results from the all-order RPA and the all-order non-RPA contributions at the CCSD level. The importance of including non-RPA correlation effects can be realized from the differences in the results between the MBPT(2) and MBPT(3) methods as the non-RPA contributions first start appearing at the MBPT(3) approximation in a perturbative theory framework. The MCDF method very often cannot capture the polarization effects arising from the deep core efficiently for practical reasons. The large differences seen among the results from the LCCSD and CCSD methods and among the results obtained with various levels of truncation in the CCSD$^{(k)}$ calculations suggest that there are strong cancellations between the linear and nonlinear RCC terms for estimating $\mathcal{R}$ values. More detailed discussions on these results can be found elsewhere [458, 459]. It is, therefore, imperative to use an all-order approach like our CCSD method to

Table 15. Calculated values of $\mathcal{R}$ due to both T-PT (given as $\mathcal{R}^{TPT}$ in $\times 10^{-20}\langle\sigma\rangle|e|\,\mathrm{cm}$) and NSM (given as $\mathcal{R}^{NSM}$ in $\times[10^{-17}/|e|\,\mathrm{fm}^3]|e|\,\mathrm{cm}$) interactions in the ^{129}Xe and ^{223}Rn noble gas atoms. The final recommended values with uncertainties are given as "Best value" for the respective quantities.

Method	^{129}Xe				^{223}Rn			
	This work		Others		This work		Others	
	$\mathcal{R}^{TPT}$	$\mathcal{R}^{NSM}$	$\mathcal{R}^{TPT}$	$\mathcal{R}^{NSM}$	$\mathcal{R}^{TPT}$	$\mathcal{R}^{NSM}$	$\mathcal{R}^{TPT}$	$\mathcal{R}^{NSM}$
DF	0.447	0.288	0.45 [443]	0.29 [443]	4.485	2.459	4.6 [443]	2.5 [443], 2.47 [450]
MBPT(2)	0.405	0.266			3.927	2.356		
MBPT(3)	0.515	0.339	0.52 [447]		4.137	2.398		
RPA	0.562	0.375	0.57 [443], 0.564 [448]	0.38 [443]	5.400	3.311	5.6 [443]	3.3 [443], 3.33 [450]
LCCSD	0.608	0.417			5.069	3.055		
CCSD$^{(3)}$	0.501	0.336			4.947	2.925		
CCSD$^{(5)}$	0.489	0.334			4.851	2.890		
CCSD$^{(\infty)}$	0.475	0.333			4.459	2.782		
Best value	0.475(4)	0.333(4)			4.46(6)	2.78(4)		

Table 16. Calculated values of $\mathcal{R}$ due to both T-PT (given as $\mathcal{R}^{TPT}$ in $\times 10^{-20}\langle\sigma\rangle|e|\,\mathrm{cm}$) and NSM (given as $\mathcal{R}^{NSM}$ in $\times[10^{-17}/|e|\,\mathrm{fm}^3]|e|\,\mathrm{cm}$) interactions in the ^{199}Hg and ^{225}Ra diamagnetic atoms. The final recommended values with uncertainties are given as "Best value" for the respective quantities.

Method	^{199}Hg				^{225}Ra			
	This work		Others		This work		Others	
	$\mathcal{R}^{TPT}$	$\mathcal{R}^{NSM}$	$\mathcal{R}^{TPT}$	$\mathcal{R}^{NSM}$	$\mathcal{R}^{TPT}$	$\mathcal{R}^{NSM}$	$\mathcal{R}^{TPT}$	$\mathcal{R}^{NSM}$
DF	−2.39	−1.20	−2.0 [447]	−1.19 [450]	−3.46	−1.86	−3.5 [443]	−1.8 [443]
			−2.4 [443]	−1.2 [443]				
			−7.29 [457]^a	−2.86 [457]^a				
MBPT(2)	−4.48	−2.30			−11.00	−5.48		
MBPT(3)	−3.33	−1.72			−10.59	−5.30		
RPA	−5.89	−2.94	−6.0 [447]	−2.8 [450]	−16.66	−8.12	−17 [443]	−8.3 [443]
			−5.9 [443]	−3.0 [443]			−16.59 [448]	−8.5 [450]
CI+MBPT			−5.1 [443]	−2.6 [443]			−18 [443]	−8.8 [443]
PRCC			−4.3 [449]	−2.46 [449]				
MCDF			−4.84 [457]^a	−2.22 [457]^a				
LCCSD	−4.52	−2.24			−13.84	−8.40		
CCSD$^{(3)}$	−3.82	−2.00			−10.40	−6.94		
CCSD$^{(5)}$	−4.02	−2.00			−10.01	−6.79		
CCSD$^{(\infty)}$	−3.38	−1.78			−9.926	−6.215		
Best value	−3.4(5)	−1.8(3)			−9.93(8)	−6.22(6)		

^{a} Only the *ab initio* results are cited for the comparison.

capture both the RPA and non-RPA correlation contributions. To assess the accuracies of our CCSD results, we also estimate order of magnitudes of the neglected effects, such as corrections due to the truncated basis in the construction of atomic orbitals and higher level excitations (estimating from the leading-order triply excitations). We provide recommended values along with the net uncertainties at the end of table 15 quoting as "Best value". These results in combination with the measured EDMs of the ^{129}Xe and ^{223}Rn atoms would provide best limits on C_T and S when they become available.

The diamagnetic atoms, ^{199}Hg and ^{225}Ra, are the two current leading candidates for EDM experiments. The electron correlation effects in these two atoms are strong. The primary reason for this is that the leading ground-state configuration which has two s electrons, mixes fairly strongly with low-lying opposite configurations with s and p electrons and the correlation effects modifying them make substantial contributions. We present $\mathcal{R}$ values in table 16 from all the methods that we have discussed earlier in the same sequence as were given in table 15. As can be seen, the trends in the results are completely different

Table 17. Breakdown of contributions to the $\mathcal{R}$ values from the CCSD method due to the T-PT interaction (in $\times 10^{-20}\langle\sigma\rangle|e|\,\mathrm{cm}$) in the considered diamagnetic atoms.

CC term	^{129}Xe	^{223}Rn	^{199}Hg	^{225}Ra
$DT_1^{(1)}$	0.459	4.345	−4.400	−13.10
$T_1^{(0)\dagger}DT_1^{(1)}$	−0.001	0.005	0.027	−0.100
$T_2^{(0)\dagger}DT_1^{(1)}$	0.039	0.333	1.224	3.303
$T_1^{(0)\dagger}DT_2^{(1)}$	−0.006	−0.069	−0.058	−0.086
$T_2^{(0)\dagger}DT_2^{(1)}$	−0.009	−0.108	0.107	0.778
Extra	−0.007	−0.047	−0.28	−0.721

Table 18. Breakdown of contributions to the $\mathcal{R}$ values from the CCSD method due to the NSM interaction (in $\times[10^{-17}/|e|\,\mathrm{fm}^3]|e|\,\mathrm{cm}$) in the considered diamagnetic atoms.

CC term	^{129}Xe	^{223}Rn	^{199}Hg	^{225}Ra
$DT_1^{(1)}$	0.313	2.695	−2.388	−7.577
$T_1^{(0)\dagger}DT_1^{(1)}$	−0.001	−0.004	0.018	0.008
$T_2^{(0)\dagger}DT_1^{(1)}$	0.023	0.134	0.607	1.557
$T_1^{(0)\dagger}DT_2^{(1)}$	0.0002	−0.006	0.011	0.046
$T_2^{(0)\dagger}DT_2^{(1)}$	0.004	0.020	−0.026	−0.594
Extra	−0.006	−0.057	−0.002	0.345

from those in the noble gas atom discussed in the previous paragraph. Unlike the noble gas atoms, the differences between the results from RPA and RCC methods are quite large. The final results, especially for ^{225}Ra, are significantly different from their corresponding DF results (refer to [451, 460] for more discussions). In fact, our DF and RPA results are in close agreement with calculations reported earlier, but our final CCSD result for Ra is very different from that of the CI+MBPT method. This makes a strong case for using a suitable relativistic many-body theory that can treat both the core polarization and pair correlations to all orders and treat them on equal footing. Adopting a procedure similar to the one discussed earlier, we also estimate uncertainties of the calculated $\mathcal{R}$ values of ^{199}Hg and ^{225}Ra and quoted the "Best values" towards the bottom of table 16. Moreover, we had evaluated dipole polarizabilities of the considered systems by replacing the P,T-odd interaction Hamiltonians by the dipole operator and had compared them against the available experimental values and other sophisticated calculations to gauge validity of our methods (more discussions are given in our previous works [451, 458–460]). In this view, we find our results are the most accurate calculations to date due to a balanced treatment of all possible electron correlation effects exhibited by these atoms.

5.4 Analyzing the CCSD results

It is possible to get insights into the contributions from the singly excited and doubly excited configurations for the calculation of $\mathcal{R}$ values using the expression given in eq. (259). The total sum of contributions from CCSD terms associated with $T_1^{(1)}$ and $T_2^{(2)}$ represent contributions from the singly excited and doubly excited configurations, respectively. Unlike a CI method where configurations are explicitly selected in the calculations, the RCC operators generate all possible configurations automatically that are allowed. In table 17 and table 18, we present contributions from various CCSD terms to the $\mathcal{R}$ values due to the T-PT interaction and NSM respectively for all the atoms we have considered. The net contributions from the leading doubly excited odd-parity configuration state functions. Though it appears as if the contribution due to the leading singly excited odd-parity configuration state functions, while the remaining terms represent for the contributions from the leading doubly excited odd-parity configuration state functions. Though it appears as if the contributions from the non-linear terms, given as "Extra", in the table are small, but actually the major contributions from the nonlinear RCC terms have been included through the evaluation of the $T^{(0)}$ and $T^{(1)}$ amplitude equations. It is also worth mentioning here is that in accordance with the description in in sect. 5.2.4, corrections due to the normalization of the wave functions are not necessary here.

Now comparing the trends of contributions to $\mathcal{R}$ due to the T-PT interaction from all the atoms given in table 17, we find that the correlation trends for ^{129}Xe and ^{223}Rn are almost similar, but they are very different for ^{199}Hg and ^{225}Ra. With respect to the DF values given in tables 15 and 16, the $DT_1^{(1)}$ contributions are very large in ^{225}Ra than for other atoms. This means the correlation effects are very strong in ^{225}Ra and to account for these effects rigorously, it is imperative to use a powerful many-body method like our RCC theory. Though correlation trends between the ^{199}Hg and ^{225}Ra atoms are almost the same, but the strong correlation effects in the ^{225}Ra atom suggest that the latter behaves more like an open-shell atom.

Since both the rank and parity of the P and T odd interaction Hamiltonians given by eqs. (207) and (208) are the same, one would expect that the correlation trends for $\mathcal{R}$ values due to the T-PT interaction and due to the interaction of the atomic electrons with the NSM to be similar. However, a comparison between these values given in tables 17 and 18 from the different CCSD terms reveals that this is not the case. The reason may be due to an extra r dependence appearing in eq. (207). One can also see that the trends for the contributions from the NSM interaction are different for all the atoms.

6 Experiments on EDMs of closed-shell atoms

The EDM is a property of a spin carrying particle, and is detected through observation of the difference in energy between two spin states, *i.e.* with $\boldsymbol{s}$ parallel and antiparallel to a static electric field $\boldsymbol{E}$. In a typical EDM measurement, the particle is placed under a static magnetic field $\boldsymbol{B}$ so that the Zeeman energy splitting between the

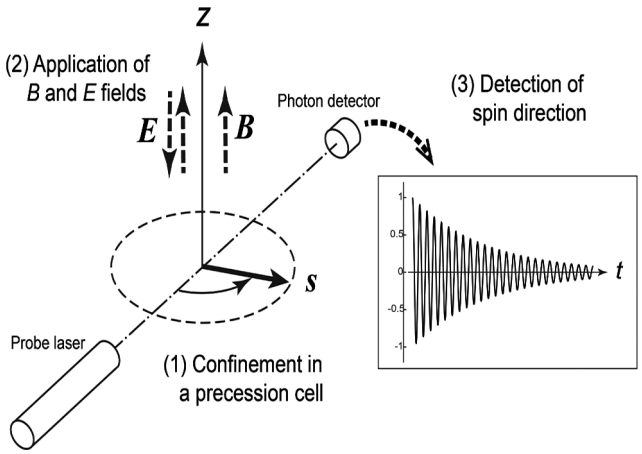

Fig. 16. Geometry and concepts relevant to typical EDM measurements.

magnetic substates $m = +1/2$ and $-1/2$, or the spin precession frequency ω, changes upon a reversal of $\boldsymbol{E}$. Thus, the EDM d is determined from a relation

$$d_{at} = \frac{\hbar(\omega_+ - \omega_-)}{4E}\,, \tag{261}$$

where symbols + and − refer to the directions of the E field parallel and antiparallel, respectively, to the B field. In order to measure the precession frequencies $\omega_\pm$, typically the spin is polarized and is pointed toward a direction transverse to $\boldsymbol{B}$ at time $t = 0$, from which the spin starts precession about the $\boldsymbol{B}$ direction. Figure 16 schematically illustrates geometry and concepts relevant to such an experiment: 1) confinement of polarized spins within some space (*e.g.*, in a gas cell for the cases of Hg [29] and Xe [22] atoms, in an optical dipole trap for the Ra case [461], or in a beam path for the TlF case [462,463]), 2) application of static B and E fields, and 3) detection of spin direction (typically through transmission of a circularly polarized laser light). To get a feeling on the typical scales for experimental settings and signals, one might recall that a size of EDM of $10^{-28}\,e\,$cm aimed to be detected poses to experimenter a requirement of frequency determination with a nHz precision under an applied E field of 10 kV/cm and a stabilization or monitoring of the B field within 0.1 fT.

With such demanding conditions required, any experiment which either have provided the present lowest limits or are newly proposed to revise them are equipped with their own advantageous features: Currently the best restricting limit on the EDM of a closed-shell atom has been obtained for ^{199}Hg in [25, 29], in which a four-cell scheme is employed with the inner two cells placed under applied electric fields pointing opposite directions to each other and the two outer cells under a zero E field. The signal for the EDM is observed as a difference of the precession frequencies for the middle two cells, and the other combinations of the four cells are used to measure the averaged magnetic field and its gradient. Optical pumping is being used to spin-polarize the atoms orthogonal to the applied magnetic field, and the Faraday rotation of near-resonant light is observed to determine an electric-field–induced perturbation to the Larmor precession frequency carrying information on EDM. As a result, they obtained $d(^{199}\mathrm{Hg}) = (-2.20 \pm 2.75(\mathrm{stat}) \pm 1.48(\mathrm{sys})) \times 10^{-30}\,e\,$cm corresponding to a new upper limit $|d(^{199}\mathrm{Hg})| < 7.4 \times 10^{-30}\,e\,$cm with 95% confidence level [29].

The EDM of ^{129}Xe has been studied in [22] by taking advantage of high Xe polarization obtained using spin exchange optical pumping technique and of unlimitedly long spin coherence time realized by virtue of a spin maser, yielding the result $d(^{129}\mathrm{Xe}) = [0.7 \pm 3.3(\mathrm{stat}) \pm 0.1(\mathrm{syst})] \times 10^{-27}\,e\,$cm. Also there are several currently ongoing developments on the ^{129}Xe EDM: Tokyo Tech-RIKEN group introduces a new scheme for the spin-coherence time elongation, an external feedback spin oscillator [42, 47, 464] which works even at very low B fields below $0.2\mu\,$T. Heil *et al.* [46] take advantage of remarkably long transverse relaxation times which are only realized under extremely high homogeneity of their magnetic field. Kuchler *et al.* [45] proposes a completely new method for detecting the EDM, in which a rotating E field is used instead of a static one.

Still another way is at work to confront the demanding conditions posed to EDM experiments on closed-shell atoms: As discussed in sect. 4 the nuclear octupole deformation/vibration, the parity-odd–type collective degrees of freedom in the nucleus, can bring a large enhancement to the Schiff moment [441]. At present, the appearance of the octupole collectivity is known to be in rather limited regions of the nuclear chart, and the candidate nuclei currently attracting attention are radioactve isotopes: EDM measurements of the radioactive ^{225}Ra atom have been carried out recently [28, 461]. EDM of ^{225}Ra nucleus is calculated to be 2-3 orders of magnitude larger than that of ^{199}Hg [430, 442, 450] due to octupole deformation. This means that even a one to two orders of magnitude less accurate determination of the EDM of ^{225}Ra atom than that of ^{199}Hg is still advantageous for extracting the required physics. To measure the EDM of ^{225}Ra atom, a cold-atom technique has been developed to detect spin precession of this atom held in an optical dipole trap and an upper limit has been set as $|d(^{225}\mathrm{Ra})| < 1.4 \times 10^{-23}\,e\,$cm with 95% confidence level [28]. Likewise, an experiment to measure EDM of ^{223}Rn is under development [43, 44].

7 Discussion

7.1 EDMs of diamagnetic atoms and the underlying elementary particle physics

By combining coefficients related to CP-violating processes mentioned in the previous sections, we can write a general formula for the dependence of the EDMs of diamagnetic atoms on elementary level CP violation in the following manner:

$$d_{at} = \sum_i K_i x_i, \tag{262}$$

where $x_i = d_e$, d_u, d_d, d_s, d_u^c, d_d^c, d_s^c, w, C_{eq}^{T}, C_{eq}^{SP}, C_{eq}^{PS}, and other CP-odd four-quark couplings (i is the index

of CP-odd effects considered) and K_i is the ratio of the atomic EDM to the CP-violating coefficient. We list these coefficients obtained from different levels of calculations in table 19.

We present first the "conventional" way of obtaining constraints from the EDM experimental and theoretical results by assuming a single source of CP violation at the atomic level. It has already been stated earlier that, currently, the most precise measurement of EDM of diamagnetic atoms comes from ^{199}Hg. Thus, by combining the EDM of this atom reported as $|d(^{199}\mathrm{Hg})| < 7.4 \times 10^{-30}|e|\,\mathrm{cm}$ with 95% confidence level [29] with the corresponding $\mathcal{R}$ value for the NSM and T-PT CP-odd electron-nucleus interaction using the CCSD method given in table 17, we get

$$C_N^{\mathrm{T}} < 6.5 \times 10^{-10} \tag{263}$$

and

$$S_{\mathrm{Hg}} < 4.1 \times 10^{-13}|e|\,\mathrm{fm}^3. \tag{264}$$

The NSM of ^{199}Hg in terms of $\bar{g}_{\pi NN}^{(i)}$'s is given by

$$\boldsymbol{S}_{\mathrm{Hg}} = \left[(0.23\pm0.15)\bar{g}_{\pi NN}^{(0)} - (0.007\pm0.011)\bar{g}_{\pi NN}^{(1)}\right]|e|\,\mathrm{fm}^3, \tag{265}$$

where we have adopted the central value of several mean-field calculations from ref. [431], with the standard deviation as the error bar. From the above limit on the NSM, we can infer constraints on $\bar{g}_{\pi NN}^{(0)}$ as

$$|\bar{g}_{\pi NN}^{(0)}| < 5.1 \times 10^{-12}. \tag{266}$$

Here we note that we have maximized the upper limit of $|\bar{g}_{\pi NN}^{(0)}|$ by minimizing the isoscalar coefficient of eq. (265) within the error bar.

Furthermore, using the relation of eq. (103), we can extract the upper limits on $\bar{\theta}$ as

$$|\bar{\theta}| < 5.7 \times 10^{-10}, \tag{267}$$

where we have again maximized the allowed region, given that the error bars of the coefficient of eqs. (103) and (265) are uncorrelated, to obtain the most conservative constraint. While inferring this limit, we have assumed that the PQ mechanism is not active. As can be noticed the above inferred limit of $\bar{\theta}$ from ^{199}Hg and that is obtained from the combination of measured d_n and EFT calculation in eq. (61) are of same order.

We emphasize here that, in giving each of the above limits, we have assumed that only one CP-odd coupling is finite, and the others are zero. The above way of reasoning is expected to work well to constrain the θ-term, since the θ-term is the largest contribution to the atomic EDM under the current upper limit given by experiment, compared with the effects of other TeV scale new physics or the CP violation of the CKM matrix. In these optimistic approximation, it would be useful to provide linear relationship between different atomic EDMs with $\bar{\theta}$ following table 19 as

– EDM of ^{129}Xe atom:

$$d_{\mathrm{Xe}} = (7.5 \pm 3.4) \times 10^{-22}\bar{\theta}\,e\,\mathrm{cm}, \tag{268}$$

– EDM of ^{199}Hg atom:

$$d_{\mathrm{Hg}} = (4.1 \pm 2.8) \times 10^{-20}\bar{\theta}\,e\,\mathrm{cm}, \tag{269}$$

and

– EDM of ^{225}Ra atom:

$$d_{\mathrm{Ra}} = (-3.1 \pm 1.9) \times 10^{-17}\bar{\theta}\,e\,\mathrm{cm}. \tag{270}$$

It is to be noted that the θ-term contribution to the atomic EDM has a sizable theoretical uncertainty, mainly coming from the nuclear structure calculation. Moreover, the CP-odd interactions used in the calculation of the nuclear level coefficients, with restricted model space, may differ from the bare ones, and this fact may bring additional unknown systematics.

This single source assumption is however not valid when several sources contribute to the atomic EDM with similar orders of magnitude, which is the case for the majority of the TeV scale new physics (when the PQ mechanism is invoked and the θ-term is unphysical). As a concrete example, d_{Xe} and d_{Hg} have similar orders enhancement factors for the quark EDMs and chromo-EDMs (see table 19), which is due to the absence of the enhancement or suppression of the contributions from the nucleon EDMs and the CP-odd force between the nucleons. Another important case is the effect of P,CP-odd e-N interaction. We see that the effect of the quark level C_{eu}^{PS} and C_{ed}^{PS} is comparable to that of $C_{eq}^{\mathrm{T}}(q = u, d)$, although T-PT interaction contributes larger than the S-PS interaction in the diamagnetic atoms. This counterbalancing is due to the enhancement of the nucleon pseudoscalar charge (see eqs. (91) and (92)). From these properties, we see that it is not possible to give limits by simply assuming a single elementary level process. Rather, we have to accurately evaluate the contributions from each process to the final observable EDMs, as there could be a destructive interference between the quark EDM and the chromo-EDM, reducing the sensitivity and loosening the constraint. This fact increases the error bars of the constraints on the CP-violating parameters of the new physics generating the quark EDM and the chromo-EDM of the same order of magnitude. A typical example is the generic SUSY model, which generates the quark EDM and the chromo-EDM of the same order of magnitude. This also concerns the general new physics candidates which generate the chromo-EDM or the Weinberg operator at the TeV scale, as the RGE renders quark EDM and chromo-EDM of the same order at the hadronic scale.

In relation to the quark chromo-EDM contribution, the EDM of ^{225}Ra is a cleaner system, since the effect of the CP-odd nuclear force is much more enhanced compared to the nucleon EDM. As was pointed in sect. 4.4, this enhancement is due to the nuclear octupole deformation. On the contrary, the NSM due to the intrinsic nucleon EDM is suppressed, and the upper limit on its contribution is

Table 19. The coefficients relating to the EDMs of the diamagnetic atoms with the elementary level CP-violating processes as given by eq. (262). The renormalization point of quark and gluon level operators is taken as $\mu = 1\,\mathrm{GeV}$. The θ-term contribution is estimated with the single source assumption.

^{129}Xe			
K_{Xe}	Central value	Error bar	Largest sources of error
$K_{\mathrm{Xe},\theta}$	$7\times10^{-22}e\,\mathrm{cm}$	$O(50\%)$	Hadronic level (θ-term contribution to the nucleon EDM)
K_{Xe,d_e}	10^{-3}	$O(100\%)$	Atomic level (higher-order contribution from hyperfine interaction)
K_{Xe,d_u}	2.2×10^{-6}	$O(30\%)$	Nuclear level (nucleon EDM contribution to Schiff moment)
K_{Xe,d_d}	-8.5×10^{-6}	$O(30\%)$	Nuclear level (nucleon EDM contribution to Schiff moment)
K_{Xe,d_u^c}	$-6\times10^{-6}e$	$O(70\%)$	Hadronic level (light quark chromo-EDM contribution to nucleon EDM)
K_{Xe,d_d^c}	$-2\times10^{-5}e$	$O(70\%)$	Hadronic level (light quark chromo-EDM contribution to nucleon EDM)
K_{Xe,d_s^c}	$10^{-6}e$	$O(100\%)$	Hadronic level (strange quark chromo-EDM contribution to nucleon EDM)
$K_{\mathrm{Xe},w}$	$10^{-21}[e\,\mathrm{GeV}^2\,\mathrm{cm}]$	$O(100\%)$	Hadronic level (Weinberg operator contribution to d_N)
$K_{\mathrm{Xe},C_{eu}^{\mathrm{SP}}}$	$10^{-23}[e\,\mathrm{cm}]$	$O(100\%)$	Atomic level (higher-order contribution from analytical expression)
$K_{\mathrm{Xe},C_{ed}^{\mathrm{SP}}}$	$10^{-23}[e\,\mathrm{cm}]$	$O(100\%)$	Atomic level (higher-order contribution from analytical expression)
$K_{\mathrm{Xe},C_{es}^{\mathrm{SP}}}$	$10^{-25}[e\,\mathrm{cm}]$	$O(100\%)$	Atomic level (higher-order contribution from analytical expression)
$K_{\mathrm{Xe},C_{eu}^{\mathrm{T}}}$	$-2.2\times10^{-22}[e\,\mathrm{cm}]$	$O(30\%)$	Nuclear level (nuclear spin matrix element)
$K_{\mathrm{Xe},C_{ed}^{\mathrm{T}}}$	$8.8\times10^{-22}[e\,\mathrm{cm}]$	$O(30\%)$	Nuclear level (nuclear spin matrix element)
$K_{\mathrm{Xe},C_{eu}^{\mathrm{PS}}}$	$-5.2\times10^{-22}[e\,\mathrm{cm}]$	$O(60\%)$	Hadronic level (nucleon pseudoscalar density)
$K_{\mathrm{Xe},C_{ed}^{\mathrm{PS}}}$	$5.5\times10^{-22}[e\,\mathrm{cm}]$	$O(60\%)$	Hadronic level (nucleon pseudoscalar density)
$K_{\mathrm{Xe},C_{es}^{\mathrm{PS}}}$	$-1.6\times10^{-23}[e\,\mathrm{cm}]$	$O(60\%)$	Hadronic level (nucleon pseudoscalar density)
$K_{\mathrm{Xe},C_{LR}}$	$10^{-19}[e\,\mathrm{GeV}^2\,\mathrm{cm}]$	$O(100\%)$	Hadronic level (CP-odd four-quark interaction contribution to $\bar{g}_{\pi NN}^{(1)}$)
^{199}Hg			
K_{Hg}	Central value	Error bar	Largest sources of error
$K_{\mathrm{Hg},\theta}$	$10^{-20}e\,\mathrm{cm}$	$O(100\%)$	Nuclear level (d_N and $\bar{g}_{\pi NN}^{(0)}$ contribution to Schiff moment)
K_{Hg,d_e}	10^{-2}	$O(100\%)$	Atomic level (higher-order contribution from analytical expression)
K_{Hg,d_u}	10^{-5}	$O(100\%)$	Nuclear level (nucleon EDM contribution to Schiff moment)
K_{Hg,d_d}	10^{-4}	$O(100\%)$	Nuclear level (nucleon EDM contribution to Schiff moment)
K_{Hg,d_u^c}	$10^{-4}e$	$O(100\%)$	Nuclear level (CP-odd nuclear force contribution to Schiff moment)
K_{Hg,d_d^c}	$10^{-3}e$	$O(100\%)$	Nuclear level (CP-odd nuclear force contribution to Schiff moment)
K_{Hg,d_s^c}	$10^{-4}e$	$O(100\%)$	Hadronic level (strange quark chromo-EDM contribution to nucleon EDM)
$K_{\mathrm{Hg},w}$	$10^{-19}[e\,\mathrm{GeV}^2\,\mathrm{cm}]$	$O(100\%)$	Hadronic level (Weinberg operator contribution to d_N)
$K_{\mathrm{Hg},C_{eu}^{\mathrm{SP}}}$	$10^{-21}[e\,\mathrm{cm}]$	$O(100\%)$	Atomic level (higher-order contribution from analytical expression)
$K_{\mathrm{Hg},C_{ed}^{\mathrm{SP}}}$	$10^{-21}[e\,\mathrm{cm}]$	$O(100\%)$	Atomic level (higher-order contribution from analytical expression)
$K_{\mathrm{Hg},C_{es}^{\mathrm{SP}}}$	$10^{-23}[e\,\mathrm{cm}]$	$O(100\%)$	Atomic level (higher-order contribution from analytical expression)
$K_{\mathrm{Hg},C_{eu}^{\mathrm{T}}}$	$10^{-21}[e\,\mathrm{cm}]$	$O(100\%)$	Nuclear level (unknown nuclear spin matrix element)
$K_{\mathrm{Hg},C_{ed}^{\mathrm{T}}}$	$10^{-21}[e\,\mathrm{cm}]$	$O(100\%)$	Nuclear level (unknown nuclear spin matrix element)
$K_{\mathrm{Hg},C_{eu}^{\mathrm{PS}}}$	$10^{-21}[e\,\mathrm{cm}]$	$O(100\%)$	Nuclear level (unknown nuclear spin matrix element)
$K_{\mathrm{Hg},C_{ed}^{\mathrm{PS}}}$	$10^{-21}[e\,\mathrm{cm}]$	$O(100\%)$	Nuclear level (unknown nuclear spin matrix element)
$K_{\mathrm{Hg},C_{es}^{\mathrm{PS}}}$	$10^{-22}[e\,\mathrm{cm}]$	$O(100\%)$	Nuclear level (unknown nuclear spin matrix element)
$K_{\mathrm{Hg},C_{LR}}$	$10^{-18}[e\,\mathrm{GeV}^2\,\mathrm{cm}]$	$O(100\%)$	Hadronic level (CP-odd four-quark interaction contribution to $\bar{g}_{\pi NN}^{(1)}$)
^{225}Ra			
K_{Ra}	Central value	Error bar	Largest sources of error
$K_{\mathrm{Ra},\theta}$	$-3\times10^{-17}e\,\mathrm{cm}$	$O(60\%)$	Nuclear level ($\bar{g}_{\pi NN}^{(0)}$ contribution to Schiff moment)
K_{Ra,d_e}	10^{-2}	$O(100\%)$	Atomic level (higher-order contribution from analytical expression)
K_{Ra,d_u}	10^{-5}	$O(100\%)$	Nuclear level (unknown nucleon EDM contribution to Schiff moment)
K_{Ra,d_d}	10^{-4}	$O(100\%)$	Nuclear level (unknown nucleon EDM contribution to Schiff moment)
K_{Ra,d_u^c}	$-6e$	$O(70\%)$	Nuclear level (CP-odd nuclear force contribution to Schiff moment)
K_{Ra,d_d^c}	$6e$	$O(70\%)$	Nuclear level (CP-odd nuclear force contribution to Schiff moment)
K_{Ra,d_s^c}	$10^{-4}e$	$O(100\%)$	Hadronic level (strange quark chromo-EDM contribution to nucleon EDM)
$K_{\mathrm{Ra},w}$	$10^{-19}[e\,\mathrm{GeV}^2\,\mathrm{cm}]$	$O(100\%)$	Hadronic level (Weinberg operator contribution to d_N)
$K_{\mathrm{Ra},C_{eu}^{\mathrm{SP}}}$	$10^{-21}[e\,\mathrm{cm}]$	$O(100\%)$	Atomic level (higher-order contribution from analytical expression)
$K_{\mathrm{Ra},C_{ed}^{\mathrm{SP}}}$	$10^{-21}[e\,\mathrm{cm}]$	$O(100\%)$	Atomic level (higher-order contribution from analytical expression)
$K_{\mathrm{Ra},C_{es}^{\mathrm{SP}}}$	$10^{-23}[e\,\mathrm{cm}]$	$O(100\%)$	Atomic level (higher-order contribution from analytical expression)
$K_{\mathrm{Ra},C_{eu}^{\mathrm{T}}}$	$10^{-21}[e\,\mathrm{cm}]$	$O(100\%)$	Nuclear level (unknown nuclear spin matrix element)
$K_{\mathrm{Ra},C_{ed}^{\mathrm{T}}}$	$10^{-21}[e\,\mathrm{cm}]$	$O(100\%)$	Nuclear level (unknown nuclear spin matrix element)
$K_{\mathrm{Ra},C_{eu}^{\mathrm{PS}}}$	$10^{-21}[e\,\mathrm{cm}]$	$O(100\%)$	Nuclear level (unknown nuclear spin matrix element)
$K_{\mathrm{Ra},C_{ed}^{\mathrm{PS}}}$	$10^{-21}[e\,\mathrm{cm}]$	$O(100\%)$	Nuclear level (unknown nuclear spin matrix element)
$K_{\mathrm{Ra},C_{es}^{\mathrm{PS}}}$	$10^{-23}[e\,\mathrm{cm}]$	$O(100\%)$	Nuclear level (unknown nuclear spin matrix element)
$K_{\mathrm{Ra},C_{LR}}$	$10^{-14}[e\,\mathrm{GeV}^2\,\mathrm{cm}]$	$O(100\%)$	Hadronic level (CP-odd four-quark interaction contribution to $\bar{g}_{\pi NN}^{(1)}$)

suppressed by several orders of magnitude, when it is expressed in terms of $\bar{g}^{(0)}_{\pi NN}$. This is a very remarkable property, as the CP-odd nuclear force is singularly sensitive to the quark chromo-EDM, or the left-right symmetric-type four-quark operator. Of course, this enhancement is only a nuclear level effect, and it does not prohibit the suppression of the quark chromo-EDM effect at the elementary level, which may counterbalance the effect of other sources. In the analysis of the EDMs of diamagnetic atoms, careful inspections of the contributions from all possible important sources of CP violation are required.

7.2 Implication for particle physics

We now discuss the implications of our current knowledge of the EDMs of diamagnetic atoms for different particle physics models. The first case we consider is the SUSY class of models. In the generic SUSY model, the EDM and the chromo-EDM of quarks are generated at the one-loop level. In sect. 2.3.2, we have seen that d_q and d^c_q are of the order of $10^{-25} e\,\mathrm{cm}$, at the TeV scale with typical parameters in TeV scale SUSY breaking scenarios. The RGE can be calculated without large theoretical uncertainty, but the hadron and nuclear level evaluations involve a large error bar. As can be seen in table 19, the error might be enlarged due to the destructive interference for the EDMs of ^{129}Xe and ^{199}Hg. If we consider the most conservative case, the best limit of the EDM of ^{199}Hg cannot even constrain the SUSY CP phases (θ_μ and θ_A), related to d_q and d^c_q by eqs. (15) and (16). The EDM of ^{225}Ra can overcome this problem, since its sensitivity to the chromo-EDM is enhanced. In ordinary SUSY models, the right-handed current of light quarks is strongly suppressed due to the Yukawa couplings, so there is no possibility of destructive interference with the left-right four-quark interaction [465, 466].

In the split SUSY scenarios, the leading CP violation is given by the quark and electron EDMs, as mentioned in sect. 2.3.2. In that case, the hadronic uncertainty is better controlled since the quark EDM contribution to the NSM is better known. In this case however, we have to consider the interference between the electron and quark EDMs. It is also important to note that ^{225}Ra EDM is not sensitive to the split SUSY scenario, since the quark chromo-EDM is suppressed. The same remarks apply to several R-parity–violating models for which the leading contribution comes from the Barr-Zee–type diagrams with heavy leptons in the inner loop. In the baryon number violating R-parity–violating scenarios, the right-handed quark current is also generated, which leads to the left-right–type four-quark interaction and may interfere with the quark chromo-EDM [337, 467].

In the Higgs doublet models, the leading process is the Barr-Zee–type diagram of quarks and electrons, as discussed in sect. 2.3.1. Here the quark chromo-EDM gives the most important contribution, as the electromagnetic Barr-Zee–type diagram is suppressed by α_{em}. As for the one-loop level SUSY fermion EDM and chromo-EDM, this process generates after the renormalization group evolution down to the hadronic scale a quark EDM with the same order of magnitude. The ^{225}Ra EDM is again the most efficient way of probing it. The Weinberg operator also contributes to the hadronic effective CP-odd interaction, but it is subleading since its Wilson coefficient at the TeV scale is smaller by about two orders of magnitude for the Higgs mass $m_H = 125\,\mathrm{GeV}$. It is also additionally suppressed by the RGE, down to the hadronic scale, so that its final contribution to the nucleon EDM is smaller than that generated by the quark chromo-EDM by more than an order of magnitude.

In the left-right symmetric models, the leading CP violation is given by the left-right–type four-quark interaction (see sect. 2.3.3), which generates the isovector CP-odd π-N-N interaction at the hadron level, without largely mixing with other hadronic interactions (see sect. 2.4.1). This process can therefore be probed with all diamagnetic atoms. If we can observe a clear hierarchy respecting the coefficients a_1 times the coefficients relating the NSM and the atomic EDM in the experimental values of the EDMs of ^{129}Xe, ^{199}Hg, and ^{225}Ra, it is strongly probable that the left-right symmetric model is the source of CP violation. We might think that this hierarchy can be mimicked by the electron EDM or the CP-odd e-N interactions, but the huge enhancement of the EDM of ^{225}Ra is difficult to realize. Of course, continuous efforts in determining the NSM and reducing theoretical uncertainties are desirable.

Regarding the leptoquark model, the EDM of diamagnetic atoms is singularly important, as it is sensitive to the tensor-type CP-odd e-N interaction. Current limit of ^{199}Hg EDM can exclude the mass of the leptoquark to the PeV level, assuming $O(0.1)$ couplings with $O(1)$ CP phase.

We also discuss below the case of vectorlike fermions without direct interaction with the SM fermions. In this case the leading process is the Weinberg operator, which generates the quark EDM and chromo-EDM with similar orders of magnitude through the renormalization group evolution from the TeV scale to the hadronic scale. We therefore have to accurately determine its contribution to the nucleon EDM as well as those from the quark EDM and the chromo-EDM. Unfortunately, the accuracy is currently not high. The isoscalar chromo-EDM generated by the Weinberg operator at the hadronic scale can be probed using the ^{225}Ra through the CP-odd nuclear force. We have to note that the Weinberg operator is also expected to contribute to the short-range contact interaction of the CP-odd nuclear force. This contribution is also currently unknown, and has to be determined to unveil the CP violation of vectorlike fermions.

Finally, we consider the SM contributions generated by the CP phase of the CKM matrix. Here we have to compare the CP violation due to the CP-odd e-N interaction and that from the NSM. The CP-odd e-N interaction contribution is estimated as $C_N^{\mathrm{SP}} \sim O(10^{-17})$ (see sect. 3.2). Combing with the atomic level coefficients that are determined using the analytical relations, we obtain atomic EDMs less than $10^{-38} e\,\mathrm{cm}$. The NSM contribution was

estimated in ref. [269] as

$$d_{\rm Xe} \sim 10^{-36} e\,{\rm cm}, \quad (271)$$

$$d_{\rm Hg} \sim 10^{-35} e\,{\rm cm}, \quad (272)$$

$$d_{\rm Ra} \sim 10^{-32} e\,{\rm cm}. \quad (273)$$

In the SM, the NSM is giving the largest contribution. It is of course well below the current experimental sensitivity. Here we note that we are using the same CP-odd π-N-N coupling to estimate the CP-odd e-N interaction (see fig. 6) and the nuclear Schiff moment. The hierarchy between them has therefore a smaller error bar than the values themselves.

8 Summary and outlook

The EDMs of diamagnetic atoms depend on the hadronic CP violation, CP-odd e-N interaction and the electron EDM. In particular they are sensitive to the isoscalar and isovector CP-odd π-N-N interactions. The neutron EDM, which is sensitive to the hadronic CP violation, is also rather sensitive to isoscalar interactions. Diamagnetic atoms are, on the contrary, sensitive to the isovector CP-odd π-N-N interaction. Another remarkable point is that the EDMs of these atoms can probe the tensor-type CP-odd e-N interaction, which is singularly sensitive to the leptoquark model. For each microscopic CP-violating process, there are other competitive or even more sensitive experimental probes, such as the EDMs of paramagnetic atoms or d_n. However, as we have mentioned in the introduction, the BSMs which can generate CP violation in several sectors at the same time cannot be constrained with only those singularly sensitive experimental observables.

The sensitivity of the EDM of diamagnetic atoms on elementary level CP violation is orthogonal with those of other observables due to its dependence on a number of quantities, so it is very useful in constraining models that encompass a large parameter space. An excellent example is the analysis of SUSY models, which have a very large degree of freedom. Previous analyses often assumed that only a restricted number of parameters are active (the so-called "single source dominance" assertion) and the constraints on CP phases were given by the most sensitive experimental data on them. There may be cancellations if we consider several couplings and CP phases at the same time. In such a scenario, the EDM of diamagnetic atoms can constrain the CP violation which spreads over several sectors, or disentangle the CP-violating sources if a non-vanishing CP violation is found in some other experiments.

Among the several diamagnetic atoms that have so far been the subject of experimental EDM studies, ^{199}Hg has yielded the best result; the current upper limit of its EDM being $7.4 \times 10^{-30}\,e\,{\rm cm}$ at the 95% confidence level [29]. This is a remarkably stringent limit, not only because it is nominally the lowest among the upper limits ever placed on the EDM of an elementary particle or a composite system, but also because it holds promising possibilities for EDMs of other diamagnetic atoms, suggesting that they can be measured with similar or even better accuracy. In fact, the detection sensitivity of the ongoing search for EDM in ^{225}Ra is rapidly improving [28, 461]. By virtue of the large enhancement expected for the Schiff moment in this quadrupole- and octupole-deformed nucleus, its sensitivity to the CP-violating sources will reach comparable or even superior levels to that of mercury. ^{223}Rn would also be another promising candidate in the search for EDMs in diamagnetic atomic systems [43,44]. We note here also that important developments are taking place in the search for the EDM of ^{129}Xe atom, which have been undertaken by several groups taking advantage of the exceptionally long spin coherence times realizable for this species [42, 45, 46].

It is evident from our discussion on the atomic calculations of the ratio of the EDMs of diamagnetic to different CP-violating coupling constants that significant progress has been made in this area during the past decade. This has been possible due to advances in the RCC theory and the hybrid CI+MBPT method. In particular, the ability of the former method to capture the strong electron effects in Ra is truly impressive. The errors in the calculations which is of the order of two to five percent for the diamagnetic atoms can be reduced further by using the normal coupled-cluster and the extended coupled-cluster methods [468].

The NSM provides a very important contribution to the diamagnetic atomic EDM. In the beginning of its study, the Schiff moment might be enhanced due to the collective motion in the nucleus in a similar way as quadrupole vibrations enhance the quadrupole moments and transitions. It has been found later that this is not the case. On the contrary the single-particle estimate of the Schiff moment is even quenched due to the many-body effects. The exception might be the octupole deformation seen in actinide Ra regions, where the octupole deformation forms parity doublet states with spin 1/2. It is the same for the nuclear EDMs coming from the intrinsic nucleon EDMs. Nuclear EDMs are also quenched due to the many-body correlations. It is therefore important to incorporate the many-body effects in the nuclear wave function. In this respect the nuclear shell model is superior to the other mean-field theories.

The theoretical uncertainty for the nuclear calculations is fairly large. In addition to the sizeable error bar in the result of the calculation of the NSM, several nuclear level quantities, such as the nuclear spin matrix elements, are not known. The nuclear spin matrix elements are useful in determining the CP-odd e-N interaction contribution to the EDMs of atoms. Their evaluation is expected to be much easier than the NSM, so future work in this direction is very desirable. Another open question is to relate the "bare" CP-odd nuclear force to the effective CP-odd nuclear force which is relevant in theories with restricted model space. This procedure is required in bridging from hadron to nuclear physics. The uncertainty in the evaluation of the hadron matrix elements is larger than those of all the quantities that are needed for the determination of the EDMs of diamagnetic atoms. It is very challenging

to reduce it and it cannot be achieved without performing large scale lattice QCD computations. Results for several quantities that contribute to the atomic EDMs such as the nucleon scalar densities and tensor changes have been obtained recently. The most important quark level CP-odd quantity that needs to be evaluated is probably the quark chromo-EDM [469]. It is currently being computed on lattices by several groups and new results are expected soon. The chiral EFT approach is also useful in controlling the theoretical uncertainties originating in unknown hadronic effective interactions which are difficult to obtain on a lattice.

Given that our understanding of the challenging experimental and theoretical issues of the EDMs of diamagnetic atoms is steadily improving, one can be optimistic about new and improved results in this field in the foreseeable future. This will not only deepen our knowledge of CP violation, but also provide important insights into physics of BSM.

We thank Professor T. Fukuyama for useful discussions. This work was supported partly by INSA-JSPS under project no. IA/INSA-JSPS Project/2013-2016/February 28,2013/4098. BKS acknowledges Dr. Y. Singh and Dr. D.K. Nandy for many useful discussions and participating in development of RCC codes and use of PRL HPC cluster at Ahmedabad, India. The work of NY was completed due to support of the RSF grant 15-12-20008 and of Riken iTHES project.

References

1. S.L. Glashow, Nucl. Phys. **22**, 579 (1961).
2. S. Weinberg, Phys. Rev. Lett. **17**, 616 (1966).
3. A. Salam, in *Proceedings of the Eighth Nobel Symposium*, edited by N. Svartholm (Wiley-Interscience, New York, 1968).
4. ATLAS Collaboration (G. Aad *et al.*), Phys. Lett. B **716**, 1 (2012).
5. CMS Collaboration (S. Chatrchyan *et al.*), Phys. Lett. B **716**, 30 (2012).
6. A.D. Sakharov, Pisma Zh. Eksp. Teor. Fiz. **5**, 32 (1967) (JETP Lett. **5**, 24 (1967)).
7. I.B. Khriplovich, S.K. Lamoreaux, *CP Violation without Strangeness: Electric Dipole Moments of Particles, Atoms, and Molecules* (Springer, Berlin, 1997).
8. I.I. Bigi, A.I. Sanda, *CP Violation* (Cambridge University Press, 2000).
9. B.L. Roberts, W.J. Marciano, *Lepton Dipole Moments, Advanced Series on Directions in High Energy Physics*, Vol. **20** (World Scientific, Singapore, 2010).
10. J.H. Christenson, J.W. Cronin, V.L. Fitch, R. Turlay, Phys. Rev. Lett. **13**, 138 (1964).
11. K. Abe *et al.*, Phys. Rev. Lett. **87**, 091802 (2001).
12. B. Aubert *et al.*, Phys. Rev. Lett. **87**, 091801 (2001).
13. R. Aaij *et al.*, Phys. Rev. Lett. **110**, 221601 (2013).
14. E. Áavarez, A. Szynkman, Mod. Phys. Lett. A **23**, 2085 (2008).
15. M. Kobayashi, T. Maskawa, Prog. Theor. Phys. **49**, 652 (1973).
16. C. Jarlskog, Phys. Rev. Lett. **55**, 1039 (1985).
17. G.R. Farrar, M.E. Shaposhnikov, Phys. Rev. D **50**, 774 (1994).
18. P. Huet, E. Sather, Phys. Rev. D **51**, 379 (1995).
19. M. Dine, A. Kusenko, Rev. Mod. Phys. **76**, 1 (2003).
20. E.M. Purcell, N.F. Ramsey, Phys. Rev. **78**, 807 (1950).
21. S.K. Lamoreaux, J.P. Jacobs, B.R. Heckel, F.J. Raab, N. Fortson, Phys. Rev. Lett. **59**, 2275 (1987).
22. M.A. Rosenberry, T.E. Chupp, Phys. Rev. Lett. **86**, 22 (2001).
23. B.C. Regan, E.D. Commins, C.J. Schmidt, D. DeMille, Phys. Rev. Lett. **88**, 071805 (2002).
24. C.A. Baker *et al.*, Phys. Rev. Lett. **97**, 131801 (2006).
25. W.C. Griffith *et al.*, Phys. Rev. Lett. **102**, 101601 (2009).
26. J.J. Hudson *et al.*, Nature **473**, 493 (2011).
27. ACME Collaboration (J. Baron *et al.*), Science **343**, 269 (2014).
28. M. Bishof, R.H. Parker, K.G. Bailey, J.P. Greene, R.J. Holt, M.R. Kalita, W. Korsch, N.D. Lemke, Z.-T. Lu, P. Mueller, T.P. OConnor, J.T. Singh, M.R. Dietrich, Phys. Rev. C **94**, 025501 (2016).
29. B. Graner, Y. Chen, E.G. Lindahl, B.R. Heckel, Phys. Rev. Lett. **116**, 161601 (2016).
30. J.M. Pendlebury *et al.*, Phys. Rev. D **92**, 092003 (2015).
31. N.F. Ramsey, Annu. Rev. Nucl. Part. Sci. **32**, 211 (1982).
32. N. Fortson, P. Sandars, S. Barr, Phys. Today **56**, 33 (2003) (issue No. 6, doi: 10.1063/1.1595052).
33. G. Lüders, Ann. Phys. (N.Y.) **281**, 1004 (2000).
34. W. Bernreuther, M. Suzuki, Rev. Mod. Phys. **63**, 313 (1991).
35. S.M. Barr, Int. J. Mod. Phys. A **8**, 209 (1993).
36. M. Pospelov, A. Ritz, Ann. Phys. (N.Y.) **318**, 119 (2005).
37. M.J. Ramsey-Musolf, S. Su, Phys. Rep. **456**, 1 (2008).
38. D.S. Weiss, private communication.
39. D. Heinzen, private communication.
40. K. Harada, T. Aoki, K. Kato, H. Kawamura, T. Inoue, T. Aoki, A. Uchiyama, K. Sakamoto, S. Ito, M. Itoh, T. Hayamizu, A. Hatakeyama, K. Hatanata, T. Wakasa, Y. Sakemi, J. Phys.: Conf. Ser. **691**, 012017 (2016).
41. T. Furukawa *et al.*, J. Phys.: Conf. Ser. **312**, 102005 (2011).
42. T. Inoue *et al.*, Hyperfine Interact. **220**, 59 (2013).
43. E.T. Rand *et al.*, J. Phys.: Conf. Ser. **312**, 102013 (2011).
44. E.R. Tardiff, *Towards a Measurement of the Electric Dipole Moment of* ^{223}Rn, PhD Thesis, University of Michigan (2009).
45. F. Kuchler *et al.*, Hyperfine Interact. **237**, 1 (2016).
46. W. Heil, C. Gemmel, S. Karpuk, Y. Sobolev, K. Tullney, F. Allmendinger, U. Schmidt, M. Burghoff, W. Kilian, S.K.-Grüneberg, A. Schnabel, F. Seifert, L. Trahms, Ann. Phys. **525**, 539 (2013).
47. A. Yoshimi *et al.*, Phys. Lett. A **304**, 13 (2002).
48. X.-G. He, B.H.J. McKellar, S. Pakvasa, Int. J. Mod. Phys. A **4**, 5011 (1989) **6**, 1063(E) (1991).
49. J.S.M. Ginges, V.V. Flambaum, Phys. Rep. **397**, 63 (2004).
50. T. Fukuyama, Int. J. Mod. Phys. A **27**, 1230015 (2012).
51. V.A. Dzuba, V.V. Flambaum, Int. J. Mod. Phys. E **21**, 1230010 (2012).
52. J. Engel, M.J. Ramsey-Musolf, U. van Kolck, Prog. Part. Nucl. Phys. **71**, 21 (2013).
53. L.I. Schiff, Phys. Rev. **132**, 2194 (1963).
54. S.L. Glashow, J. Iliopoulos, L. Maiani, Phys. Rev. D **2**, 1285 (1970).

55. J. Donoghue, Phys. Rev. D **18**, 1632 (1978).
56. E.P. Shabalin, Yad. Fiz. **28**, 151 (1978) (Sov. J. Nucl. Phys. **28**, 75 (1978)).
57. E.P. Shabalin, Yad. Fiz. **31**, 1665 (1980) (Sov. J. Nucl. Phys. **31**, 864 (1980)).
58. A. Czarnecki, B. Krause, Phys. Rev. Lett. **78**, 4339 (1997).
59. M.E. Pospelov, I.B. Khriplovich, Sov. J. Nucl. Phys. **53**, 638 (1991) (Yad. Fiz. **53**, 1030 (1991)).
60. M.J. Booth, arXiv:hep-ph/9301293.
61. M. Pospelov, A. Ritz, Phys. Rev. D **89**, 056006 (2014).
62. J.P. Archambault, A. Czarnecki, M.E. Pospelov, Phys. Rev. D **70**, 073006 (2004).
63. X.-G. He, C.-J. Lee, S.-F. Li, J. Tandean, Phys. Rev. D **89**, 091901 (2014).
64. X.-G. He, C.-J. Lee, S.-F. Li, J. Tandean, JHEP **08**, 019 (2014).
65. H. Novales-Sánchez, M. Salinas, J.J. Toscano, O. Vázquez-Hernández, arXiv:1610.06649 [hep-ph].
66. J.R. Ellis, M.K. Gaillard, Nucl. Phys. B **150**, 141 (1979).
67. I.B. Khriplovich, Phys. Lett. B **173**, 193 (1986) Yad. Fiz. **44**, 1019 (1986) (Sov. J. Nucl. Phys. **44**, 659 (1986)).
68. M.E. Pospelov, Phys. Lett. B **328**, 441 (1994).
69. J. Ellis, M.K. Gaillard, D.V. Nanopoulos, Nucl. Phys. B **109**, 213 (1976).
70. D.V. Nanopoulos, A. Yildiz, P.H. Cox, Phys. Lett. B **87**, 53 (1979).
71. N.G. Deshpande, G. Eilam, W.L. Spence, Phys. Lett. B **108**, 42 (1982).
72. M.B. Gavela, A. Le Yaouanc, L. Oliver, O. Pene, J.C. Raynal, T.N. Pham, Phys. Lett. B **109**, 215 (1982).
73. I.B. Khriplovich, A.R. Zhitnitsky, Phys. Lett. B **109**, 490 (1982).
74. J.O. Eeg, I. Picek, Nucl. Phys. B **244**, 77 (1984).
75. C. Hamzaoui, A. Barroso, Phys. Lett. B **154**, 202 (1985).
76. B. McKellar, S.R. Choudhury, X.-G. He, S. Pakvasa, Phys. Lett. B **197**, 556 (1987).
77. T. Mannel, N. Uraltsev, Phys. Rev. D **85**, 096002 (2012).
78. C.-Y. Seng, Phys. Rev. C **91**, 025502 (2015).
79. S.M. Barr, A. Zee, Phys. Rev. Lett. **65**, 21 (1990) 2920(E) (1990).
80. S. Weinberg, Phys. Rev. Lett. **63**, 2333 (1989).
81. D.A. Dicus, Phys. Rev. D **41**, 999 (1990).
82. D. Chang, W.-Y. Keung, T.C. Yuan, Phys. Lett. B **251**, 608 (1990).
83. R.G. Leigh, S. Paban, R.-M. Xu, Nucl. Phys. B **352**, 45 (1991).
84. D. Chang, W.-Y. Keung, T.C. Yuan, Phys. Rev. D **43**, R14 (1991).
85. U. Mahanta, Phys. Lett. B **281**, 320 (1992).
86. C. Kao, R.-M. Xu, Phys. Lett. B **296**, 435 (1992).
87. V. Barger, A. Das, C. Kao, Phys. Rev. D **55**, 7099 (1997).
88. D. Bowser-Chao, D. Chang, W.-Y. Keung, Phys. Rev. Lett. **79**, 1988 (1997).
89. A.J. Buras, G. Isidori, P. Paradisi, Phys. Lett. B **694**, 402 (2011).
90. J. Brod, U. Haisch, J. Zupan, JHEP **11**, 180 (2013).
91. S. Inoue, M.J. Ramsey-Musolf, Y. Zhang, Phys. Rev. D **89**, 115023 (2014).
92. K. Cheung, J.S. Lee, E. Senaha, P.-Y. Tseng, JHEP **06**, 149 (2014).
93. M. Jung, A. Pich, JHEP **04**, 076 (2014).
94. T. Abe, J. Hisano, T. Kitahara, K. Tobioka, JHEP **01**, 106 (2014).
95. L. Bian, N. Chen, arXiv:1608.07975 [hep-ph].
96. C.-Y. Chen, S. Dawson, Y. Zhang, JHEP **06**, 056 (2015).
97. J.O. Eeg, arXiv:1611.07778 [hep-ph].
98. H.-K. Guo, Y.-Y. Li, T. Liu, M. Ramsey-Musolf, J. Shu, arXiv:1609.09849 [hep-ph].
99. S.M. Barr, A. Masiero, Phys. Rev. Lett. **58**, 187 (1987).
100. S.M. Barr, Phys. Rev. D **45**, 4148 (1992).
101. H.E. Haber, G.L. Kane, Phys. Rep. **117**, 75 (1985).
102. J.F. Gunion, H.E. Haber, Nucl. Phys. B **272**, 1 (1986).
103. S.P. Martin, in *Perspectives on Supersymmetry II*, edited by G.L. Kane (World Scientific, Singapore, 2010) p. 1, arXiv:hep-ph/9709356.
104. F. Gabbiani, E. Gabrielli, A. Masiero, L. Silvestrini, Nucl. Phys. B **477**, 321 (1996).
105. J.R. Ellis, S. Ferrera, D.V. Nanopoulos, Phys. Lett. B **114**, 231 (1982).
106. W. Buchmüller, D. Wyler, Phys. Lett. B **121**, 321 (1983).
107. J. Polchinski, M.B. Wise, Phys. Lett. B **125**, 393 (1983).
108. F. del Aguila, M.B. Gavela, J.A. Grifols, A. Mendez, Phys. Lett. B **126**, 71 (1983).
109. D.V. Nanopoulos, M. Srednicki, Phys. Lett. B **128**, 61 (1983).
110. M. Dugan, B. Grinstein, L.J. Hall, Nucl. Phys. B **255**, 413 (1985).
111. P. Nath, Phys. Rev. Lett. **66**, 2565 (1991).
112. Y. Kizukuri, N. Oshimo, Phys. Rev. D **45**, 1806 (1992).
113. Y. Kizukuri, N. Oshimo, Phys. Rev. D **46**, 3025 (1992).
114. T. Inui, Y. Mimura, N. Sakai, T. Sasaki, Nucl. Phys. B **449**, 49 (1995).
115. J.R. Ellis, J.S. Lee, A. Pilaftsis, JHEP **10**, 049 (2008).
116. B. Li, C.E.M. Wagner, Phys. Rev. D **91**, 095019 (2015).
117. T. Fukuyama, K. Asahi, Int. J. Mod. Phys. A **31**, 1650082 (2016).
118. T.H. West, Phys. Rev. D **50**, 7025 (1994).
119. T. Kadoyoshi, N. Oshimo, Phys. Rev. D **55**, 1481 (1997).
120. D. Chang, W.-Y. Keung, A. Pilaftsis, Phys. Rev. Lett. **82**, 900 (1999).
121. A. Pilaftsis, Phys. Lett. B **471**, 174 (1999).
122. D. Chang, W.-F. Chang, W.-Y. Keung, Phys. Lett. B **478**, 239 (2000).
123. A. Pilaftsis, Phys. Rev. D **62**, 016007 (2000).
124. D. Demir, O. Lebedev, K.A. Olive, M. Pospelov, A. Ritz, Nucl. Phys. B **680**, 339 (2004).
125. T.-F. Feng, X.-Q. Li, L. Lin, J. Maalampi, X.-M. Zhang, Phys. Rev. D **71**, 056005 (2005).
126. T.-F. Feng, X.-Q. Li, L. Lin, J. Maalampi, H.-S. Song, Phys. Rev. D **73**, 116001 (2006).
127. Y. Li, S. Profumo, M.J. Ramsey-Musolf, Phys. Rev. D **78**, 075009 (2008).
128. N. Yamanaka, Phys. Rev. D **87**, 011701 (2013).
129. M. Carena, J. Ellis, J.S. Lee, A. Pilaftsis, C.E.M. Wagner, JHEP **02**, 123 (2016).
130. Y. Nakai, M. Reece, arXiv:1612.08090 [hep-ph].
131. J. Dai, H. Dykstra, R.G. Leigh, S. Paban, D. Dicus, Phys. Lett. B **237**, 216 (1990).
132. R. Arnowitt, J.L. Lopez, D.V. Nanopoulos, Phys. Rev. D **42**, 2423 (1990).
133. R. Arnowitt, M.J. Duff, K.S. Stelle, Phys. Rev. D **43**, 3085 (1991).
134. W. Fischler, S. Paban, S.D. Thomas, Phys. Lett. B **289**, 373 (1992).

135. T. Falk, K.A. Olive, M. Pospelov, R. Roiban, Nucl. Phys. B **560**, 3 (1999).
136. O. Lebedev, M. Pospelov, Phys. Rev. Lett. **89**, 101801 (2002).
137. A. Pilaftsis, Nucl. Phys. B **644**, 263 (2002).
138. S.A. Abel, W.N. Cottingham, I.B. Whittingham, Phys. Lett. B **370**, 106 (1996).
139. R. Gariato, J.D. Wells, Phys. Rev. D **55**, 1611 (1997).
140. A. Romanino, A. Strumia, Nucl. Phys. B **490**, 3 (1997).
141. A. Bartl, T. Gajdosik, W. Porod, P. Stöckinger, H. Stremnitzer, Phys. Rev. D **60**, 073003 (1999).
142. M. Brhlik, L.L. Everett, G.L. Kane, J.D. Lykken, Phys. Rev. Lett. **83**, 2124 (1999).
143. E. Accomando, R.L. Arnowitt, B. Dutta, Phys. Rev. D **61**, 115003 (2000).
144. N. Arkani-Hamed, S. Dimopoulos, JHEP **06**, 073 (2005).
145. N. Arkani-Hamed, S. Dimopoulos, G.F. Giudice, A. Romanino, Nucl. Phys. B **709**, 3 (2005).
146. D. Chang, W.-F. Chang, W.-Y. Keung, Phys. Rev. D **71**, 076006 (2005).
147. G.F. Giudice, A. Romanino, Phys. Lett. B **634**, 307 (2006).
148. M. Dhuria, A. Misra, Phys. Rev. D **90**, 085023 (2014).
149. S.A.R. Ellis, G.L. Kane, JHEP **01**, 077 (2016).
150. Y. Grossman, M.P. Worah, Phys. Lett. B **395**, 241 (1997).
151. R. Barbieri, A. Strumia, Nucl. Phys. B **508**, 3 (1997).
152. Belle Collaboration (K. Abe *et al.*), Phys. Rev. Lett. **91**, 261602 (2003).
153. J. Hisano, Y. Shimizu, Phys. Lett. B **581**, 224 (2004).
154. J. Hisano, Y. Shimizu, Phys. Rev. D **70**, 093001 (2004).
155. M. Endo, M. Kakizaki, M. Yamaguchi, Phys. Lett. B **583**, 186 (2004).
156. G.-C. Cho, N. Haba, M. Honda, Mod. Phys. Lett. A **20**, 2969 (2005).
157. J. Hisano, M. Nagai, P. Paradisi, Phys. Lett. B **642**, 510 (2006).
158. J. Hisano, M. Nagai, P. Paradisi, Phys. Rev. D **78**, 075019 (2008).
159. J. Hisano, M. Nagai, P. Paradisi, Phys. Rev. D **80**, 095014 (2009).
160. W. Altmannshofer, A.J. Buras, P. Paradisi, Phys. Lett. B **688**, 202 (2010).
161. M. Maniatis, Int. J. Mod. Phys. A **25**, 3505 (2010).
162. S.F. King, M. Muhlleitner, R. Nevzorov, K. Walz, Nucl. Phys. B **901**, 526 (2015).
163. P.F. Perez, Phys. Lett. B **711**, 353 (2012).
164. J.M. Arnold, P.F. Perez, B. Fornal, S. Spinner, Phys. Rev. D **85**, 115024 (2012).
165. S.-M. Zhao, T.-F. Feng, X.-J. Zhan, H.-B. Zhang, B. Yan, JHEP **07**, 124 (2015).
166. G. Bhattacharyya, arXiv:hep-ph/9709395.
167. H.K. Dreiner, in *Perspectives on Supersymmetry II*, edited by G.L. Kane (World Scientific, Singapore, 1997) p. 565, arXiv:hep-ph/9707435.
168. M. Chemtob, Prog. Part. Nucl. Phys. **54**, 71 (2005).
169. R. Barbier *et al.*, Phys. Rep. **420**, 1 (2005).
170. Y.Y. Keum, Otto C.W. Kong, Phys. Rev. Lett. **86**, 393 (2001).
171. Y.Y. Keum, Otto C.W. Kong, Phys. Rev. D **63**, 113012 (2001).
172. K. Choi, E.J. Chun, K. Hwang, Phys. Rev. D **63**, 013002 (2001).
173. C.-C. Chiou, O.C.W. Kong, R.D. Vaidya, Phys. Rev. D **76**, 013003 (2007).
174. R.M. Godbole, S. Pakvasa, S.D. Rindani, X. Tata, Phys. Rev. D **61**, 113003 (2000).
175. S.A. Abel, A. Dedes, H.K. Dreiner, JHEP **05**, 13 (2000).
176. D. Chang, W.-F. Chang, M. Frank, W.-Y. Keung, Phys. Rev. D **62**, 095002 (2000).
177. N. Yamanaka, Phys. Rev. D **85**, 115012 (2012).
178. N. Yamanaka, Phys. Rev. D **86**, 075029 (2012).
179. N. Yamanaka, T. Sato, T. Kubota, Phys. Rev. D **87**, 115011 (2013).
180. N. Yamanaka, arXiv:1212.5800 [hep-ph].
181. P. Herczeg, Phys. Rev. D **61**, 095010 (2000).
182. A. Faessler, T. Gutsche, S. Kovalenko, V.E. Lyubovitskij, Phys. Rev. D **73**, 114023 (2006).
183. A. Faessler, T. Gutsche, S. Kovalenko, V.E. Lyubovitskij, Phys. Rev. D **74**, 074013 (2006).
184. T. Ibrahim, P. Nath, Phys. Rev. D **57**, 478 (1998).
185. T. Ibrahim, P. Nath, Phys. Lett. B **418**, 98 (1998).
186. T. Ibrahim, P. Nath, Phys. Rev. D **58**, 111301 (1998).
187. M. Brhlik, G.J. Good, G.L. Kane, Phys. Rev. D **59**, 115004 (1999).
188. S. Pokorski, J. Rosiek, C.A. Savoy, Nucl. Phys. B **570**, 81 (2000).
189. S. Abel, S. Khalil, O. Lebedev, Nucl. Phys. B **606**, 151 (2001).
190. K.A. Olive, M. Pospelov, A. Ritz, Y. Santoso, Phys. Rev. D **72**, 075001 (2005).
191. S.Y. Ayazi, Y. Farzan, Phys. Rev. D **74**, 055008 (2006).
192. S.Y. Ayazi, Y. Farzan, JHEP **06**, 013 (2007).
193. J. Ellis, J.S. Lee, A. Pilaftsis, JHEP **10**, 049 (2010).
194. Y. Li, S. Profumo, M.J. Ramsey-Musolf, JHEP **08**, 062 (2010).
195. J. Ellis, J.S. Lee, A. Pilaftsis, JHEP **02**, 045 (2011).
196. J. Ellis, J.S. Lee, A. Pilaftsis, arXiv:1009.1151 [math.OC].
197. N. Yamanaka, *Analysis of the Electric Dipole Moment in the R-parity Violating Supersymmetric Standard Model* (Springer, Berlin, Germany, 2014).
198. N. Yamanaka, T. Sato, T. Kubota, JHEP **12**, 110 (2014).
199. R.N. Mohapatra, J.C. Pati, Phys. Rev. D **11**, 566 (1975).
200. R.N. Mohapatra, J.C. Pati, Phys. Rev. D **11**, 2558 (1975).
201. G. Senjanovic, R.N. Mohapatra, Phys. Rev. D **12**, 1502 (1975).
202. A. Maiezza, M. Nemevšek, Phys. Rev. D **82**, 055022 (2010).
203. CMS Collaboration (S. Chatrchyan *et al.*), JHEP **05**, 108 (2014).
204. ATLAS Collaboration (G. Aad *et al.*), Phys. Lett. B **743**, 235 (2015).
205. CMS Collaboration (V. Khachatryan *et al.*), Phys. Lett. B **755**, 196 (2016).
206. CMS Collaboration (V. Khachatryan *et al.*), JHEP **02**, 122 (2016).
207. G. Beall, A. Soni, Phys. Rev. Lett. **47**, 552 (1981).
208. D. Chang, C.S. Li, T.C. Yuan, Phys. Rev. D **42**, 867 (1990).
209. J.-M. Frère, J. Galand, A. Le Yaouanc, L. Oliver, O. Pène, J.-C. Raynal, Phys. Rev. D **45**, 259 (1992).
210. Y. Zhang, H. An, X. Ji, R.N. Mohapatra, Phys. Rev. D **76**, 091301 (2007).
211. Y. Zhang, H. An, X. Ji, R.N. Mohapatra, Nucl. Phys. B **802**, 247 (2008).
212. F. Xu, H. An, X. Ji, JHEP **03**, 088 (2010).

213. J. de Vries, E. Mereghetti, R.G.E. Timmermans, U. van Kolck, Ann. Phys. **338**, 50 (2013).
214. A. Maiezza, M. Nemevšek, Phys. Rev. D **90**, 095002 (2014).
215. W. Dekens, J. de Vries, J. Bsaisou, W. Bernreuther, C. Hanhart, U.-G. Meißner, A. Nogga, A. Wirzba, JHEP **07**, 069 (2014).
216. C.-Y. Seng, J. de Vries, E. Mereghetti, H.H. Patel, M. Ramsey-Musolf, Phys. Lett. B **736**, 147 (2014).
217. J.A. Aguilar-Saavedra, R. Benbrik, S. Heinemeyer, M. Pérez-Victoria, Phys. Rev. D **88**, 094010 (2013).
218. A. Djouadi, A. Lenz, Phys. Lett. B **715**, 310 (2012).
219. S. Dimopoulos, J. Preskill, Nucl. Phys. B **199**, 206 (1982).
220. D.B. Kaplan, Nucl. Phys. B **365**, 259 (1991).
221. K.A. Peterson, Phys. Lett. B **255**, 567 (1991).
222. R. Contino, T. Kramer, M. Son, R. Sundrum, JHEP **05**, 074 (2007).
223. J.L. Hewett, T.G. Rizzo, Phys. Rep. **183**, 193 (1989).
224. F. del Aguila, M.J. Bowick, Nucl. Phys. B **224**, 107 (1983).
225. G.C. Branco, L. Lavoura, Nucl. Phys. B **278**, 738 (1986).
226. Y. Nir, D.J. Silverman, Phys. Rev. D **42**, 1477 (1990).
227. G.C. Branco, T. Morozumi, P.A. Parada, M.N. Rebelo, Phys. Rev. D **48**, 1167 (1993).
228. F. del Aguila, J.A. Aguilar-Saavedra, G.C. Branco, Nucl. Phys. B **510**, 39 (1998).
229. G. Barenboim, F.J. Botella, G.C. Branco, O. Vives, Phys. Lett. B **422**, 277 (1998).
230. T. Appelquist, M. Piai, R. Shrock, Phys. Lett. B **593**, 175 (2004).
231. T. Appelquist, M. Piai, R. Shrock, Phys. Lett. B **595**, 442 (2004).
232. Y. Adachi, N. Kurahashi, C.S. Lim, N. Maru, JHEP **11**, 150 (2010).
233. K. Ishiwata, M.B. Wise, Phys. Rev. D **88**, 055009 (2013).
234. M. König, M. Neubert, D.M. Straub, Eur. Phys. J. C **74**, 2945 (2014).
235. Y. Liao, X. Li, Phys. Lett. B **503**, 301 (2001).
236. E.O. Iltan, Eur. Phys. J. C **51**, 689 (2007).
237. W.-F. Chang, J.N. Ng, JHEP **12**, 077 (2002).
238. K. Agashe, G. Perez, A. Soni, Phys. Rev. D **71**, 016002 (2005).
239. C.S. Lim, N. Maru, K. Nishiwaki, Phys. Rev. D **81**, 076006 (2010).
240. M.W. Kalinowski, Eur. Phys. J. C **74**, 2742 (2014).
241. J. Fan, M. Reece, JHEP **06**, 004 (2013).
242. K. Choi, S.H. Im, H. Kim, D.Y. Mo, Phys. Lett. B **760**, 666 (2016).
243. T. Appelquist, G.-H. Wu, Phys. Rev. D **51**, 240 (1995).
244. CMS Collaboration (V. Khachatryan *et al.*), Phys. Lett. B **739**, 229 (2014).
245. CMS Collaboration (V. Khachatryan *et al.*), JHEP **07**, 042 (2015).
246. CMS Collaboration (V. Khachatryan *et al.*), Phys. Rev. D **93**, 032004 (2016).
247. CMS Collaboration (V. Khachatryan *et al.*), Phys. Rev. D **93**, 032005 (2016).
248. ATLAS Collaboration (G. Aad *et al.*), Eur. Phys. J. C **76**, 5 (2016).
249. ATLAS Collaboration (M. Aaboud *et al.*), New J. Phys. **18**, 093016 (2016).
250. S. Davidson, D. Bailey, B.A. Campbell, Z. Phys. C **61**, 613 (1994).
251. C.Q. Geng, Z. Phys. C **48**, 279 (1990).
252. X.-G. He, B.H.J. McKellar, S. Pakvasa, Phys. Lett. B **283**, 348 (1992).
253. P. Herczeg, Phys. Rev. D **68**, 116004 (2003).
254. W. Dekens, J. de Vries, JHEP **05**, 149 (2013).
255. W. Altmannshofer, J. Brod, M. Schmaltz, JHEP **05**, 125 (2015).
256. V. Cirigliano, W. Dekens, J. de Vries, E. Mereghetti, Phys. Rev. D **94**, 016002 (2016).
257. V. Cirigliano, W. Dekens, J. de Vries, E. Mereghetti, Phys. Rev. D **94**, 034031 (2016).
258. X. Artru, M. Mekhfi, Z. Phys. C **45**, 669 (1990).
259. E. Braaten, C.S. Li, T.C. Yuan, Phys. Rev. Lett. **64**, 1709 (1990).
260. G. Boyd, A.K. Gupta, S.P. Trivedi, M.B. Wise, Phys. Lett. B **241**, 584 (1990).
261. E. Braaten, C.S. Li, T.C. Yuan, Phys. Rev. D **42**, 276 (1990).
262. M. Dine, W. Fischler, Phys. Lett. B **242**, 239 (1990).
263. V. Barone, Phys. Lett. B **409**, 499 (1997).
264. G. Degrassi, S. Marchetti, E. Franco, L. Silvestrini, JHEP **11**, 044 (2005).
265. J. Hisano, K. Tsumura, M.J.S. Yang, Phys. Lett. B **713**, 473 (2012).
266. Particle Data Group (K.A. Olive *et al.*), Chin. Phys. C **40**, 100001 (2016).
267. G. Buchalla, A.J. Buras, M.E. Lautenbacher, Rev. Mod. Phys. **68**, 1125 (1996).
268. A.J. Buras, M. Jamin, M.E. Lautenbacher, P.H. Weisz, Nucl. Phys. B **370**, 69 (1992) **375**, 501(E) (1992).
269. N. Yamanaka, E. Hiyama, JHEP **02**, 067 (2016).
270. R.J. Crewther, P. Di Vecchia, G. Veneziano, E. Witten, Phys. Lett. B **88**, 123 (1979) **91**, 487(E) (1980).
271. A. Pich, E. de Rafael, Nucl. Phys. B **367**, 313 (1991).
272. B. Borasoy, Phys. Rev. D **61**, 114017 (2000).
273. C. Dib, A. Faessler, T. Gutsche, S.G. Kovalenko, J. Kuckei, V.E. Lyubovitskij, K. Pumsa-ard, J. Phys. G **32**, 547 (2006).
274. J. Kuckei, C. Dib, A. Faessler, T. Gutsche, S.G. Kovalenko, V.E. Lyubovitskij, K. Pumsa-ard, Phys. Atom. Nucl. **70**, 349 (2007).
275. S. Narison, Phys. Lett. B **666**, 455 (2008).
276. M. Pospelov, A. Ritz, Phys. Rev. Lett. **83**, 2526 (1999).
277. M. Pospelov, A. Ritz, Nucl. Phys. B **573**, 177 (2000).
278. D.K. Hong, H.-C. Kim, S. Siwach, H.-U. Yee, JHEP **11**, 036 (2007).
279. L. Bartolini, F. Bigazzi, S. Bolognesi, A.L. Cotrone, A. Manenti, arXiv:1609.09513 [hep-ph].
280. S. Aoki, A. Gocksch, A.V. Manohar, Stephen R. Sharpe, Phys. Rev. Lett. **65**, 1092 (1990).
281. E. Shintani *et al.*, Phys. Rev. D **72**, 014504 (2005).
282. F. Berruto, T. Blum, K. Orginos, A. Soni, Phys. Rev. D **73**, 054509 (2006).
283. E. Shintani, S. Aoki, Y. Kuramashi, Phys. Rev. D **78**, 014503 (2008).
284. F.-K. Guo, R. Horsley, U.-G. Meissner, Y. Nakamura, H. Perlt, P.E.L. Rakow, G. Schierholz, A. Schiller, J.M. Zanotti, Phys. Rev. Lett. **115**, 062001 (2015).
285. A. Shindler, T. Luu, J. de Vries, Phys. Rev. D **92**, 094518 (2015).
286. C. Alexandrou, A. Athenodorou, M. Constantinou, K. Hadjiyiannakou, K. Jansen, G. Koutsou, K. Ottnad, M. Petschlies, Phys. Rev. D **93**, 074503 (2016).

287. E. Shintani, T. Blum, T. Izubuchi, A. Soni, Phys. Rev. D **93**, 094503 (2016).
288. K. Ottnad, B. Kubis, U.-G. Meißner, F.-K. Guo, Phys. Lett. B **687**, 42 (2010).
289. E. Mereghetti, W.H. Hockings, U. van Kolck, Ann. Phys. **325**, 2363 (2010).
290. E. Mereghetti, J. de Vries, W.H. Hockings, C.M. Maekawa, U. van Kolck, Phys. Lett. B **696**, 97 (2011).
291. F.-K. Guo, U.-G. Meißner, JHEP **12**, 097 (2012).
292. J. de Vries, E. Mereghetti, A. Walker-Loud, Phys. Rev. C **92**, 045201 (2015).
293. J. de Vries, Ulf-G. Meißner, Int. J. Mod. Phys. E **25**, 1641008 (2016).
294. R.D. Peccei, H.R. Quinn, Phys. Rev. Lett. **38**, 1440 (1977).
295. M.A. Shifman, A.I. Vainshtein, V.I. Zakharov, Nucl. Phys. B **166**, 493 (1980).
296. I. Bigi, N.G. Ural'tsev, Zh. Eksp. Teor. Fiz. **100**, 363 (1991) (Sov. Phys. JETP **73**, 198 (1991)).
297. I. Bigi, N.G. Ural'tsev, Nucl. Phys. B **353**, 321 (1991).
298. V.M. Belayev, I.B. Ioffe, Sov. Phys. JETP **100**, 493 (1982).
299. V.M. Belayev, Ya.I. Kogan, Sov. J. Nucl. Phys. **40**, 659 (1984).
300. H. An, X. Ji, F. Xu, JHEP **02**, 043 (2010).
301. G. Barton, E.G. White, Phys. Rev. **184**, 1660 (1969).
302. W.C. Haxton, E.M. Henley, Phys. Rev. Lett. **51**, 1937 (1983).
303. M. Gorchtein, arXiv:0803.2906 [hep-ph].
304. T. Gutsche, A.N. Hiller Blin, S. Kovalenko, S. Kuleshov, V.E. Lyubovitskij, M.J. Vicente Vacas, A. Zhevlakov, arXiv:1612.02276 [hep-ph].
305. J. de Vries, R. Higa, C.-P. Liu, E. Mereghetti, I. Stetcu, R.G.E. Timmermans, U. van Kolck, Phys. Rev. C **84**, 065501 (2011).
306. C.-P. Liu, R.G.E. Timmermans, Phys. Rev. C **70**, 055501 (2004).
307. I. Stetcu, C.-P. Liu, J.L. Friar, A.C. Hayes, P. Navratil, Phys. Lett. B **665**, 168 (2008).
308. Y.-H. Song, R. Lazauskas, V. Gudkov, Phys. Rev. C **87**, 015501 (2013).
309. J. Bsaisou, J. de Vries, C. Hanhart, S. Liebig, U.-G. Meißner, D. Minossi, A. Nogga, A. Wirzba, JHEP **03**, 104 (2015) **05**, 083(E) (2015).
310. J. Bsaisou, U.-G. Meißner, A. Nogga, A. Wirzba, Ann. Phys. **359**, 317 (2015).
311. N. Yamanaka, E. Hiyama, Phys. Rev. C **91**, 054005 (2015).
312. N. Brambilla *et al.*, Eur. Phys. J. C **74**, 2981 (2014).
313. S. Collins, talk given at the *34th International Symposium on Lattice Field Theory, 24-30 July 2016*.
314. T.P. Cheng, R. Dashen, Phys. Rev. Lett. **26**, 594 (1971).
315. J. Gasser, Ann. Phys. **136**, 62 (1981).
316. J. Gasser, H. Leutwyler, M.E. Sainio, Phys. Lett. B **213**, 85 (1988).
317. J. Gasser, H. Leutwyler, M.E. Sainio, Phys. Lett. B **253**, 252 (1991).
318. J. Gasser, H. Leutwyler, M.E. Sainio, Phys. Lett. B **253**, 260 (1991).
319. J.M. Alarcon, J. Martin Camalich, J.A. Oller, Phys. Rev. D **85**, 051503 (2012).
320. J.M. Alarcon, J. Martin Camalich, J.A. Oller, Ann. Phys. **336**, 413 (2013).
321. X.-L. Ren, L.-S. Geng, J. Meng, Phys. Rev. D **91**, 051502 (2015).
322. M. Hoferichter, J. Ruiz de Elvira, B. Kubis, U.-G. Meißner, Phys. Rev. Lett. **115**, 092301 (2015).
323. D.-L. Yao *et al.*, JHEP **05**, 038 (2016).
324. H. Ohki *et al.*, Phys. Rev. D **78**, 054502 (2008).
325. R.D. Young, A.W. Thomas, Phys. Rev. D **81**, 014503 (2010).
326. S. Dürr *et al.*, Phys. Rev. D **85**, 014509 (2012).
327. ETM Collaboration (S. Dinter *et al.*), JHEP **08**, 037 (2012).
328. QCDSF Collaboration (G.S. Bali *et al.*), Phys. Rev. D **85**, 054502 (2012).
329. QCDSF Collaboration (G.S. Bali *et al.*), Nucl. Phys. B **866**, 1 (2013).
330. QCDSF-UKQCD Collaboration (R. Horsley *et al.*), Phys. Rev. D **85**, 034506 (2012).
331. S. Durr *et al.*, Phys. Rev. Lett. **116**, 172001 (2016).
332. G.S. Bali, S. Collins, D. Richtmann, A. Schäfer, W. Söldner, A. Sternbeck, Phys. Rev. D **93**, 094504 (2016).
333. A. Abdel-Rehim, C. Alexandrou, M. Constantinou, K. Hadjiyiannakou, K. Jansen, Ch. Kallidonis, G. Koutsou, A. Vaquero Avilés-Casco, Phys. Rev. Lett. **116**, 252001 (2016).
334. Y.-B. Yang *et al.*, Phys. Rev. D **94**, 054503 (2016).
335. S. Adler, E. Colglazier, J. Healy, I. Karliner, J. Lieberman, Y. Ng, H. Tsao, Phys. Rev. D **11**, 3309 (1975).
336. N. Yamanaka, T. Sato, T. Kubota, J. Phys. G **37**, 055104 (2010).
337. N. Yamanaka, T. Sato, T. Kubota, Phys. Rev. D **86**, 075032 (2012).
338. M. González-Alonso, J. Martin Camalich, Phys. Rev. Lett. **112**, 042501 (2014).
339. P.J. Mohr, B.N. Taylor, D.B. Newell, Rev. Mod. Phys. **84**, 1527 (2012).
340. A.W. Thomas, X.G. Wang, R.D. Young, Phys. Rev. C **91**, 015209 (2015).
341. H.-W. Lin, T. Blum, S. Ohta, S. Sasaki, T. Yamazaki, Phys. Rev. D **78**, 014505 (2008).
342. Y. Aoki, T. Blum, H.-W. Lin, S. Ohta, S. Sasaki, R. Tweedie, J. Zanotti, T. Yamazaki, Phys. Rev. D **82**, 014501 (2010).
343. J.R. Green, J.W. Negele, A.V. Pochinsky, S.N. Syritsyn, M. Engelhardt, S. Krieg, Phys. Rev. D **86**, 114509 (2012).
344. T. Bhattacharya, S.D. Cohen, R. Gupta, A. Joseph, H.-W. Lin, B. Yoon, Phys. Rev. D **89**, 094502 (2014).
345. RQCD Collaboration (G.S. Bali *et al.*), Phys. Rev. D **91**, 054501 (2015).
346. Y.-B. Yang, A. Alexandru, T. Draper, M. Gong, K.-F. Liu, Phys. Rev. D **93**, 034503 (2016).
347. PNDME Collaboration (T. Bhattacharya *et al.*), Phys. Rev. D **94**, 054508 (2016).
348. A. Abdel-Rehim *et al.*, Phys. Rev. D **92**, 114513 (2015) **93**, 039904(E) (2016).
349. T. Hatsuda, T. Kunihiro, Z. Phys. C **51**, 49 (1991).
350. T. Hatsuda, T. Kunihiro, Nucl. Phys. B **387**, 715 (1992).
351. T. Hatsuda, T. Kunihiro, Phys. Rep. **247**, 221 (1994).
352. N. Yamanaka, S. Imai, T.M. Doi, H. Suganuma, Phys. Rev. D **89**, 074017 (2014).
353. K. Takeda, S. Aoki, S. Hashimoto, T. Kaneko, J. Noaki, T. Onogi, Phys. Rev. D **83**, 114506 (2011).
354. JLQCD Collaboration (H. Ohki, K. Takeda, S. Aoki, S. Hashimoto, T. Kaneko, H. Matsufuru, J. Noaki, T. Onogi), Phys. Rev. D **87**, 034509 (2013).

355. A. Abdel-Rehim *et al.*, Phys. Rev. D **89**, 034501 (2014).
356. C. Alexandrou, M. Constantinou, S. Dinter, V. Drach, K. Hadjiyiannakou, K. Jansen, G. Koutsou, A. Vaquero, Phys. Rev. D **91**, 094503 (2015).
357. MILC Collaboration (D. Toussaint, W. Freeman), Phys. Rev. Lett. **103**, 122002 (2009).
358. M. Engelhardt, Phys. Rev. D **86**, 114510 (2012).
359. P.M. Junnarkar, A. Walker-Loud, Phys. Rev. D **87**, 114510 (2013).
360. MILC Collaboration (W. Freeman, D. Toussaint), Phys. Rev. D **88**, 054503 (2013).
361. χQCD Collaboration (M. Gong *et al.*), Phys. Rev. D **88**, 014503 (2013).
362. J.M. Alarcon, L.S. Geng, J. Martin Camalich, J.A. Oller, Phys. Lett. B **730**, 342 (2014).
363. P. Gubler, K. Ohtani, Phys. Rev. D **90**, 094002 (2014).
364. P. Gubler, W. Weise, Phys. Lett. B **751**, 396 (2015).
365. P. Gubler, W. Weise, Nucl. Phys. A **954**, 125 (2016).
366. E. Witten, Nucl. Phys. B **104**, 445 (1976).
367. M.A. Shifman, A.I. Vainshtein, V.I. Zakharov, Phys. Lett. B **78**, 443 (1978).
368. A.R. Zhitnitsky, Phys. Rev. D **55**, 3006 (1997).
369. M. Franz, M.V. Polyakov, K. Goeke, Phys. Rev. D **62**, 074024 (2000).
370. H.-Y. Cheng, Phys. Lett. B **219**, 347 (1989).
371. T.P. Cheng, L.F. Li, Phys. Rev. Lett. **62**, 1441 (1989).
372. K.R. Dienes, J. Kumar, B. Thomas, D. Yaylali, Phys. Rev. D **90**, 015012 (2014).
373. C. Adolph *et al.*, Phys. Lett. B **753**, 18 (2016).
374. QCDSF Collaboration (G.S. Bali *et al.*), Phys. Rev. Lett. **108**, 222001 (2012).
375. H.-Y. Cheng, C.-W. Chiang, JHEP **07**, 009 (2012).
376. S. Scopel, H. Yu, arXiv:1701.02215 [hep-ph].
377. S. Aoki, M. Doui, T. Hatsuda, Y. Kuramashi, Phys. Rev. D **56**, 433 (1997).
378. T. Bhattacharya, V. Cirigliano, R. Gupta, H.-W. Lin, B. Yoon, Phys. Rev. Lett. **115**, 212002 (2015).
379. T. Bhattacharya, V. Cirigliano, S.D. Cohen, R. Gupta, A. Joseph, H.-W. Lin, B. Yoon, Phys. Rev. D **92**, 094511 (2015).
380. JLQCD Collaboration (N. Yamanaka, H. Ohki, S. Hashimoto, T. Kaneko), PoS **LATTICE2015**, 121 (2016).
381. N. Yamanaka, T.M. Doi, S. Imai, H. Suganuma, Phys. Rev. D **88**, 074036 (2013).
382. M. Pitschmann, C.-Y. Seng, C.D. Roberts, S.M. Schmidt, Phys. Rev. D **91**, 074004 (2015).
383. A. Bacchetta, A. Courtoy, M. Radici, JHEP **03**, 119 (2013).
384. M. Anselmino, M. Boglione, U. D'Alesio, S. Melis, F. Murgia, A. Prokudin, Phys. Rev. D **87**, 094019 (2013).
385. A. Courtoy, S. Baeßler, M. González-Alonso, S. Liuti, Phys. Rev. Lett. **115**, 162001 (2015).
386. M. Radici, A. Courtoy, A. Bacchetta, M. Guagnelli, JHEP **05**, 123 (2015).
387. Z.-B. Kang, A. Prokudin, P. Sun, F. Yuan, Phys. Rev. D **93**, 014009 (2016).
388. Z. Ye *et al.*, Phys. Lett. B **767**, 91 (2017).
389. K. Choi, J. Hong, Phys. Lett. B **259**, 340 (1991).
390. D.V. Chubukov, L.N. Labzowsky, Phys. Rev. A **93**, 062503 (2016).
391. J. Bsaisou, C. Hanhart, S. Liebig, U.-G. Meißner, A. Nogga, A. Wirzba, Eur. Phys. J. A **49**, 31 (2013).
392. M. Pospelov, Phys. Lett. B **530**, 123 (2002).
393. K. Fuyuto, J. Hisano, N. Nagata, Phys. Rev. D **87**, 054018 (2013).
394. R. Dashen, Phys. Rev. D **3**, 1879 (1971).
395. C.-Y. Seng, M. Ramsey-Musolf, arXiv:1611.08063 [hep-ph].
396. V. Cirigliano, W. Dekens, J. de Vries, E. Mereghetti, Phys. Lett. B **767**, 1 (2017).
397. V.M. Khatsimovsky, I.B. Khriplovich, A.S. Yelkhovsky, Ann. Phys. (N.Y.) **186**, 1 (1988).
398. X.-G. He, B. McKellar, Phys. Rev. D **47**, 4055 (1993).
399. X.-G. He, B. McKellar, Phys. Lett. B **390**, 318 (1997).
400. C. Hamzaoui, M. Pospelov, Phys. Rev. D **60**, 036003 (1999).
401. O.P. Sushkov, V.V. Flambaum, I.B. Khriplovich, Zh. Eksp. Teor. Fiz. **87**, 1521 (1984) (Sov. Phys. JETP **60**, 873 (1984)).
402. V.V. Flambaum, I.B. Khriplovich, O.P. Sushkov, Nucl. Phys. A **449**, 750 (1986).
403. X.-G. He, B. McKellar, Phys. Rev. D **46**, 2131 (1992).
404. N. Yamanaka, arXiv:1605.00161 [nucl-th].
405. V.M. Khatsymovsky, I.B. Khriplovich, Phys. Lett. B **296**, 219 (1992).
406. J. de Vries, R.G.E. Timmermans, E. Mereghetti, U. van Kolck, Phys. Lett. B **695**, 268 (2011).
407. UCNA Collaboration (B. Plaster *et al.*), Phys. Rev. C **86**, 055501 (2012).
408. M. Pospelov, A. Ritz, Phys. Rev. D **63**, 073015 (2001).
409. J. Hisano, J.-Y. Lee, N. Nagata, Y. Shimizu, Phys. Rev. D **85**, 114044 (2012).
410. T. Bhattacharya, V. Cirigliano, R. Gupta, E. Mereghetti, B. Yoon, Phys. Rev. D **92**, 114026 (2015).
411. T. Bhattacharya, V. Cirigliano, R. Gupta, E. Mereghetti, B. Yoon, PoS **LATTICE2015**, 238 (2015).
412. R. Gupta, T. Bhattacharya, V. Cirigliano, B. Yoon, arXiv:1701.04132 [hep-lat].
413. M. Abramczyk, S. Aoki, T. Blum, T. Izubuchi, H. Ohki, S. Syritsyn, arXiv:1701.07792 [hep-lat].
414. D. Demir, M. Pospelov, A. Ritz, Phys. Rev. D **67**, 015007 (2003).
415. V.P. Gudkov, X.-G. He, B.H.J. McKellar, Phys. Rev. C **47**, 2365 (1993).
416. I.S. Towner, A.C. Hayes, Phys. Rev. C **49**, 2391 (1994).
417. I.B. Khriplovich, R.A. Korkin, Nucl. Phys. A **665**, 365 (2000).
418. N. Yamanaka, arXiv:1609.04759 [nucl-th].
419. L. Tiator, C. Bennhold, S.S. Kamalov, Nucl. Phys. A **580**, 455 (1994).
420. R.A. Senkov, N. Auerbach, V.V. Flambaum, V.G. Zelevinsky, Phys. Rev. A **77**, 014101 (2008).
421. V.V. Flambaum, A. Kozlov, Phys. Rev. C **85**, 068502 (2012).
422. For a review, see M. Baldo, *Nuclear Methods and the Nuclear Equation of State*, in *International Review of Nuclear Physics*, Vol. **8** (World Scientific, 1999).
423. V.F. Dmitriev, R.A. Senkov, Phys. Rev. Lett. **91**, 212303 (2003).
424. V.F. Dmitriev, R.A. Sen'kov, N. Auerbach, Phys. Rev. C **71**, 035501 (2005).
425. J. Engel, M. Bender, J. Dobaczewski, J.H. de Jesus, P. Olbratowski, Phys. Rev. C **68**, 025501 (2003).
426. P.G.H. Sandars, Phys. Lett. **14**, 194 (1965).
427. P.G.H. Sandars, Phys. Lett. **22**, 290 (1966).

428. V.V. Flambaum, Yad. Fiz. **24**, 383 (1976) (Sov. J. Nucl. Phys. **24**, 199 (1976)).
429. J.H. de Jesus, J. Engel, Phys. Rev. C **72**, 045503 (2005).
430. J. Dobaczewski, J. Engel, Phys. Rev. Lett. **94**, 232502 (2005).
431. S. Ban, J. Dobaczewski, J. Engel, A. Shukla, Phys. Rev. C **82**, 015501 (2010).
432. N. Auerbach, V.F. Dmitriev, V.V. Flambaum, A. Lisetskiy, R.A. Sen'kov, V.G. Zelevinsky, Phys. Rev. C **74**, 025502 (2006).
433. N. Yoshinaga, K. Higashiyama, R. Arai, E. Teruya, Phys. Rev. C **87**, 044332 (2013) **89**, 069902(E) (2014).
434. K. Higashiyama, N. Yoshinaga, K. Tanabe, Phys. Rev. C **67**, 044305 (2003).
435. N. Yoshinaga, K. Higashiyama, Phys. Rev. C **69**, 054309 (2004).
436. K. Higashiyama, N. Yoshinaga, Phys. Rev. C **83**, 034321 (2011) **89**, 049903(E) (2014).
437. E. Teruya, N. Yoshinaga, K. Higashiyama, K. Asahi, Submitted.
438. N. Yoshinaga, K. Higashiyama, R. Arai, Prog. Theor. Phys. **124**, 1115 (2010).
439. T. Fujita, S. Oshima, J. Phys. G **39**, 095106 (2012).
440. N. Yoshinaga, K. Higashiyama, R. Arai, E. Teruya, Phys. Rev. C **89**, 045501 (2014).
441. N. Auerbach, V.V. Flambaum, V. Spevak, Phys. Rev. Lett. **76**, 4316 (1996).
442. V. Spevak, N. Auerbach, V.V. Flambaum, Phys. Rev. C **56**, 1357 (1997).
443. V.A. Dzuba, V.V. Flambaum, S.G. Porsev, Phys. Rev. A **80**, 032120 (2009).
444. V.V. Flambaum, I.B. Khriplovich, Zh. Eksp. Teor. Fiz. **89**, 1505 (1985) (Sov. Phys. JETP **62**, 872 (1985)).
445. V.V. Flambaum, J.S.M. Ginges, Phys. Rev. A **72**, 052115 (2005).
446. B.K. Sahoo, Phys. Rev. A **93**, 022503 (2016).
447. A.M. Martensson-Pendrill, Phys. Rev. Lett. **54**, 1153 (1985).
448. K.V.P. Latha, P.R. Amjith, Phys. Rev. A **87**, 022509 (2013).
449. K.V.P. Latha, D. Angom, B.P. Das, D. Mukherjee, Phys. Rev. Lett. **103**, 083001 (2009) **115**, 059902(E) (2015).
450. V.A. Dzuba, V.V. Flambaum, J.S.M. Ginges, M.G. Kozlov, Phys. Rev. A **66**, 012111 (2002).
451. Y. Singh, B.K. Sahoo, Phys. Rev. A **91**, 030501(R) (2015).
452. I. Lindgren, J. Morrison, *Atomic Many-Body Theory*, second edition (Springer-Verlag, Berlin, 1986).
453. Y. Singh, B.K. Sahoo, B.P. Das, Phys. Rev. A **88**, 062504 (2013).
454. Y. Singh, B.K. Sahoo, Phys. Rev. A **90**, 022511 (2014).
455. S. Pal, M.D. Prasad, D. Mukherjee, Pramana **18**, 261 (1982).
456. I. Shavitt, R.J. Bartlett, *Many-Body Methods in Chemistry and Physics: MBPT and Coupled-Cluster Theory* (Cambridge University Press, 2009).
457. L. Radziute, G. Gaigalas, P. Jönsson, Jacek Bieron, Phys. Rev. A **93**, 062508 (2016).
458. Y. Singh, B.K. Sahoo, B.P. Das, Phys. Rev. A **89**, 030502(R) (2014).
459. B.K. Sahoo, Y. Singh, B.P. Das, Phys. Rev. A **90**, 050501(R) (2014).
460. Y. Singh, B.K. Sahoo, Phys. Rev. A **92**, 022502 (2015).
461. R.H. Parker *et al.*, Phys. Rev. Lett. **114**, 233002 (2015).
462. D. Cho, K. Sangster, E.A. Hinds, Phys. Rev. Lett. **63**, 2559 (1989).
463. D. Cho, K. Sangster, E.A. Hinds, Phys. Rev. A **44**, 2783 (1991).
464. A. Yoshimi, T. Inoue, T. Furukawa, T. Nanao, K. Suzuki, M. Chikamori, M. Tsuchiya, H. Hayashi, M. Uchida, N. Hatakeyama, S. Kagami, Y. Ichikawa, H. Miyatake, K. Asahi, Phys. Lett. A **376**, 1924 (2012).
465. E. Christova, M. Fabbrichesi, Phys. Lett. B **315**, 113 (1993).
466. M. Drees, M. Rauch, Eur. Phys. J. C **29**, 573 (2003).
467. J. Ng, S. Tulin, Phys. Rev. D **85**, 033001 (2012).
468. R.F. Bishop, *Microscopic Quantum Many-Body Theories and their Applications*, in *Lecture Notes in Physics*, Vol. **510** (Springer, Berlin, Heidelberg, 1998).
469. J. de Vries, E. Mereghetti, C.-Y. Seng, A. Walker-Loud, Phys. Lett. B **766**, 254 (2017).